Validation Test Report:
Offline Testing of a Regionalized Travel-Time Model and Source-Specific Stations Corrections for Asia

March 2002

Valeriu Burlacu[1], Mark D. Fisk[1], Vitaly I. Khalturin[2], Won-Young Kim[2], Paul G. Richards[2], John Armbruster[2], Igor Morozov[3], Elena Morozova[3]

Columbia University, Group 1 Consortium

1. Mission Research Corporation
2. Lamont-Doherty Earth Observatory of Columbia University
3. University of Wyoming

TABLE OF CONTENTS

LIST OF FIGURES

LIST OF TABLES

1. INTRODUCTION

1.1. Identification

This document describes the development and validation testing of Source Specific Station Corrections (SSSCs), by the Group 1 consortium (led by Prof. Paul Richards of Columbia University), for regional Pn travel times at seismic stations in Central Asia.

The SSSCs were computed by the method of Bondár (1999), using regionalized 1-D travel-time curves for Asia based on published studies, and by applying a kriging algorithm (e.g., Bottone et al., 2001) to empirical travel-time observations from events with ground-truth (GT) locations. The resulting SSSCs are in the form of grid files (in a standard format for operational use) with one-degree resolution, extending out to 20 degrees from a given station. They represent travel-time corrections relative to the IASPEI91 travel-time tables (Kennett, 1991).

Off-line validation testing was performed at the Center for Monitoring Research (CMR) by relocating GT events using the program *EvLoc* (e.g., IDC7.1.5, 2001), with and without the use of SSSCs. All events used in this analysis have published locations that are considered accurate to within 10 km; the majority of events have GT locations accurate to within 1 km. (For definitions of GT location categories, see Yang and Romney, 1999.) A leave-one-out approach was used so that events were not simultaneously used to both compute and test the SSSCs. Performance metrics are provided in terms of statistics of travel-time residuals, mislocation errors, the size of location error ellipses, and their coverage.

1.2. Scope and Audience

The goal of this effort is to provide Pn SSSCs for operational use that improve the accuracy of location estimates of seismic events, and reduce the uncertainty of these estimates, on the basis of the interpretation of the arrival times of regional seismic waves observed at seven stations of the International Monitoring System (IMS) located in Central Asia (see Table 1 and Figure 10).

This document describes our regionalization of Asia, travel-time curves for these regions, the calculation of Pn SSSCs (using Bondár's method and kriging), and the validation testing and

performance metrics. SSSCs for other regional phases (i.e., Pg, Sn, and Lg) and for other IMS seismic stations in Eastern Asia will be provided in the future.

The intended audience is the CMR Research and Development Support System (RDSS) staff who perform integration testing of SSSCs (and other system enhancements), the Configuration Control Board (CCB) who review and approve changes to the operational system, and other interested members of the scientific community. This document will accompany a future CCB proposal to implement, into routine processing, Pn SSSCs for seven stations located in Central Asia.

1.3. Overview

This document is divided into five main sections: Regionalization and Travel-Time Curves for Asia (Section 2), Data Sets (Section 3), Computation of SSSCs (Section 4), and Validation Testing and Evaluation (Section 5), Conclusions and Recommendations (Section 6).

Section 2 provides a comprehensive description of the regionalization of Asia, accompanied by the review of a wide variety of data concerning the propagation of the regional seismic waves and the estimation of the travel times, in each subregion, as a function of distance for regional seismic phases Pg, Pn, Sn, and Lg. Section 3 describes the GT data sets used for kriging empirical observations and in the off-line validation test. Section 4 presents the methods (Bondár's and kriging) used to generate the SSSCs and the resulting grids. Section 5 describes the validation test and the results expressed as standard evaluation metrics, which demonstrate significant improvements in location performance due to the Pn SSSCs. In Section 6 we provide conclusions regarding the results of the validation test and recommendations for use of these SSSCs in the operational system. An appendix provides plots the explicit SSSCs and modeling errors for seven seismographic stations in Central Asia.

2. REGIONALIZATION AND TRAVEL-TIME CURVES FOR ASIA

Here we document and justify our approach to obtaining travel times by a process of regionalization of Eastern Asia. We pay particular attention to Central Asia and nearby regions. Our approach has been to use the procedure suggested by Bondár (1999), which directly emphasizes acquisition of travel-time information (and forming averages of subregion travel times to predict total travel times for paths that cross regional boundaries), rather than using models of crust and upper mantle.

The work of acquiring travel times of seismic waves in Eastern Asia, for purposes of calibrating IMS stations, can conveniently be split into two steps. The first step is to identify the boundaries of subregions, within which travel times show little evidence of lateral variability. Our consortium began with this step in February 2001 at an Experts Group Review Meeting held at Lamont, during which consortium members worked together with two outside advisors (Dr. Charles Langston, of the University of Memphis; and Dr. E. Robert Engdahl, of the University of Colorado) and made a preliminary choice of subregion boundaries. The second step is to review a wide variety of data and previous technical reports and publications, concerning the propagation of regional seismic waves in each subregion, and to obtain best estimates of the travel time as a function of distance, within each subregion, for each major observed seismic phase (notably, Pg, Pn, Sn, and Lg).

Subsequent to February 2001, the predictions of our preliminary regionalization have been compared with a variety of empirical travel times; and our regionalization has been modified both as to the regional boundaries in some instances, and as to the travel times within some subregions, in order to conform better with gross features of empirical data such as the travel times from Soviet-era Peaceful Nuclear Explosions recorded in Eastern Asia. At present (December 2001) we are working with version 3 of our regionalization, which is described in detail at the URL http://www.LDEO.columbia.edu/~armb. For example, this website gives latitude and longitude at closely spaced points along the boundaries between subregions, as well as maps and tables of travel-time relations (i.e. travel time as a function of distance, for different regional phases) that are included in the present document.

Figure 1 shows two maps of the boundaries of the different subregions in this version 3 of our work. The upper map shows boundaries together with topography. The lower map shows boundaries together with our numbering scheme for the different subregions.

In sections that follow we describe our approach to the regionalization of Eastern Asia, paying particular attention to the subregions that are of importance to the calibration of the first set of stations, in or near Central Asia, for which we are proposing SSSCs at this time, namely AAK, AKTO, BRVK, KURK, MAKZ, NIL, ZAL. The IMS station code for these sites, and the host country, are presented in Table 1.

Table 1. IMS Stations for which Pn SSSCs are computed.

IMS Code	Country	Station Name	Station Code
PS23	Kazakhstan	Makanchi	MAKZ
PS29	Pakistan	Pari	NIL
PS33	Russian Federation	Zalesovo	ZAL
AS57	Kazakhstan	Borovoye	BRVK
AS58	Kazakhstan	Kurchatov	KURK
AS59	Kazakhstan	Aktyubinsk	AKTO
AS60	Kyrgyzstan	Ala-Archa	AAK

NIL (Nilore, Pakistan) is a station very close to the planned IMS primary station at Pari. We note that at present only the Nilore and Zalesovo stations are contributing data that are being used for routine analysis at the IDC. An array at Makanchi is currently contributing data to Vienna, and it may be expected that these data will shortly be incorporated into routine analysis by the IDC. Borovoye, Kurchatov, Makanchi and Ala-Archa are sites at which a variety of broadband instrumentation has been operated in recent years. These data are used by regional network operators but not yet by the IDC. Aktyubinsk has been operated for several years by Russian seismologists, and intermittently since 1994 by Kazakhstan. In addition to these stations, we have computed Pn SSSCs at stations MAG, NRI (NRIS), SEY, TIK (TIXI), TLY, YAK, and ULN, which are useful surrogates for other IMS stations that we are attempting to calibrate in Asia.

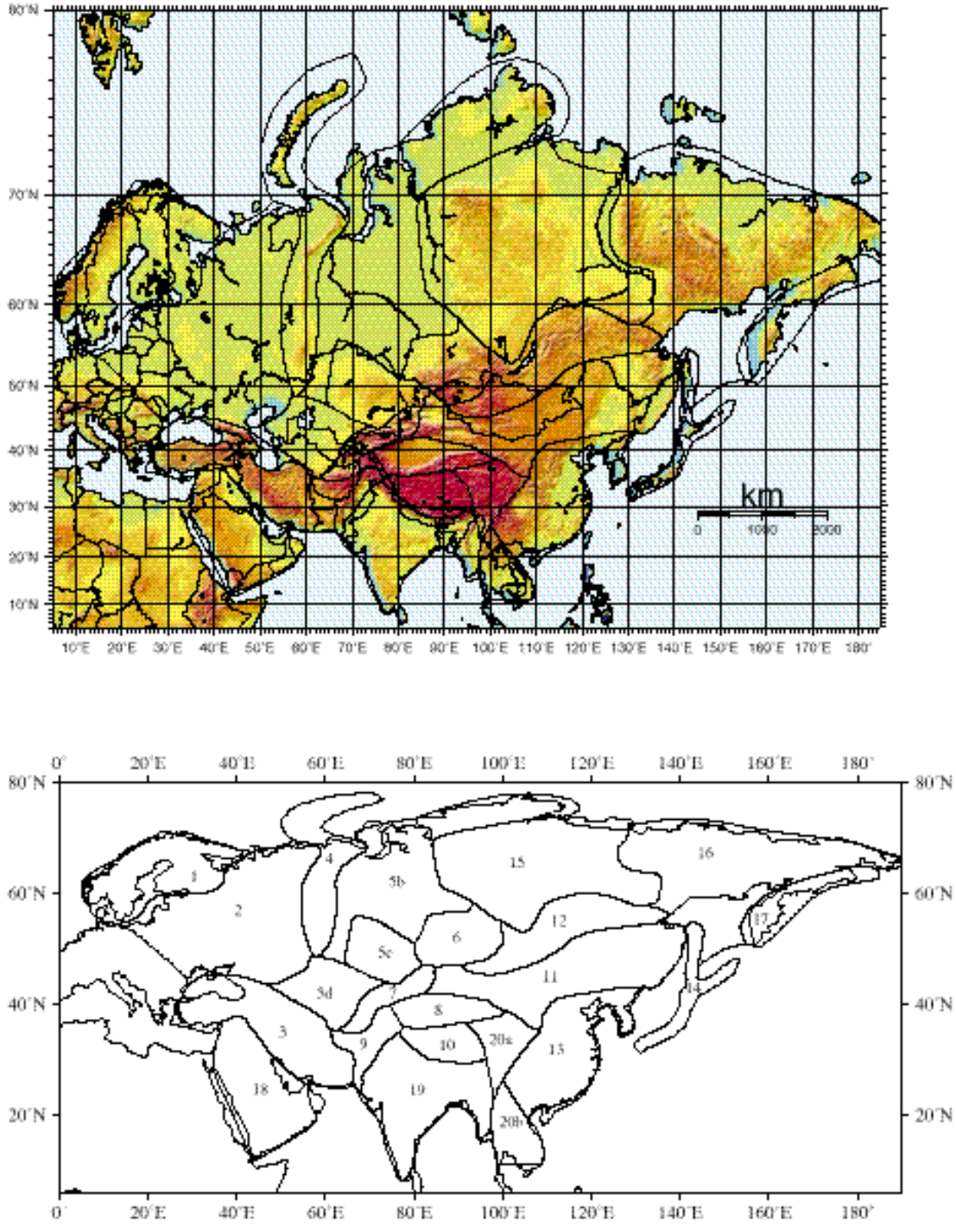

Figure 1. Maps of topography and regionalization boundaries (upper) and the numbering convention used for the various subregions (lower).

2.1. Subregion Boundaries

Our choice of subregion boundaries has been based on expert interpretation of maps of tectonic provinces and taking into account published velocity structures of the crust and upper mantle (including lithospheric thickness), seismic activity, heat flow, and gravity. The tectonic approach is based on structural types such as shields, ancient and young platforms, and fold belts. While information on geophysical parameters has mostly been acquired in recent decades, the basic identification of different geologic provinces was made in most cases much earlier. Useful sources used for identifying subregions were

- The Tectonic map of Eurasia, compiled by the Geological Institute of the Soviet Academy of Science, 1:5,000,000, Moscow, 1966 (in Russian), and
- Seismotectonic map of Asia and Europe, 1:8,000,000, published by the Geological Institute of the Chinese Academy of Sciences, Beijing, 1981 (in Chinese).

The more important sources of information on the velocity structure of the crust and upper mantle, also used to assign subregion boundaries, were Beloussov et al. (1991), Beloussov et al. (1992), Egorkin (1980), Karus (1984), Kirichenko and Kraev (2000), Kosminskaya (1980), Nersesov (1987), Pavlenkova (1996), Volvovsky (1991).

At the present stage of our consortium's work, regionalization of the territory of the former USSR including Central Asia is more detailed and reliable than for surrounded areas such as Iran, Pakistan, India, China. This is because of the major efforts made (a) in association with the program of activities known as Deep Seismic Sounding (DSS), and (b) in detailed geological mapping carried out during the Soviet era. The DSS profiles associated with nuclear explosions are well known from extensive publications in western journals. Less well known are earlier DSS profiles carried out with chemical explosions.

We next describe the regional phases associated with the IASPEI91 model, contrasted with features generally observed in Eastern Asia that differ from the IASPEI91 model; then we give our main sources of general information on travel times, followed by more detailed comments on subregion travel times with particular attention to the subregions that are most important for obtaining SSSCs for IMS stations in and near Central Asia.

2.2. Comparison of Observed Regional Phases in Asia to IASPEI91

Regional phases are seismic waves propagated in the crust, lithosphere and upper mantle down to the region of anomalous velocity gradient at a depth of around 410 km. The Pg, Lg and Rg waves propagate within the continental crust with near constant velocity along the path and having only small regional variations. In most regions, the Pg apparent velocity is 6.10 - 6.25 km/s, Lg velocities are 3.50 - 3.60 km/s, and Rg velocity is in the range 2.7 - 3.0 km/s depending upon the period of maximum phase in the wave train.

According to the IASPEI91 travel-time table there are two groups of Pn waves: Pn1 and Pn2. The Pn1 wave is the first arrival in the interval 200 - 1700 km with near constant apparent velocity, slightly increasing from 8.08 km/s to 8.14 km/s (+1.2%).

The Pn2 wave of IASPEI91 appears as a first arrival at around 1700 km with velocity 8.5 km/s (+4.4%) in the interval 1700 - 1800 km and velocity 8.9 km/s (+4.7%) in the range 1900 - 2000 km.

In the IASPEI91 table, the apparent velocity of P waves sharply increases around 2000 km from 8.9 km/s up to 9.5 km/s at 2000 - 2100 km and increasing further to 10.0 km/s (2100 - 2200 km). Thus this reference table indicates velocity increases totaling 11.2% over a short interval (2000 - 2200 km). The P waves with velocities of 9.5 km/s and greater, propagate beneath the 410 km and are usually called “teleseismic” P waves though they are observed at distances where the regional phase Pn can also be seen. These teleseismic waves can be divided into two types, P1 and P2, for distances up to 2700 - 3000 km. The P1 waves propagate beneath the 410 km boundary and above the 660 km boundary. They are observed as a first arrival at distances between 2000 and 2600 km, with velocity slightly increasing from 10.0 km/s at 2200 km up to 10.6 km/s (+6%) at 2600 km. The P2 wave appears as a first arrival in the 2600 - 2700 km distance range, where the P wave velocity increases from 10.6 km/s to 12.2 km/s (+15%). Beyond 2700 km the P2 velocity increases only 0.5% per 100 km.

In contrast to these travel times for IASPEI91, we find evidence in general for significant regional variation of P-wave velocities out to distances of 2200 km, and less significant out to 2700 km. Of particular importance is the fact that our tables for some regions of Eastern Asia indicate that Pn is observed as the first arrival out to distances of 2100 - 2200 km.

For Pn waves we use the designations Pn1, Pn2, and in some regions Pn3, in cases where the apparent velocity changes slightly with distance but does not exceed 9.5 km/s.

Sn waves experience significant regional variations in amplitude. Sn waves also have travel-time variations that are 3 to 5 times larger than regional variation of Pn travel times.

It is known that intensive Sn waves are observed in the areas south of the Alpine belt and very often this phase cannot be detected on records of the events located north of this belt. (This “Alpine belt” includes mountains extending far to the east of the European Alps, through the Caucasus, the Kopet Mountains, the Tian Shan, and Altay Sayan to Lake Baykal, all of which broadly are associated with the same major event, namely the closing of the Tethys Ocean.)

In Northern Eurasia, Sn waves are observed with apparent velocities 4.5 - 4.7 km/s in the distance range 1400 - 1700 km. Teleseismic S waves can be observed from 1500 - 1700 km and at greater distances, with apparent velocities 5.6 - 5.8 km/s. A time gap of about 20 - 30 s can be observed between regional Sn and teleseismic S waves on the same record, at distances 1400 - 1600 km. If only one S phase is observed in this distance range, uncertainty as to identification (whether Sn or S) can result in significant scatter in empirical data, and significant travel-time residuals to the extent that the wrong phase is identified and used for interpretation.

2.3. Main Sources of Information on Regional Travel Times

Although hundreds of papers (mostly based on DSS results) are devoted to the velocity structure of the crust and upper mantle of different regions of the former USSR and surrounding areas, only a few of them quote the primary travel-time data on which these studies are based. Note that our whole approach to IMS station calibration emphasizes the acquisition and use of empirical travel times, rather than relying upon a modeling approach. References to specific publications that are important for particular subregions are given below. Here, we note that more general data about travel times from DSS data were found in the following papers: Karus (1984), Ryaboy (1989), Ryaboy (1991), Volvovsky (1991), Zunnunov (1985).

It was easier to obtain travel-time information for seismically active zones for which regional seismologists have collected many observational results, but unfortunately most of them were

limited to distance ranges up to only 800 - 1000 km. Travel-time data for greater distances were published only in a few papers. The most important among them is Nersesov and Rautian (1964).

This main paper covered a very wide region, extending from Central Asia to the north and east as far as the Lena River (north of Lake Baykal). Subregional versions of the data in the main paper were described in three reports and one paper: Khalturin (1974), Khalturin at al. (1978), Khalturin et al. (1994), Khalturin et al. (2001).

Other significant seismological publications containing travel-time information for more than one of our subregions are: Atabaev and Butovskaya (1986), Gorbunova (1990), Kirichenko and Kraev (2000), Lukk and Nersesov (1967), Nersesov (1960).

Table 2 lists 27 Deep Seismic Sounding profiles in Central Asia carried out with chemical explosions. This table is assembled from information in Antonenko (1984), Shatsilov (1993), Zunnunov (1985) and the book “Seismic Models of the Lithosphere of the main Geostructures in territory of the USSR” published in 1980. Figure 2 shows the location of these 27 profiles, some of which consisted of more than one segment. Table 3 gives the empirical travel time of Pn arrivals picked from seven DSS profiles using chemical explosions in and near Kazakhstan (information from Zunnunov, 1985). Table 4 gives a simple (straight line) travel time as a function of distance, for the Pn wave on these seven profiles, and also the distance over which this time - distance relation applies. Figure 3 shows seven values for the average Pn velocity obtained from the data associated with Table 1 and Table 2. All of this information was used in our regionalization of Central Asia and surrounding areas.

We next give more detailed comments on regional travel times within specific subregions of Eastern Asia, together with figures showing the residual against the IASPEI91 travel times for some subregions within and near Central Asia.

Table 2. List of DSS Profiles, using chemical explosions, conducted in or near Kazakhstan.

N	Name or position	Profile end points	Length, km
1.	Turkestanski	42.5N 65.0E to 44.7N 75.0E 46.3N 81.0E to 49.0N 83.4E	1,550
2.	Charsky - Sinyuha	49.3N 80.8E to 50.4N 83.2E	220
3.	Sayakski, first line second line	43.1N 74.9E to 46.5N 76.8E 46.6N 77.3E to 51.1N 82.1E	600
4.	Aktogaysky	44.7N 78.6E to 47.5N 80.5E	350
5.	Kentierlausskiy	47.1N 72.9E to 47.5N 80.5E	570
6.	Zhalanash - Taldi-Kurgan	43.0N 78.5E to 45.0N 78.5E	220
7.	Issikski	43.3N 77.7E to 46.2N 77.3E	315
8.	Central Kazakhstansky	47.4N 70.7E to 49.0N 77.7E	540
9.	Issik-Kul - Balkhash	43.3N 77.0E to 46.0N 75.0E	430
10.	Slavgorodsky	46.2N 73.8E to 51.4N 77.5E	520
11.	Shchuchinsk - Severnoe	53.4N 71.6E to 56.3N 76.3E	700
12.	Karkaralinsky	48.8N 75.2E to 50.6N 69.2E	780
13a.	Temirtay-Petropavlovsk	50.3N 72.9E to 54.8N 69.4E	600
13b.	Balkhash-Temirtau	46.9N 75.0E to 50.3N 72.9E	500
14.	Uvanassky	43.6N 74.0E to 46.1N 65.2E	740
15.	Aris'- Balkhash	42.5N 68.7E to 45.7N 73.4E	510
16.	Temirtau - Kuybishev	50.3N 72.9E to 52.2N 54.0E	1,360
17.	Peschaniy	43.9N 68.8E to 47.0N 72.6E	460
18.	Karatau - Tengiz Lake	43.2N 70.5E to 50.2N 69.0E	900
19.	Kzil-Orda - Dzheti-Konur	44.8N 65.6E to 47.7N 68.8E	400
20.	Meridian	42.8N 67.4E to 49.5N 68.3E	740
21.	1-T-70	47.4N 65.8E to 48.6N 58.6E	550
22.	Aktyubinsky	50.0N 62.1E to 50.2N 57.5E	300
23.	Kopet-Dag - Aral Sea	40.0N 58.0E to 43.8N 61.3E	650
24.	Kandagachsky	49.0N 59.5E to 50.8N 52.0E	540
25.	Chelkar - Volgograd	48.5N 58.0E to 49.0N 54.OE	930
26.	OP-1 and 11	41.2N 54.5E to 52.3N 53.7E	1,680
27.	Farab - Tamdi-Bulak	40.0N 63.5E to 43.0N 65.0E	430

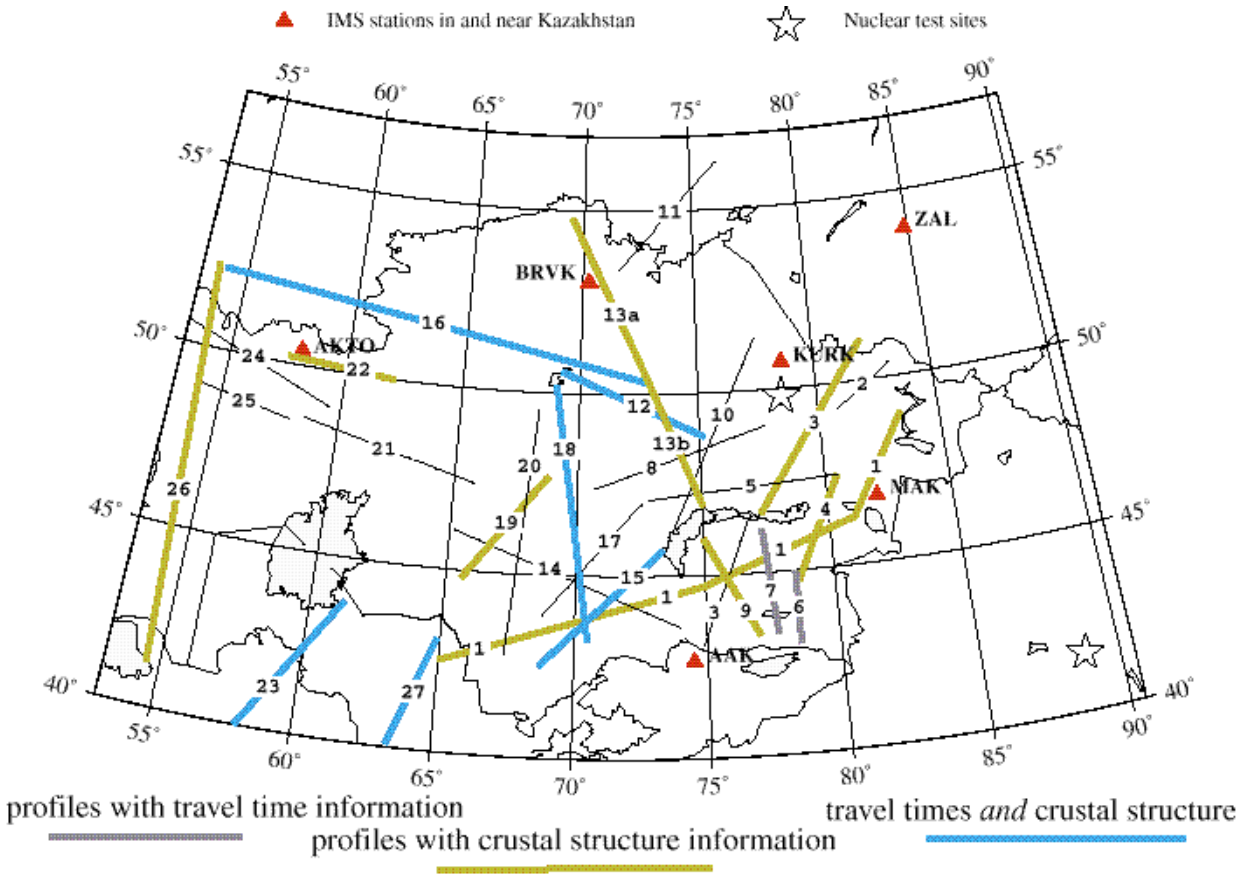

Figure 2. Major Deep Seismic Sounding profiles of Kazakhstan and nearby regions.

Table 3. Empirical travel times reported for seven DSS profiles in and near Kazakhstan.

	Profiles numbers on the map (Figure 2)							
R, km	**6**	**7**	**15**	**16**	**18**	**23**	**27**	IASPEI91
160	-	-	-	27.5	-	27.5	28.1	-
200	35.8	-	34.4	32.6	33.0	33.0	33.4	32.3
240	40.9	40.9	38.4	37.7	38.3	38.2	38.0	37.2
280	45.5	45.6	43.3	43.2	43.1	43.0	42.9	42.2
320	50.4	50.6	47.9	47.8	47.8	47.7	-	47.1
360	55.1	55.4	52.9	52.6	52.6	52.8	-	52.1
400	60.7	60.9	58.2	57.5	57.5	57.2	-	57.0
440	-	-	64.0	-	62.5	62.3	-	62.0
480	-	-	69.5	-	66.8	67.3	-	66.9
520	-	-	74.2	-	71.4	72.7	-	71.9
560	-	-	-	-	76.2	77.6	-	76.8
600	-	-	-	-	81.1	82.5	-	81.7
640	-	-	-	-	86.0	-	-	86.7
680	-	-	-	-	91.1	-	-	91.6
720	-	-	-	-	96.2	-	-	96.6
760	-	-	-	-	101.4	-	-	101.5
800	-	-	-	-	105.5	-	-	106.5
840	-	-	-	-	110.4	-	-	111.4
880	-	-	-	-	115.3	-	-	116.4

The numbering of profiles here is the same as in Table 2 and Figures 2 and 3. Thus,

#6 - Zhalanash - Taldy-Kurgan. From N. Tian-Shan to North.

#7 - Issik. From N. Tian-Shan to Balkhash Lake.

#15 - From Aris' (42.4N; 69.0E) to NE to Balkhash Lake, across South Kazakhstan.

#16 - From Temirtau (50N; 73E) to WNW direction to South Ural.

#18 - From Karatay (43.2N; 70.5E), S. Kazakhstan, across the Central Kazakhstan to Tengiz Lake.

#23 - From West Turkmenia to eastern part of Aral Lake.

#27 - Farab - Tamdibulak. West Uzbekistan, between Amu-Darya and Syr-Darya rivers.

Table 4. Apparent Pn velocity measured from seven DSS profiles in and near Kazakhstan.

#	Profile	Distance Range (km)	Apparent Velocity (km/s)	Travel-Time equation
6	Zhalanash-Taldykurgan	200 - 400	8.03	t = R/8.03 + 10.9
7	Issiksky	240 - 400	8.00	t = R/8.00 + 10.9
15	Aris'- Balkhash	200 - 520	8.04	t = R/8.04 + 9.3
16	Temir-Tau - Kuybishev	160 - 400	8.03	t = R/8.03 + 7.8
18	Karatay - Tengiz Lake	200 - 760 760 - 880	8.23 8.63	t = R/8.23 + 8.5 t = R/8.63 + 13.3
23	Kopet-Dag - Aral Sea	180 - 600	8.08	t = R/8.08 + 8.3
27	Farab - Tamdi-Bulak	200 - 360	8.11	t = R/8.11 + 8.5
-	IASPEI91	200 - 900	8.11	t = R/8.11 + 7.6

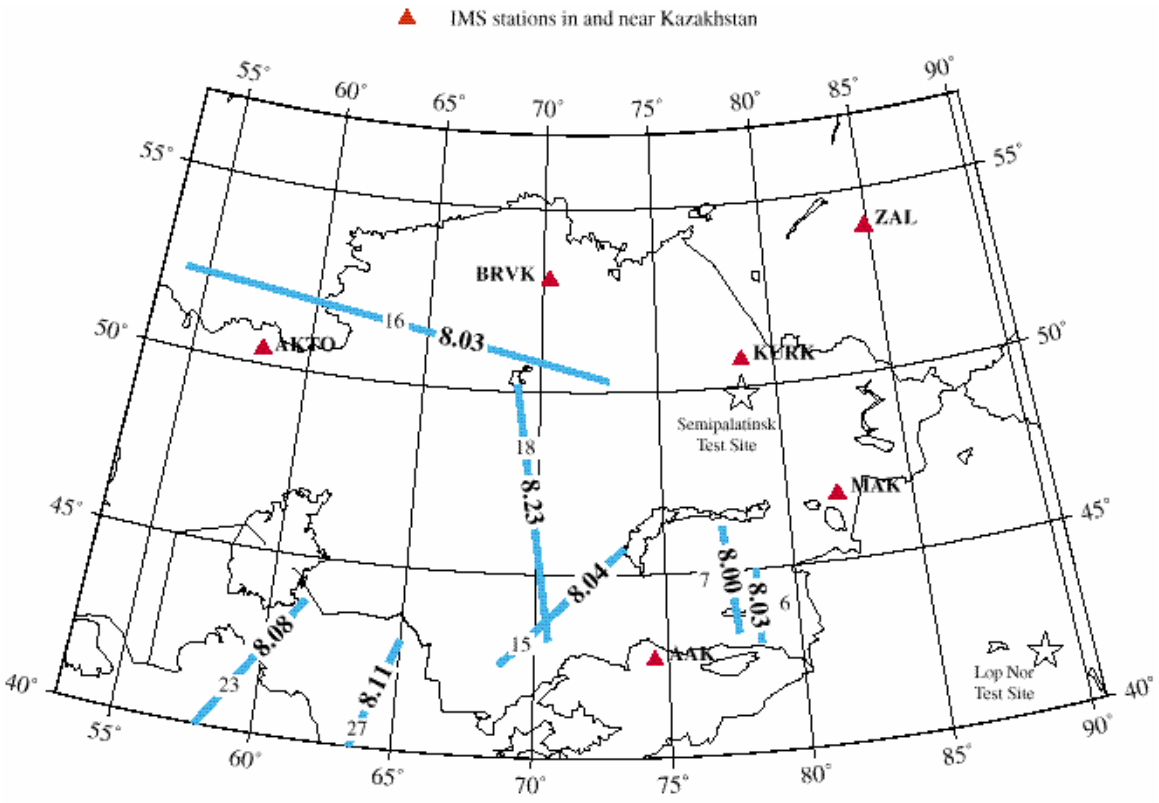

Figure 3. Pn velocities (km/s) from DSS profiles (chemical explosions) in and near Kazakhstan.

2.4. Description of Regional Travel Times in each Subregion

2.4.1. Scandinavian Shield (Region #1)

This region consists of Scandinavia (Norway and Sweden), Finland, Karelia, and the Kola Peninsula of Russia. In this region there is little sedimentary cover, and granites are widely apparent at the surface. The eastern part (Kola and Karelia) is the region of the oldest (pre-Riphean) folding of an earlier platform. In the western part (Finland and Sweden) are younger (pre-Carelian) structures. Part of the western section (Norway) includes the early Caledonian fold belt. This is the only region in Europe where 1.5 - 2.0 billion year old rocks appear at the surface. Seismic activity and heat flow are low. All tectonic and geophysical factors indicate a high-velocity structure for the crust and upper mantle in this region. The border between the Scandinavian Shield and the East European platform is clearly identifiable and passes from the White Sea, to Onega and Ladoga Lake, then along the central part of Baltic Sea and north from Denmark.

Careful seismological observations were made in this region first by Markus Båth. He was also among the first researchers to study Lg waves which are clearly seen and which propagate efficiently in this region. His travel-time relations for regional phases Pg, Lg, Rg and Sn (Båth, 1977) are still used by local seismologists and can be recommended for location of seismic events:

H = 0 km	
t(Pg) = R/6.22 + 0	0 - 1500 km
t(Sn) = R/4.65 + 13.0	200 - 1500 km
t(Lg) = R/3.58 + 0	0 - 1500 km
t(Rg) = R/3.02 + 0	0 - 1000 km

For Pn waves, reliable data based on DSS were described by Bondár and Ryaboy (1997):

t(Pn1) = R/7.94 + 6.8	195 - 300 km
t(Pn2) = R/8.17 + 7.9	300 - 370 km
t(Pn3) = R/8.32 + 8.7	370 - 800 km

For distances more than 800 km, Pn travel-time data obtained for the East European Platform (Ryaboy, 1989) can be used. These are based on recent DSS studies of the structure and velocity-

cross section (beneath 100 - 150 km) of the upper mantle of both regions, which are nearly similar for depths below 100 - 150 km. The following travel-time relations for Pn and P waves are therefore appropriate for distances greater than 800 km:

t(Pn3) = R/8.32 + 8.7	800 - 1200 km
t(Pn4) = R/8.61 + 13.5	1200 - 2200 km
t(P) = R/10.14 + 52.0	2200 - 2700 km

The main peculiarities of the P wave travel-time data for Scandinavia are:

(a) The low velocity Pn (7.94 km/s) in the distance range 200 - 300 km;

(b) The near constant and relatively high Pn velocity (8.32 km/s) for a wide range of epicentral distances, 400 - 1200 km, indicating that the P-wave speed for the top 200 km of the upper mantle is approximately constant. An increase in apparent velocity of Pn at about 1200 km distance corresponds to a discontinuous increase in P-wave speed at a depth of about 250 km, which has been detected in several regions;

(c) The apparent velocity of 8.61 km/s is observed out to a distance of 2200 km without significant change;

(d) At the so-called “20 degree discontinuity,” the apparent velocity increases sharply by 12% to 10.14 km/s without an intermediate velocity of around 9.5 km/s (as in many other regions, and in the IASPEI91 travel times).

In summary of this region, we propose use of the following travel times:

Region #1. SCANDINAVIAN SHIELD

P waves, first arrivals:

Time equations	Distance
t(Pg) = R/6.22 + 0	0 - 195 km
t(Pn1) = R/7.94 + 6.8	195 - 300 km
t(Pn2) = R/8.17 + 7.9	300 - 370 km

t(Pn3) = R/8.32 + 8.7	370 - 1200 km
t(Pn4) = R/8.61 + 13.5	1200 - 2200 km
t(P) = R/10.14 + 52.0	2200 - 2700 km

Other regional phases:

Time equations	Distance
t(Pg) = R/6.22 + 0	0 - 1500 km
t(Sn) = R/4.65 + 13.0	200 - 1500 km
t(Lg) = R/3.58 + 0	0 - 1500 km
t(Rg) = R/3.02 + 0	0 - 1000 km

2.4.2. East European Platform (Region #2)

The East European Platform (Craton) occupies a huge area of the former USSR. It is bounded to the south by the Caspian Sea, the Caucasus, and Crimea; and to the west by a linear system of troughs from the East Carpathian region to the southern part of Scandinavia. To the east, the East European Platform is bordered by the foothills of the Ural mountains.

The East European Platform is covered by sediments with average depth from 500 to 4000 m. Precambrian rocks are exposed at the surface only on the Ukranian Shield. Under most parts of the East European Platform the Moho surface is flat and average crustal thickness is within a narrow interval (38-44 km). Average P wave speed in the consolidated part of the crust is 6.5-6.6 km/s. Within this region several subareas with slightly different structures have been identified:

(a) The Scythian Plate is a younger part of the East European Platform, adjacent to the Caucasus and Crimea, with slightly lower velocities in the crust and upper mantle. Seismicity here is low;

(b) The PreCaspian Depression is a submerged part of the East European Platform, with a subcontinental type of crust in the northern part, covered by sediments having a thickness of more than 10 km. The thickness of the “non-consolidated” part of the crust in this subregion (with velocities less 5.8 km/s) has values as large as 22 km. The average crustal thickness is lower - about 40 km - and even reaches 32 - 34 km in the northern part of the Depression. This is compensated for by higher than average velocities in the consolidated part of the crust (6.7 - 6.8 km/s);

(c) Precambrian rocks are at the surface only on the Ukranian Shield, where Moho depth reaches 48 km and average velocities in the consolidated crust also are higher than average (6.7 - 6.8 km/s);

(d) The Timano-Pechora Province occupies the extreme northeastern corner of the East European Platform. Here there are Baykal age granites lying beneath the thick sediments.

The travel-time data for the East European Platform were mostly obtained by Deep Seismic Sounding. The principal results were described by Ryaboy (1989) and Krasnopevtseva (1984), and summarized by Kirichenko and Kraev (2000) and by Starovoit et al. (2000).

The travel-time data for the East European Platform are similar to those for Scandinavia. The main difference is that for the East European Platform the low apparent velocities 7.94 km/s and 8.17 km/s (which are observed in Scandinavia in the distance range 200 - 370 km) are absent. So in the East European Platform, velocities beneath the Moho immediately start from 8.32 km/s.

Observations can be summarized by the following travel-time relations:

Region #2. EAST EUROPEAN PLATFORM

P waves, first arrivals:

Time equations	Distance
t(Pg) = R/6.23 + 0.6	0 - 200 km
t(Pn) = R/8.32 + 8.7	200 - 1200 km
t(Pn) = R/8.61 + 13.5	1200 - 2200 km
t(P1) = R/10.14 + 52.0	2200 - 2700 km
t(P2) = R/12.35 + 99.7	2700 - 3000km

Other regional phases:

Time equations	Distance
t(Pg) = R/6.23 + 0.6	0 - 400 km
t(Lg) = R/3.53 + 1.0	250 - 2500 km
t(Sn) = R/4.75 + 16.0	250 - 2500 km

2.4.3. Cenozoic Folded Regions (Region #3)

This region consists of a large area of the Alpine Belt from Turkey to Pakistan. It includes the Black Sea, Crimea, Turkey, Caucasus with the southern part of the Caspian Sea, all territory of Iran and the western part of Pakistan. To the north it borders the southern part of the East European Platform (Scythian plate). To the east it is bounded along the Kopet-Dag fault zone by the Turan plate. Also to the east is Suleyman Ridge and to the south lies the Arabian plate.

The Cenozoic Folded Regions comprise an area with a high level of tectonic movement and seismic activity. For this region, high attenuation of seismic waves is typical. There is partial or full blockage of Lg and Rg waves and a high temperature gradient in the crust that leads to partial melting even in the lower crust, and a thick and shallow asthenosphere (beneath thin lithosphere). Over this large area we note several subareas with different tectonic styles and crust-upper mantle structures:

(a) the Black Sea region with thin suboceanic crust, which blocks Lg and Rg propagation;

(b) the Caucasus region (further subdivided into the Greater and Lesser Caucasus). Here, as in Eastern Turkey and Western Iran, there has been recent volcanic activity and Lg - Rg waves are partially blocked;

(c) the southern deep-water basin of the Caspian Sea, also characterized by suboceanic crust. This part of the Caspian Sea completely blocks the propagation of Lg and Rg waves;

(d) the Iranian Plateau located northeast of the Zagros Mountains and southwest of the Kopet-Dag fault zone. Here there is high attenuation of seismic waves associated with shallow depths of the asthenosphere, and a partially melted zone within the upper mantle. Geothermal observations indicate a high temperature (about 900º C), at depths in the range 30 - 40 km;

(e) the southwestern part of Iran along the Zagros area. This too is an area with low-efficiency of propagation of Lg waves.

We propose the same travel-time relations for this region, as recommended by Kirichenko and Kraev (2000):

Time equations	Distance
t(Pg) = R/6.21 + 0.9	250 - 1200 km
t(Pn) = R/8.22 + 8.8	200 - 1800 km
t(Sn) = R/4.58 + 12.1	250 - 2000 km
t(Lg) = R/3.56 + 0.9	200 - 2200 km

2.4.4. Ural Fold Zone (Region #4)

The Ural mountains form a natural border between Europe and Asia, between the East European Platform and the West Siberian Plate. This region is a folded structure of Hercynian age, composed of Precambrian rocks. The Urals are an extremely long anticlinorium reaching more than 4000 km in length, and only 250 - 300 km wide. Tectonically this region includes the Taymyr Peninsula (the northeastern part of the West Siberian Plate), Novaya Zemlya, and the Ural Mountains, including their southern part which subsides beneath sediments of the PreCaspian Depression. The average crustal thickness along the central part of the Ural Fold Zone is 50 - 53 km. High velocities of P waves (6.0 km/s and more) begin immediately at the surface. Average crustal velocity is 6.7 km/s.

Travel-time data of regional phases from local events were studied by Lomakin et al. (1978). The epicentral distances of their data ranged from a few km out to 430 km. Very intensive PmP and SmS waves are traced from 130 km out to 300 km. The amplitude of PmP and SmS waves in the distance interval 140 - 280 km are 3-5 times larger than amplitudes of Pg or Pn and Lg or Sn waves. Their travel-time relations correspond to a Moho depth of 46 km and average velocity in the crust being 6.5 km/s for P and 3.8 km/s for S waves. DSS profile data for the Ural zone were summarized by Kirichenko and Kraev (2000). We propose use of the following travel time relations:

Region #4. URAL FOLD ZONE

P waves, first arrivals:

Time equations	Distance
t(Pg) = R/6.25 + 0.2	0 - 220 km
t(Pn) = R/8.08 + 8.2	220 - 400 km

t(Pn) = R/8.32 + 9.6	400 - 1600 km
t(Pn) = R/8.60 + 15.9	1600 - 2000km

Other regional phases:

Time equations	Distance
t(Pg) = R/6.25 + 0.2	50 - 1000 km
t(Sn) = R/4.69 + 14.5	220 - 1600 km
t(Lg) = R/3.59 + 0	50 - 2000 km

2.4.5. West Siberian Platform (Region #5b)

The West Siberian Platform is located between the Ural Fold Belt in the west and the East Siberian Platform (Craton) in the east. To the north it is bordered by older structures of the Taymyr Peninsula, and to the south by the Kazakh Massif and the Altay-Sayans fold system. The West Siberian Plate is a young platform, of late Hercynian age. Geographically it is lowland with swamp prevailing on most of the land. It is covered by sediments with thickness reaching 3500 m in some places. The crust of the West Siberian Platform, with thickness in the range 33 - 39 km, is thinner than all surrounding areas. Average P-wave velocity in the crust is 6.5 - 6.6 km/s. The consolidated crust (i.e., the layers with P-wave speed greater than 5.8 km/s) begins at a depth of around 4 - 6 km.

The travel-time data for this region are obtained from long-distance DSS profiles. There are many publications giving detailed descriptions of the principal waves observed, but only in two of them were we able to find information directly on the travel time of P waves. Thus, the papers of Ryaboy (1985) and Barikhin et al. (1987) describe the results of several long DSS profiles, crossing the West Siberian Platform. In our review we have also taken into account the data from ultra-long DSS profiles (based on PNE sources) summarized by Kirichenko and Kraev (2000). The main peculiarities of West Siberian Platform travel times are:

(a) high Pn velocities (8.35 km/s) observed at distances as short as 200 km. So, directly beneath the Moho the Pn velocity jumps up to 8.35 km/s, which differs from observations in Scandinavia or in the East European Platform;

(b) in the distance range 2000 - 2200 km the apparent P velocity is 9.62 km/s, which corresponds to speed in upper mantle just beneath the 410 km discontinuity, and hence is a teleseismic arrival.

The travel-time relations summarizing all these observations are as follows:

Region #5b. WEST SIBERIAN PLATE

P waves, first arrivals:

Time equations	Distance
t(Pg) = R/6.25 + 1.3	0 - 200 km
t(Pn1) = R/8.35 + 9.3	200 - 900 km
t(Pn2) = R/8.50 + 11.1	900 - 1700 km
t(Pn3) = R/8.65 + 14.6	1700 - 2000 km
t(P1) = R/9.62 + 37.9	2000 - 2200 km

Other regional phases:

Time equations	Distance
t(Pg) = R/6.25 + 1.3	50 - 1000 km
t(Sn) = R/4.75 + 15.4	250 - 2000 km
t(Lg) = R/3.56 + 0.6	50 - 2500 km

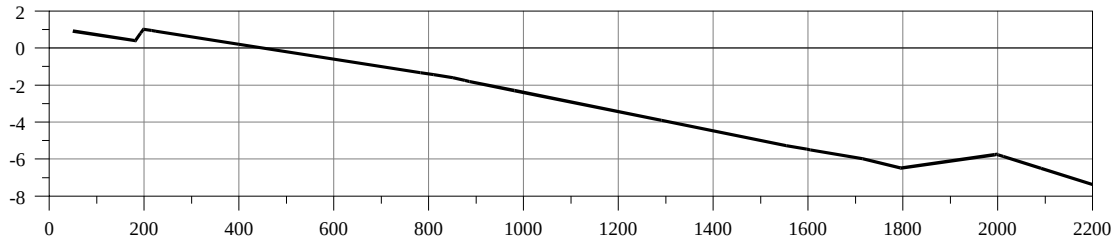

Figure 4. Travel-time residual (Region #5b - IASPEI91) for first arriving P waves out to 2200 km.

2.4.6. Kazakh Massif (Region #5c)

The Kazakh Massif is an old folded region of Caledonian and Hercynian ages. The folding process ended in the late Hercynian. This region is now dominated by flat upland with average elevation 500 - 600 m. Due to constant uplifting, erosion has revealed rocks even of Baykal age, such as the Kokchetav Mountains and Degelen Mountain. The Kazakh Massif is bounded on the north by the West Siberian Plateau, on the southwest by the Turan Plateau, on the southeast by the Tian Shan Mountain system, and on the east by the Altay-Sayan zone.

It is a stable and almost aseismic area, with activity occurring only in the eastern part of the Massif, where a very low level of seismicity is observed. The heat flow is moderate - about 50 - 70 mW/ m2. The geology and velocity structure of the region has been studied in detail by Russian geologists and geophysicists (Antonenko, 1984; Shatsilov, 1994; and many others.). Many DSS profiles crossed the area, as indicated in Figures 2 and 3. The Moho surface is flat for the northern part of the Massif. Average Moho depth there is 42 - 44 km. Moho relief becomes more complicated to the south (south of about 46.0º N) and depth there is 44 - 48 km.

The average P-wave speed in the crust is 6.6 - 6.7 km/s. Average velocity just below the Moho surface is about 7.95 - 8.05 km/s in the south part and 8.10 - 8.15 km/s in the north part. The velocity within the crust increases slowly with depth without low velocity zones. The same is typical for upper mantle cross-sections of the region.

Section 2.3 lists several publications containing travel-time data (obtained both by DSS and seismological methods) for the Kazakh Massif. See also Tables 1-3 and Figures 2 and 3. DSS data were mostly obtained from Karus (1984), Zunnunov (1985), and Volvovsky (1991). Seismological observations giving travel-time data are mostly from Nersesov and Rautian (1964) and from Khalturin et al. (1974, 1987, 1994, 2001). Information on regional travel times for this region was also extracted from Antonenko (1984), Shatsilov (1993). For this region we propose use of the following travel times:

Region #5c. KAZAKH MASSIF

P waves, first arrivals:

Time equations	Distance
t(Pg) = R/6.21 + 0.8	0 - 200 km
t(Pn1) = R/8.13 + 8.4	200 - 900 km
t(Pn2) = R/8.36 + 11.4	900 - 1600 km
t(Pn3) = R/8.73 + 19.5	1600 - 2000km
t(P1) = R/9.57 + 39.6	2000 - 2200 km
t(P2) = R/10.10 + 51.7	2200 - 2400km
t(P3) = R/10.95 + 70.1	2400 - 2700 km
t(P) = R/12.00 + 91.5	2700 - 3400 km

Other regional phases:

Time equations	Distance
t(Pg) = R/6.21 + 0.8	50 - 1200 km
t(Sn) = R/4.68 + 13.8	200 - 1300 km
t(S) = R/5.58 + 94.7	1200 - 2000 km
t(Lg1) = R/3.57 + 0.5	200 - 1100 km
t(Lg2) = R/3.61 + 4.0	1100 - 2500 km
t(Rg) = R/3.0 + 2.0 (T=6-12 s)	400 - 2000 km

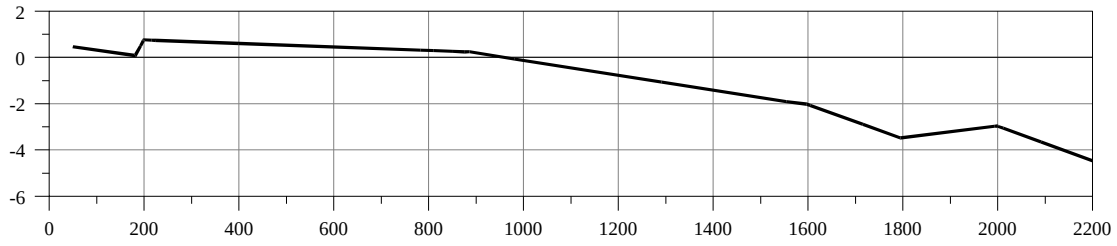

Figure 5. Travel-time residual (Region #5c - IASPEI91) for first arriving P waves out to 2200 km.

2.4.7. Turan Plateau (Region #5d)

The Turan plate is young and is a continuation of the West Siberian Platform. It is an area of Paleozoic age, folded, with a cover of thick sediments. Its tectonic relationship to neighboring regions is similar to that of the Scythian plate on the southern part of East European Platform. Both are intermediate zones between a stable platform and active Cenozoic folding areas. The Turan plate has borders with the Ural Fold Zone, the West Siberian plate, and the Kazakh Massif in the north, and with the Caucasus-Iran folded zone to the south.

The northern part of the Turan Plateau is aseismic. Scattered seismicity increases to the southwest and southeast. Recent examples of earthquakes in this region are the Gazli events, which occurred during an eight year period (1976 - 1984) and which were dominated by three earthquakes with M > 7.0 in the vicinity of (41º N, 63º E). This activity occurred in what previously was believed to be an aseismic zone. Heat flow increases from north to south, with the temperature at the depth 100 km increasing (also north to south) from 900º C to 1300º C. The Moho surface is flat, with average depth around 40 - 44 km in the northern part and 38 - 40 km in the southern part. The average P-wave speed in the crust is 6.55 - 6.45 km/s. The average velocity just below the Moho decreases slightly from 8.0 - 8.1 km/s in the north to 7.8 - 7.9 km/s in the south.

Travel-time data for the region are available from earthquake observations (Yakovleva, 1971; S.A.Fedorov, 1984) and several DSS profiles observations (Zunnunov, 1985; Volvovsky, 1991). Information from Yakovleva (1971) and Fedorov (1984) was also used to derive travel times for this region. The average P-wave velocity in the first several hundred kilometers is nearly the same for both these types of empirical data, namely, about 8.15 km/s. For this regions we propose the following travel-time relations:

Region #5d. TURAN PLATEAU

P waves, first arrivals:

Time equations	Distance
t(Pg) = R/6.25 + 1.0	20 - 190 km
t(Pn1) = R/8.15 + 8.2	190 - 800 km
t(Pn2) = R/8.36 + 10.7	800 - 1600 km

t(Pn3) = R/8.80 + 20.3	1600 - 2000 km
t(P1) = R/9.57 + 38.6	2000 - 2200 km
t(P2) = R/10.10 + 50.8	2200 - 2400 km

Other regional phases:

Time equations	Distance
t(Pg) = R/6.25 + 1.0	50 - 600 km
t(Sn) = R/4.70 + 13.7	190 - 600 km
t(Lg) = R/3.56 + 0.8	100 - 1000 km

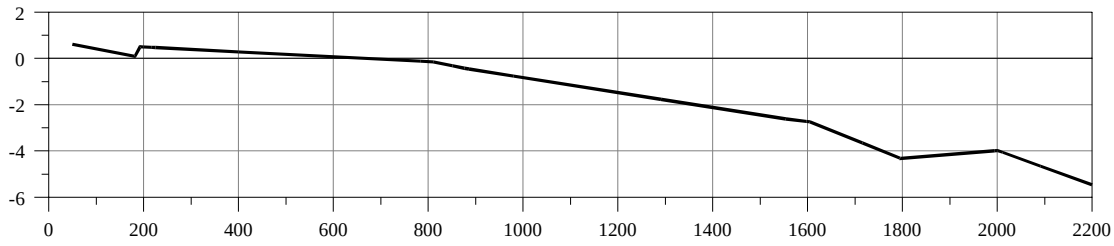

Figure 6. Travel-time residual (Region #5d - IASPEI91) for first arriving P waves out to 2200 km.

2.4.8. Altay-Sayan Folded Region (Region #6)

This is a mountainous area of Caledonian folding that evolved into intensive orogenesis. Seismicity is high in the eastern part (East Sayans) and southern part (Mongol Altay), decreasing to the west and north. Heat flow is average (about 50 mW/m2), and increasing from west to east. It is higher than in West and East Siberian platforms and significantly lower than in the Baykal Rift Zone. The relief of the Moho surface in this region is complicated. Average Moho depth is 45 - 50 km, increasing from 42 km in the northwest to 54 km in the southeast. A detailed study of crustal and upper mantle velocity structure for the region was published by V. Sereznev et al.(2000).

Pg waves have an average velocity of 6.10 km/s, increasing up to values in the range 6.20 - 6.25 km/s towards the northwest (West Siberian Plate) and the southeast (Mongolian fold zone). Lg

waves have an average velocity of 3.55 km/s, decreasing to 3.50 - 3.45 km/s to the west. Pn velocity just beneath the Moho surface is 8.00 km/s on average, decreasing to 7.9 km/s in the west, north, and east directions; and increasing to 8.15 km/s in the south direction. Very careful studies of regional-phases travel times were conducted by Tsibulchik (1967) and later by Seleznev et al. (2000). We propose to use the results summarized below:

Region #6. ALTAY-SAYAN

P waves, first arrivals:

Time equations	Distance
t(Pg) = R/6.13 + 0.3	50 - 200 km
t(Pn1) = R/8.13 + 8.3	200 - 900 km
t(Pn2) = R/8.36 + 11.3	900 - 1600 km
t(Pn3) = R/8.73 + 19.4	1600 - 2000 km
t(P1) = R/9.30 + 33.4	2000 - 2200 km
t(P2) = R/10.1 + 52.2	2200 - 2500 km

Other regional phases:

Time equations	Distance
t(Pg) = R/6.13 + 0.3	50 - 1200 km
t(Sn) = R/4.56 + 12.7	200 - 1200 km
t(Lg) = R/3.57 + 0.5	50 - 2000 km

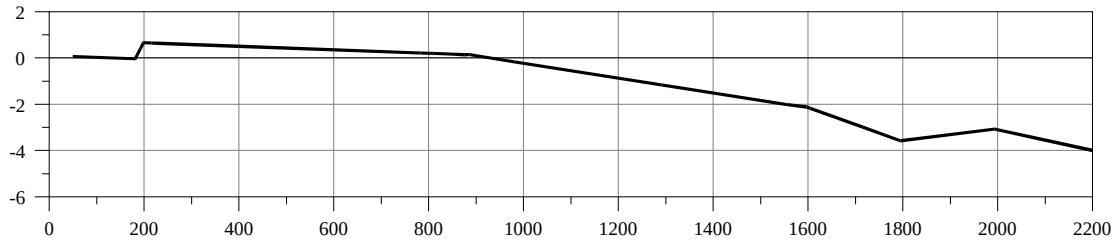

Figure 7. Travel-time residual (Region #6 - IASPEI91) for first arriving P waves out to 2200 km.

2.4.9. Tian Shan Orogenic Zone (Region #7)

The Tian Shan Orogenic Zone is located between the stable Eurasian plate and mobile regions involved in movements due to the collision with the India sub-continent. The Earth's crust in this region has been subjected to lateral compression and it has undergone considerable thickening. It is a region of linear folding with upthrusted and overthrusted sheets. Seismicity is high in this region; many earthquakes with magnitude 7 and few with magnitude 8 have also occurred. The present level of deformation within the Tian Shan is anomalously high for an intracontinental zone. Heat flow is high, reaching about 120 - 150 mW/m2. The average crustal thickness is 48 - 54 km. The Moho depth increases from 42 km at the northern part of the Tian Shan (at the border with the Kazakh Massif) to 60 km in the southern Tian Shan.

Velocity structures of the Tian Shan are described by Molnar and Tapponier (1975, 1979), Roecker et al. (1993), and Hamburger et al. (1998). Evidence of low velocity layers has been found in the crust and upper mantle, but their depth and thickness are different in the eastern and western parts of the Tian Shan. The western part (approximately west of 70º E) is simpler than the eastern part. This is clearly seen from isostatic gravity anomalies (which are high), geothermal observations (heat flow is low), and velocity observations (travel times are about 2 s shorter). The lithosphere in the western part is thick (80 - 160 km), and the asthenosphere is not clearly seen. In the eastern part the asthenosphere is thicker (between 90 - 150 km). Some authors propose that two low velocity layers exist there: one directly under the Moho or at depths of 20 - 35 km beneath it, and another between 100 to 200 km depth. We suppose that regional variability in the depth of the first low velocity zone explains the significant variations in Pn velocity at distances in the range 200 to 400 km - from 7.0 km/s in East Tian Shan (Sabitova, 1989), then 7.35 km/s (Gorbuova, 1990; Shatsilov, 1989), and up to 7.8 - 8.0 km/s in West Tian Shan (Atabaev and Butovskaya, 1986).

Travel-time data have been obtained mostly from seismological observations and less from Deep Seismic Sounding. We summarize the results of seismological observations by local networks. Average travel-time relations for 8 local areas at distances up to 250 km for Pg, Lg and Sn waves:

t(Pg) = R/6.06 + 0.5	50 - 250 km
t(Lg) = R/3.51 + 1.2	50 - 250 km
t(Sn) = R/4.58 + 16.2	50 - 250 km

The average travel-time relations at different distances for Pn waves, taken from 5 publications where data were obtained for distances in the range 600 - 1000 km (V.I. Bune et el., 1955; T.M. Sabitova. 1989; V.I.Ulomov and A.B.Aronov, 1977; I.L. Nersesov, 1960; I.V. Gorbunova, 1990) are the following:

t(Pn1) = R/7.72 + 8.6	200 - 400 km
t(Pn2) = R/8.00 + 10.4	400 - 800 km

Also, from a DSS long profile data (Ryaboy 1985) we find:

t(Pn1) = R/7.87 + 8.6	200 - 400 km
t(Pn2) = R/8.20 + 10.7	400 -1200 km
t(Pn3) = R/8.46 + 16.0	1300 -1700 km

If we average all available data (recognizing that there are differences within the region) the following time relations are the result:

t(Pn1) = R/7.75 + 8.6	225 - 400 km
t(Pn2) = R/8.03 + 10.4	400 - 800 km
t(Pn3) = R/8.13 + 11.1	800 - 1300 km
t(Pn4) = R/8.26 + 14.1	1300 - 1800 km

For travel times for events having one end of the ray path (source or station) in the Tian Shan and the other end more than 200 - 300 km outside it, then the following relations are proposed:

t(Pn1) = R/8.13 + 9.2	300 - 900 km
t(Pn3) = R/8.36 + 12.2	900 - 1600 km
t(Pn4) = R/8.73 + 19.7	1600 - 2000 km

The travel time relations summarizing all these observations for the Tian Shan are as follows:

Region #7. TIAN SHAN OROGENIC ZONE

Case A: epicenter and station located within the zone

P waves, first arrivals:

Time equations	Distance
t(Pg) = R/6.06 + 0.5	0 - 225 km
t(Pn1) = R/7.75 + 8.6	225 - 400 km
t(Pn2) = R/8.03 + 10.4	400 - 800km
t(Pn3) = R/8.13 + 11.6	800 - 1300 km
t(Pn4) = R/8.26 + 14.1	1300 - 1800 km

Other regional phases:

Time equations	Distance
t(Pg) = R/6.06 + 0.5	0 - 600km
t(Lg) = R/3.51 + 1.2	0 - 1500 km
t(Sn) = R/4.58 + 16.2	225 - 1000 km

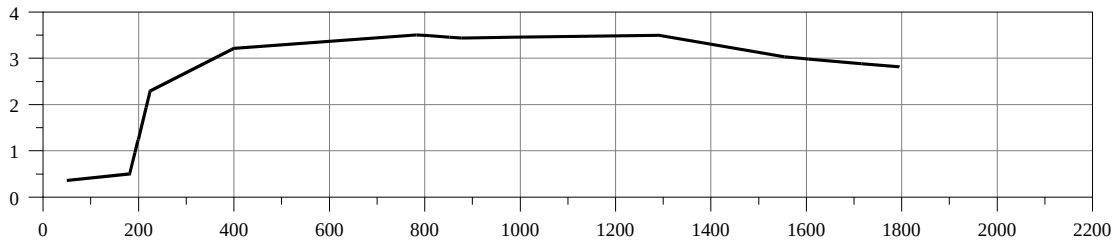

Figure 8. Travel-time residual (Region #7 - IASPEI91) for first arriving P waves out to 2200 km.

Case B. For transit rays, when source or station is located more than 200 - 300 km from the zone, and the other end of the ray is within the zone, then

P waves, first arrivals:

Time equations	Distance
t(Pn1) = R/8.13 + 9.2	300 - 900 km
t(Pn2) = R/8.36 + 12.2	900 - 1600 km
t(Pn3) = R/8.73 + 20.3	1600 - 2000 km

Other regional phases:

Time equations	Distance
t(Pg) = R/6.06 + 0.5	0 - 600 km
t(Lg) = R/3.51 + 1.2	0 - 1500 km

Travel-time data were also extracted from Bune and Butovskaya (1995), Hamburger and Ghose (1998), Khamrabaev (1977), Molnar and Tapponier (1975), Molnar and Tapponier (1979), Roecker et al. (1993), Ryaboy (1985), Sabitova (1989), Shatsilov (1989), Ulomov and Aronov (1977).

2.4.10. Tarim and North Chinese Platforms (Regions #8 and #11)

At the level of regionalization we are currently using, we propose to apply the same travel-time relations for both these cratonic regions of northwest and northeast China. This is a mostly stable region, composed mainly of cratonic terrains, that were accreted to Southern Asia prior to the India-Eurasia collision. Seismic tomography for this region indicates that it typically has higher Pn velocity, than does Southeastern China (region #13) (Hearn and Ni, 2000).

The Chinese test site (Lop Nor) is located in the Tarim basin. Travel-time data of regional phases for events located in this region were obtained by Khalturin et al. (1978). Records were analyzed from many stations of the Complex Seismological Expedition (CSE), located in East and South-east Kazakhstan and South Siberia. Sources of these signals were located in Dzungaria, Xinjiang, Kuen Lun, and other areas of China and Mongolia at epicentral distances from 800 km to 2400 km. All phases in P, Sn and Lg wave groups were measured on these records, with results as follows:

Travel-time table of Pn, Sn, S and Lg waves

P waves, first arrivals:	
Time equations	Distance
t(Pg) = R/6.18 + 0	0 - 220 km
t(Pn1) = R/8.16 + 8.5	200 - 1000 km
t(Pn2) = R/8.47 + 12.9	1000 - 1800 km
t(Pn3) = R/8.85 + 22.0	1800 - 2000 km
t(P1) = R/9.52 + 38.0	2000 - 2100 km
t(P2) = R/10.39 + 56.4	2100 - 2500 km
S waves, first arrivals	
t(Sn) = R/4.74 + 18.7	800 - 1600 km
t(S1) = R/5.68 + 99.1	1300 - 1900 km
t(S2) = R/5.75 + 103.1	1900 - 2400 km
First arrivals of Lg1 and Lg2 waves	
t(Lg1) = R/3.57 + 0.2	800 - 2300 km
t(Lg2) = R/3.36 - 6.0	800 - 2400 km

Comments:

(a) In some cases both waves Sn and S (regional and teleseismic) are observed on the records in the 1400 - 1600 km distance range. Sn wave is shorter period (few hz), S is long period (1 - 3 sec) and propagates beneath the asthenosphere. The time interval between Sn and S can be 20 - 30 sec and its regional variations are large. In general, regional variability of S (or Sn) velocity is several times larger than regional variability of P (or Pn) velocity;

(b) The Lg1 phase becomes weaker at distances greater than 2000 km, and Lg2 dominates;

(c) The Lg2 wave is not stable, but is observed on most records beyond 1000 km. The Lg2 wave has lower frequency spectral content than Lg1.

We propose the following travel time relations:

Regions #8 and #11. TARIM PLATFORM AND NORTH CHINESE PLATFORM

P waves, first arrivals:

Time equations	Distance
t(Pg) = R/6.18 + 0	50 - 215 km
t(Pn1) = R/8.16 + 8.5	215 - 1000 km
t(Pn2) = R/8.47 + 12.9	1000 - 1800 km
t(Pn3) = R/8.85 + 22.0	1800 - 2000 km
t(P1) = R/9.52 + 38.0	2000 - 2100 km
t(P2) = R/10.39 + 56.4	2100 - 2500 km

Sn, S and Lg waves, first arrivals:

Time equations	Distance
t(Sn) = R/4.74 + 18.7	800 - 1600 km
t(S) = R/5.68 + 99.1	1300 - 1900 km
t(S) = R/5.75 + 103.1	1900 - 2400 km
t(Lg) = R/3.57 + 0.2	800 - 2400 km

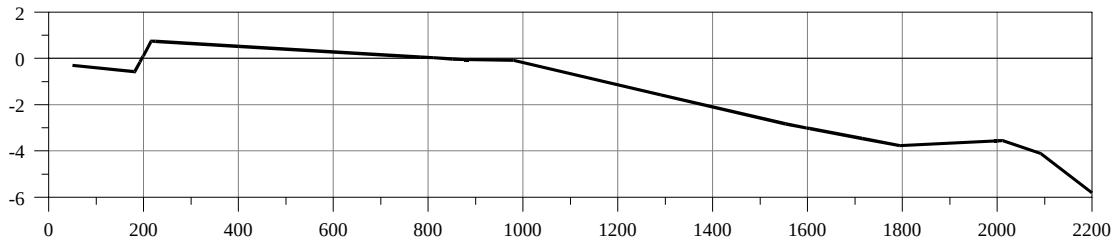

Figure 9. Travel-time residual (Region #8 or 11 - IASPEI91) for first arriving P waves out to 2200 km.

2.4.11. Pamir, Hindu Kush and Himalaya (Region #9)

This is a very complicated high-mountain region, with high levels of seismicity. As a preliminary step we take this region as a southeast continuation of the Tian Shan orogenic zone. The crustal thickness is high and reaches 60 - 65 km. At the moment we adopt, for this region #9, the region #7 travel times, with the following relations:

Region #9. PAMIR, HINDU KUSH AND HIMALAYA

Travel time of first arrivals for paths within the region

P waves, first arrivals:

Time equations	Distance
t(Pg) = R/6.06 + 0.5	0 - 225 km
t(Pn1) = R/7.75 + 8.6	225 - 400 km
t(Pn2) = R/8.03 + 10.4	400 - 800km
t(Pn3) = R/8.13 + 11.1	800 - 1300 km
t(Pn4) = R/8.26 + 14.1	1300 - 1800 km

Other regional phases:

Time equations	Distance
t(Pg) = R/6.06 + 0.5	0- 600km
t(Lg) = R/3.51 + 1.2	0 - 1500 km
t(Sn) = R/4.58 + 16.2	225 - 1000 km

2.4.12. Tibetan Plateau (Region #10)

The Tibetan massif has many geological and geophysical anomalies, associated with the India-Eurasia collision. The Earth’s crustal thickness reaches 70 km. Gravitational anomalies, and shear wave and surface wave attenuation and velocity anomalies there are very significant. The crust and upper mantle beneath Tibet are characterized by low Q as well as low shear wave velocity. P waves are not so anomalous. All these phenomena can be explained by unusually high temperatures in the lower crust and upper mantle, down to about 200 - 250 km depth. The north and south borders of Tibet completely block the propagation of Lg waves. This effect was first described by Khalturin

et al. (1977). Lg and Sn waves have low propagation efficiency within Tibet. The influence of Tibet on Pn propagation is lower, but still significant (Zhao & Xie, 1993).

The travel times of regional phase propagation within Tibet (to a distance of 1100 km) have been described in a publication of the Chinese Seismological Bureau (1989) as follows:

Time equations	Distance
t(Pg1) = R/5.55 + 0.1	Pg1 wave is a first arrival at 0 - 75 km
t(Pg2) = R/6.53 + 2.1	Pg2 wave is a first arrival at 75 - 368 km
t(Pn1) = R/7.99 + 12.3	Pn1 wave is a first arrival at 368 - 640 km
t(Pn2) = R/8.29 + 15.2	Pn2 becomes first arrival after 640 km till observations end at 1100 km
t(Sg1) = R/3.26 + 0.3	Lg1 wave is a first S arrival at 0 - 75 km
t(Sg2) = R/3.76 + 3.2	Lg2 wave is a first S arrival at 75 - 378 km
t(Sn1) = R/4.55 + 20.7	Sn1 wave is a first S arrival at 378 - 650 km
t(Sn2) = R/4.69 + 25.0	Sn2 wave is a first S arrival beyond 650 km till observations end at 1100 km

The main special features of these travel times are:

(a) Pg and Lg waves with standard velocities 6.10 and 3.55 km/s are not observed. Pg and Lg waves at distances of 0 to 75 km propagate with velocity 11% lower than standard values typical for other regions;

(b) Pg and Lg waves are observed as first arrivals out to 370 km! This is almost twice as far as for stable regions. These waves propagate in the distance range 75 - 370 km with a velocity that is 7% higher than standard values typical for other regions;

(c) Pn waves propagate with velocity about 8.0 km/s in the distance range 370 - 650 km. This is close to the Pn velocity observed in other mobile and active regions, such as the Tian Shan;

(d) The Pn velocity 8.3 km/s observed at distances greater than 650 km is similar to that of other tectonically active regions;

(e) The time delay for Pn arrivals in the distance range 800 - 1200 km for Tibet is 5 - 7 s greater than for stable regions!

In summary we propose the following travel-time relations for the Tibetan Plateau:

Region #10. TIBETAN PLATEAU

P waves, first arrivals:

Time equations	Distance
t(Pg1) = R/5.55 + 0.1	0 - 75 km
t(Pg2) = R/6.53 + 2.1	75 - 368 km
t(Pn1) = R/7.99 + 12.3	368 - 640 km
t(Pn2) = R/8.29 + 15.2	640 - 1100 km

Lg or Sn first arrivals:

Time equations	Distance
t(Lg1) = R/3.26 + 0.3	0 - 75 km
t(Lg2) = R/3.76 + 3.2	75 - 378 km
t(Sn1) = R/4.55 + 20.7	378 - 650 km
t(Sn2) = R/4.69 + 25.0	650 - 1100 km

2.4.13. Baykal-Mongolian Fold Zone (Region #12)

This zone combines two subareas with different crustal and upper mantle structures: the Baykal rift zone, and the Mongolian-Okhotsk fold zone. We describe below some of the data pertinent to each subarea, however, in our current regionalization (revision 3), we conclude with a recommendation as a first approximation to use the travel times of Kirichenko and Kraev (2000).

#12a. BAYKAL RIFT ZONE

The Baykal rift zone extends from the south-western shore of Lake Baykal, along the lake axis, to its north-eastern shore, and then for a few hundred additional km gradually changing trend from northeast to east. The rift zone has a total length of about 1400 km, about twice as long as the lake itself. This narrow zone is located between the East Siberian Platform to the northwest and the

Trans-Baykal part of the extended Mongolian-Okhotsk fold zone to the southeast. The rift zone is 200 - 300 km wide and 1400 km long. The area of low velocity in the crust and mantle, and of high heat flow, is even narrower (150 - 200 km). The crustal thickness is mostly within the range 36 - 42 km. This is an area of quite high levels of seismicity. Epicenters are concentrated along the axis of the rift zone (i.e., continuing a few hundred km east of the northeast edge of the lake).

The average velocity just beneath the Moho is anomalously low, that is, about 7.7 - 7.8 km/s. The layer with this low velocity has thickness about 20 - 30 km. The velocity beneath the low velocity layer is standard, that is, 8.0 - 8.1 km/s. Lithosphere thickness with this velocity is only 50 - 70 km. The more deeply located asthenosphere has thickness 100 km or greater.

The heat flow is exceptionally inhomogeneous. On average it is about 75 mW/m2, but reaches 200 - 500 mW/m2 in the central part of Lake Baykal and in some other regions along the axis of the rift zone. The temperature is about 800 - 1200º C at the base of the crust in the central part of the rift, and 500 - 700º C at the base of the crust in surrounding regions.

The results of regional seismological observations are based on seismic traces not only along the rift zone (from southwest to northeast) but also on traces which crossed the Baykal rift zone.

Golenetsky (1974 and 1978) fit data with the following travel-time relations:

t(Pg) = R/6.15 + 0.6	20 - 600 km
t(Pn) = R/8.04 + 7.2	180 - 600 km
t(Lg) = R/3.56 + 1.0	20 - 600 km
t(Sn) = R/4.59 + 12.5	20 - 600 km

Krilov et al. (1974) obtained from Deep Seismic Sounding and from seismological observations the following results for P-wave first arrivals:

t(Pg) = R/6.12 + 0.8	0 - 185 km
t(Pn1) = R/7.75 + 7.1	185 - 370 km
t(Pn2) = R/8.10 + 9.1	370 - 1000 km

These results were obtained only for traces along the rift axis itself, and were supported by later publications. The following travel times, for paths within the Baykal Rift Zone, having epicentral distances less 1000 km, summarize the observations:

Region #12a. BAYKAL RIFT ZONE.

P waves, first arrivals:

Time equations	Distance
t(Pg) = R/6.12 + 0.8	0 - 185 km
t(Pn1) = R/7.75 + 7.1	185 - 370 km
t(Pn2) = R/8.07 + 9.0	370 - 1000 km

Travel time table of Pg, Sn and Lg waves:

Time equations	Distance
t(Pg) = R/6.12 + 0.8	0 - 1000 km
t(Sn) =	km
t(Lg) =	km

#12b. MONGOLIAN-OKHOTSK FOLD SYSTEM

This is a long and mountainous fold system lying between the Altay-Sayan on the west and Okhotsk Sea on the east, and between the Baykal Rift Zone and East Siberian Platform on the north and the North Chinese Platform on the south. It is high land with moderate seismic activity in some areas. Geophysical data for this region are sparse. The crust thickness is about 36 - 44 km.

For the Mongolian part of this zone, regional phase velocity was estimated by Anikonova (1995). In North Mongolia, she obtained the following fit to travel-time data for Pg and Lg waves:

t(Pg) = R/6.25 + 0.2	50 - 200 km
t(Lg) = R/3.63 + 1.2	50 - 200 km

We have no data at greater distances. However, this region is the eastward continuation of the Altay-Sayans region and both regions are similar in tectonic history. So, the travel-time relations for the Altay-Sayan region could be taken to apply also to the #12b region:

Region #12b. MONGOLIAN-OKHOTSK FOLD SYSTEM

P waves, first arrivals:

Time equations	Distance
t(Pg) = R/6.13 + 0.3	50 - 200 km
t(Pn1) = R/8.13 + 8.3	200 - 900 km
t(Pn2) = R/8.36 + 11.3	900 - 1600 km
t(Pn3) = R/8.73 + 19.4	1600 - 2000 km
t(P1) = R/9.30 + 33.4	2000 - 2200 km
t(P2) = R/10.1 + 52.2	2200 - 2500 km

Other regional phases:

Time equations	Distance
t(Pg) = R/6.13 + 0.3	50 - 1200 km
t(Sn) = R/4.56 + 12.7	200 - 1200 km
t(Lg) = R/3.57 + 0.5	50 - 2000 km

We continue to study this region, but conclude that, as a first approximation, it is appropriate for revision #3 or our model to apply the travel-time relations proposed by Kirichenko and Kraev (2000), which are as follows:

Time equations	Distance
t(Pg) = R/6.13 - 0.9	400 - 1200 km
t(Pn) = R/8.21 + 6.8	400 - 2000 km
t(Sn) = R/4.64 + 12.4	400 - 2000 km
t(Lg) = R/3.48 - 6.4	400 - 2500 km

2.4.14. East Siberian Platform (Region #15)

This platform is located between two younger structures, the West Siberian Plate and North-East folding region. The natural borders are the Enisey River to the west and the Lena River to the east. To the south the East Siberian Platform borders on the Altay-Sayans, the Baykal Rift zone, and the eastern continuation of the Mongolian-Okhotsk fold system. This highland region is a stable aseismic craton of Proterozoic age. Continental crust of the region developed in early Precambrian time. There are two old Pre-Riphean age shields in the East Siberian Platform: the Anabar Shield to the north and the Aldan Shield to the south.

Heat flow values are low; about 30 mW/m2 is typical for most areas of the craton, with only 20 mW/m2 in the Anabar shield. Heat flow values increase from north to south, reaching 60 mW/m2 and more, close to the Baykal Rift Zone. These low heat flow values provide evidence for some of the lowest temperatures in Eurasia at the depth of 100 km (600 - 700º C) and 150 km (900 - 1000º C) (Mooney et.al., 2001).

The average lithosphere thickness (200 km) is the greatest in Eurasia. The asthenosphere on average is located at depths between 200 - 280 km. These properties are related to the observation that a high Pn velocity is observed starting at a distance of around 220 km, and continuing out as far as 1100 km. Crustal thickness is 40 - 48 km with average P velocity 6.6 - 6.7 km/s. The average velocity just beneath the Moho is also high: 8.25 - 8.40 km/s. In some areas of Yakutia, anomalous values of Pn velocity as high as 8.8 - 8.9 km/s have been observed.

The lack of seismicity means that only Deep Seismic Sounding data can be used to obtain travel-time relations. Results have been published by many authors, but only a few of them gave the actual travel-time data (Ryaboy, 1985; Barkhin et al., 1987; Egorkin et al., 1987). For most publications typically the Pn velocity is high (8.3 - 8.5 km/s), right from the initial distances (220 - 240 km) at which Pn is observed. The summary of available travel-time relations is given below:

Region #15. EAST SIBERIAN PLATFORM

P waves, first arrivals:

Time equations	Distance
t(Pg) = R/6.24 + 0.5	50 - 220 km
t(Pn1) = R/8.43 + 9.7	220 - 1100 km
t(Pn2) = R/8.61 + 12.4	1100 - 2000 km
t(P1) = R/9.30 + 29.6	2000 - 2200 km
t(P2) = R/10.0 + 46.2	2200 - 2500 km

Other regional phases:

Time equations	Distance
t(Pg) = R/6.24 + 0.5	50 - 1200 km
t(Sn) = R/4.77 + 17.0	600 - 2000 km
t(Lg) = R/3.53 + 0.7	250 - 2500 km

2.4.15. Northeast Territory and Chukot Peninsula (Region #16)

For this region we propose to use the Kirichenko and Kraev (2000) travel-time equations:

Region #16. NORTH-EAST TERRITORY AND CHUKOT PENINSULA

P waves, first arrivals:

Time equations	Distance
t(Pg) = R/6.19 + 1.6	50 - 205 km
t(Pn) = R/8.29 + 10.0	205 - 2000 km

Other regional phases:

Time equations	Distance
t(Pg) = R/6.19 + 1.6	100 - 1000 km
t(Sn) = R/4.51 + 6.6	500 - 2200 km
t(Lg) = R/3.50 + 0	200 - 2500 km

2.4.16. Sikkam, Sichuan-Yunan Region (Region #20a)

This region is a transition zone between the Tibetan plateau to the west and the Yangtze continental platform to the east. The zone is a consequence of the Indian-Eurasian plate collision. The Moho depth increases from southwest to northwest: it is about 38 - 40 km in the south and reaches 56 km in the north (Yunnan). This is an area with a high level of seismicity. Many earthquakes having magnitude greater than 7.0 occurred here during the last thirty years.

According to W. Chan et al. (2001), the average crust velocity is 6.25 km/s. The average velocity just beneath the Moho is only 7.75 km/s. This low value is related to high temperatures, possibly associated with the intrusion of melted materials into the lower crust. Sn waves were not observed. Available travel-time data can be fit by the following travel-time relations for the distance interval 0 - 600 km:

t(Pn) = R/7.9 + 8.5
t(Pg) = R/6.06 + 1.0
t(Lg) = R/3.52 + 1.5

To extend these Pn travel times to greater distances, for example up to 1000 - 1200 km, orogenic areas like the Tian Shan or the Pamirs can be identified as analogs. The average Pn velocity in the range 600 - 1200 km for these regions is 8.13 km/s. So the following travel-time relations are proposed for the Sikkam region for distances 600 - 1200 km:

t(Pn2) = R/8.13 + 10.7

The overall recommendation for this region is as follows:

Region #20a. SIKKAM (Sichuan-Yunan region)

P waves, first arrivals:

Time equations	Distance
t(Pg) = R/6.06 + 1.0	0 - 195 km
t(Pn1) = R/7.9 + 8.5	195 - 600 km
t(Pn2) = R/8.13 +10.7	600 - 1200

Other regional phases:

Time equations	Distance
t(Pg) = R/6.06 + 1.0	0 - 600 km
t(Lg) = R/3.52 + 1.5	0 - 600 km

We have yet to compile travel-time relations for the following regions. This will be the focus of much of our efforts in the near future. Until then, the default IASPEI91 travel-time model may be used for these regions.

#13. SOUTH-EAST CHINA

#14. JAPAN, SAKHALIN, KURILS

#17. KAMCHATKA

#18. ARABIAN PLATE

#19. INDIAN SUBCONTINENT

#20b. INDO-CHINA PENINSULA

3. DATA SETS

In order to validate the Pn SSSCs, well-located (GT) events are needed. Dr. Ivan Kitov and staff of the Institute of Dynamics of the Geosphere (IDG) have made an important contribution to this effort by acquiring and making available phase data from 83 Soviet Peaceful Nuclear Explosions (PNE), 35 underground nuclear weapon tests (UNT) at the Novaya Zemlya Test Site, and 80 underground nuclear explosions (UNE) at Semipalatinsk Test Site recorded at seismographic stations within the Former Soviet Union (FSU) and at other stations throughout Eurasia.

This data set, referred to as Kitov's data set, was obtained from the Harvard web site (http://www.seismology.harvard.edu/~ekstrom/Research/FSU_data/FSU_data.html). A description of the PNE locations and origin times is given by Sultanov et al. (1999). Bocharov et al. (1989) provide a description of the UNE's which are considered of GT0 quality, i.e., events with known locations. After parsing the information, a sustained effort was directed toward a very careful analysis of the information, including examination and exclusion of outliers. This process resulted in a collection of 156 events and 2626 Pn arrival times. Figure 10 shows a map of the event locations (red stars) and the stations that recorded them (triangles), along with great circle paths between events and stations (blue curves). This map illustrates that the source regions, station sites, and paths sample very diverse and extensive geological structures throughout Asia, making this data set extremely valuable for model validation.

Comparison with the Ground Truth Database at CMR revealed that 126 events from our list are in this database. Of these 126 events, 32 events are considered GT0 quality (0 km location accuracy), 66 events are GT1 (1 km accuracy), 13 events are GT5 (5 km accuracy), and 15 events are GT10 (10 km accuracy). The CMR Ground Truth database is described by Yang and Romney (1999).

Since Kitov's data set does not contain Pn arrivals for all of the seismic stations that we wish to calibrate (Table 1), we augmented our data set with 18 additional GT events, also shown in Figure 10. This data set includes seven underground chemical explosions (UCE) conducted at the Semipalatinsk test site, all in the CMR GT database with GT0 quality. We also added eleven underground nuclear explosions (UNE's) conducted at the Lop Nor test site in western China, eight of which have associated Pn arrivals at regional stations. Fisk (2001) describes these nuclear explosions and how IKONOS satellite imagery and seismic data were used to obtain GT1 locations

for these events. The data set is completed with two more UNE's conducted in India and Pakistan and described by Barker et al. (1999). The green curves in Figure 10 indicate the great circle paths for these 18 explosions, along with paths for PNE's recorded by BRVK for which we have made our own phase picks from waveforms.

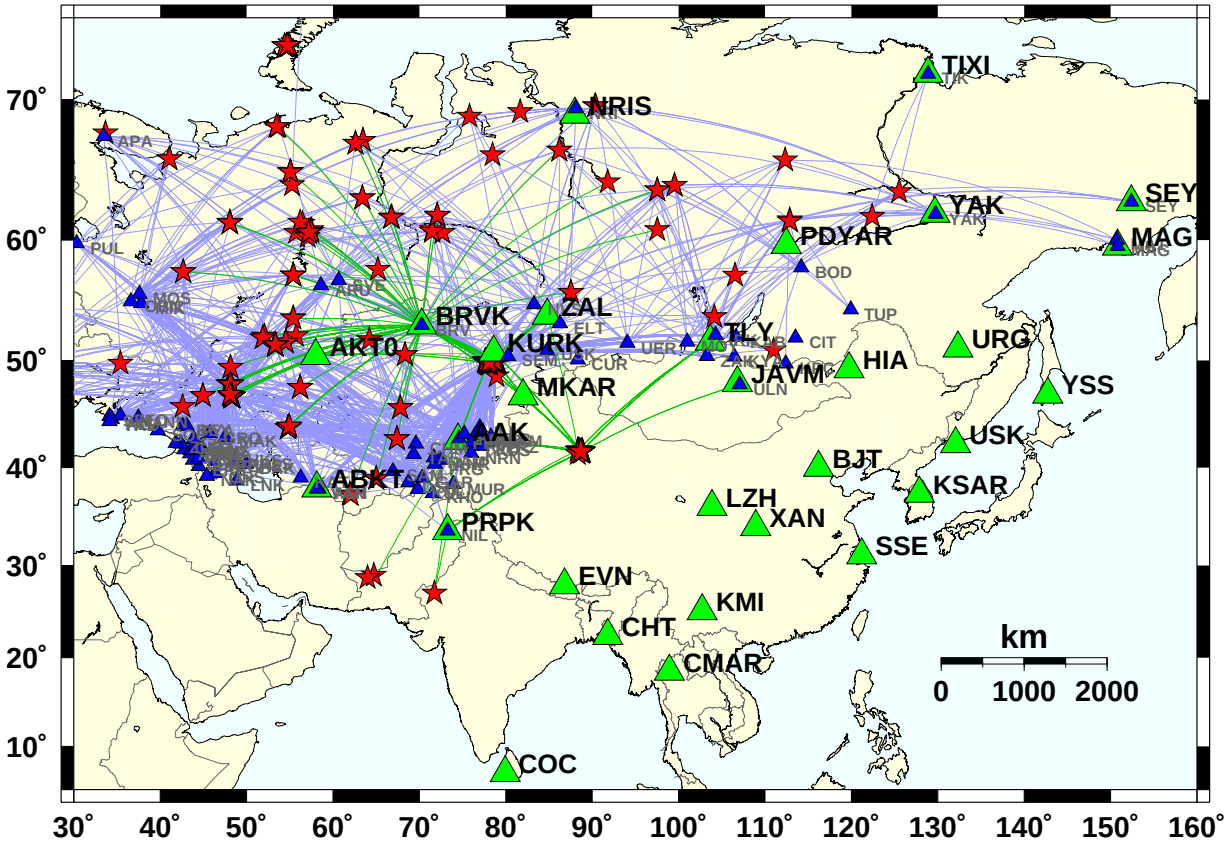

Figure 10. Map showing locations of GT explosions (red stars) and recording seismographic stations (green triangles) used for validation tests. Also shown are great circle paths between events and stations.

Figure 10 also illustrates that many of the IMS stations that we wish to calibrate are represented by existing stations or suitable surrogate stations in these data sets, including stations AAK, AKT0, BRVK, KURK, MAKZ, NIL, ZAL, MAG, NRI (NRIS), SEY, TIK (TIXI), TLY, YAK, ULN (JAVM). Although the other stations are not part of the IMS network, they are useful for validating our regionalized model and the computational methods for generating SSSCs, as demonstrated below, because nearly 3000 Pn paths are sampled in our general region of study.

4. SSSC COMPUTATIONAL APPROACH

SSSCs represent corrections relative to a reference model (e.g., IASPEI91) for a particular station and a given seismic phase. The SSSC calculation adopted here is a two-fold approach, using the method of Bondár (1999) to first compute model-based corrections, and then using phase arrival data from GT events in a kriging algorithm to refine the SSSCs empirically. The model-based approach of Bondár (1999) relies on regionalization and corresponding one-dimensional (1-D) regional travel times curves versus distance within each region. It has been applied successfully to regional phases at stations in Fennoscandia (Yang et al., 2001) and at stations in North America (Bondár et al., 1998; Yang et al., 2001). The SSSCs and the corresponding modeling errors are defined at points of a user-defined rectangular grid.

The SSSCs computed by Bondár's method can be improved using kriging if phase timing observations are available for well-located events. At each grid point, the SSSCs are updated by an optimal linear combination of travel-time residuals, weighted by a distance-dependent correlation function. In addition to the updated correction grid, the kriging algorithm estimates a corresponding uncertainty grid. The spatial distribution of the calibration points determines how much weight each calibration datum contributes to the correction surface and the relative magnitude of the uncertainty surface. For well-calibrated locations, that is, locations near many calibration points, the correction surface converges to the mean of the data close to that location and the uncertainty (variance) surface converges to the variance of nearby data, which we call the residual variance. For locations far from calibration points, the correction surface converges to the model-based SSSC value, with larger uncertainty equal to the sum of the residual variance and the calibration variance, which is the variance of the travel-time means averaged over all well-separated locations.

4.1. Bondár's Method of SSSC Computation

In the approach of Bondár (1999), SSSCs are computed over a user-defined grid for each station and for various regional phases (i.e., they are station and phase specific). The SSSCs are travel-time corrections with respect to an underlying 1-D model. The rectangular grid covers the region of interest (generally out to 20 degrees from a given station), which contains some subset of the tectonic subregions of the regionalization presented in Section 2. Each subregion is characterized

by the regional travel times and associated modeling errors. Bondár's method requires that each subregion is defined by a convex, spherical polygon, with sides given by great circles. Each subregion determined by the regionalization was therefore approximated by such a polygon. Some of these subregions could not be approximated with one convex polygon, so it was necessary to break up such subregions into the union of two, or more, convex polygons, each having the same travel-time parameters. The result is a set of convex polygons which completely cover Asia.

Since the travel-time curves for each subregion are established, it is possible to compute the total travel time for a path from each point of the grid to each of the seven IMS stations. The proper way to obtain such a travel time, for a path that crosses one or more subregion boundaries, is to integrate along the actual ray path, which in general will be laterally refracted at boundaries, so it does not stay in the same vertical plane.

A simplified approach, presented by Bondár (1999), approximates the travel time across subregion boundaries by

$$T(X) = \sum_i (x_i / X) \times T_i(X),$$

where the index i ranges over all subregions traversed by the ray path, and x_i and T_i (X) are the path length and travel time (for the full distance X) in the i-th subregion. The travel time is thus a weighted average of the travel time in each subregion, the weights being (x_i / X), which for each i is just the fraction of the total path traveling in subregion i. Once $T(X)$ is obtained, the SSSC is given by

$$T_{\mathrm{SSSC}} = T(X) - T_{\mathrm{IASP91}}.$$

The corresponding estimated modeling error is given by:

$$\sigma^2(X) = \sum_i (x_i / X) \times \sigma_i^2(X),$$

where $\sigma_i^2(X)$ is the modeling error for subregion i with path length X. Currently, the same modeling error function for Pn travel times is used for all subregions. It is an upper bound of the modeling errors that have been estimated for the various subregions in our regionalization.

Figure 11 shows Pn modeling errors as functions of epicentral distance for IASPEI91, our regionalized model (green curve), and three types of regions of Northern Eurasia (platform areas, paleozoic massifs and young platform, and tectonically active regions) defined by Kirichenko and Kraev (2001). Modeling errors were calculated as standard deviations of empirical data from the estimated travel-time curves in a 2-degree moving window with a 50% overlap (Kirichenko and Kraev, 2001). As an initial hypothesis, we defined our Pn modeling error as an upper bound of the modeling errors estimated by Kirichenko and Kraev (2001) for the various geotectonic provinces. To test the validity of our Pn model error, we computed average absolute travel-time misfits to the model-based SSSCs, binned by distance, for Pn phase arrivals in Kitov's data set (blue circles in Figure 11). While there are slight differences between the average misfit values and our modeling error curve, they are not significant with respect to the uncertainties. Furthermore, the validity of the error model was ultimately demonstrated by achieving appropriate coverage statistics.

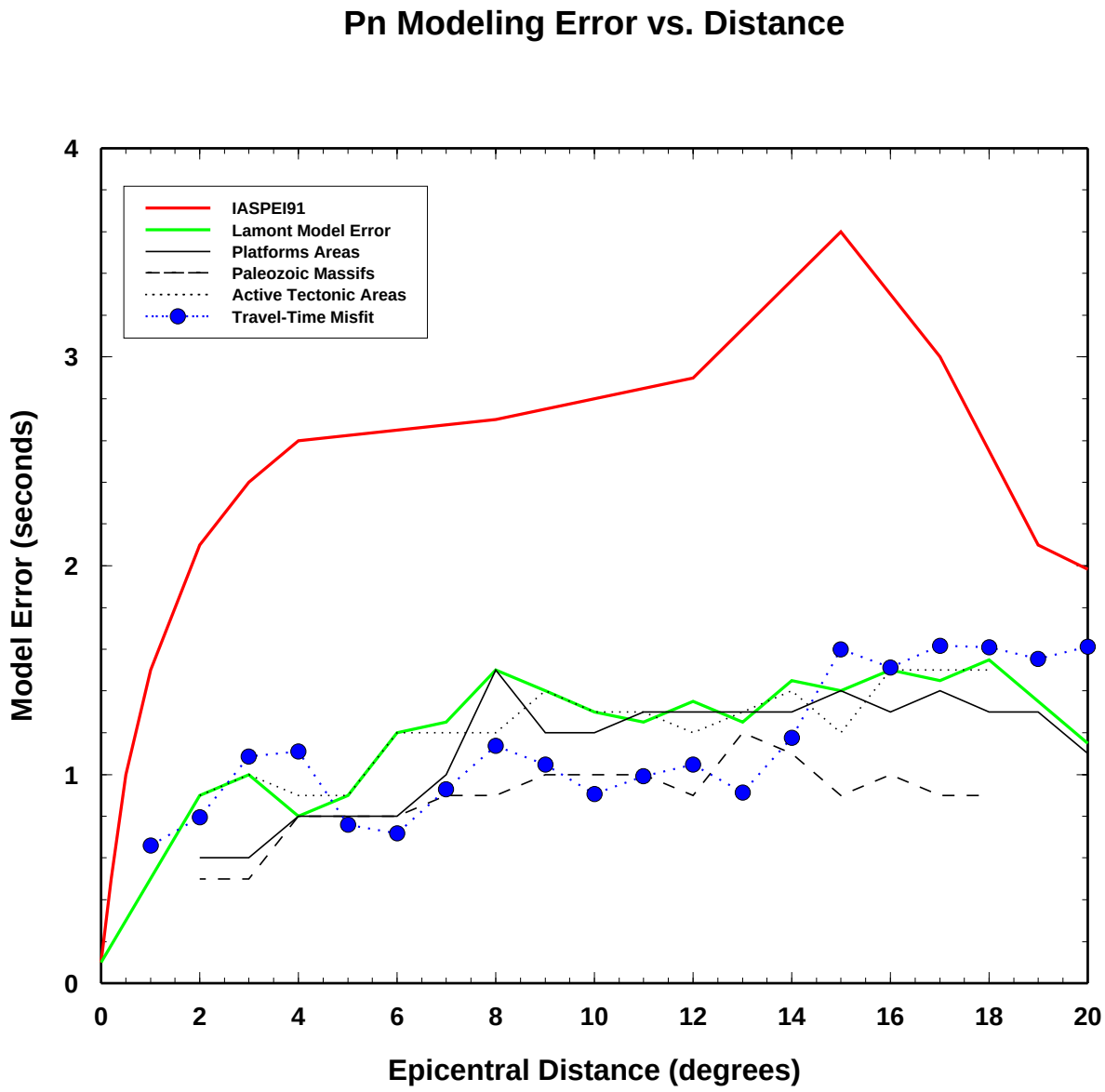

Figure 11. Pn modeling errors as functions of epicentral distance (total path length from event to station) for IASPEI91 (red curve), our regionalized model (green curve), and three types of regions of Northern Eurasia (black curves), defined by Kirichenko and Kraev (2001). Also shown are travel-time misfits to the model-based SSSCs, binned by distance, for Pn phase arrivals in Kitov's data set (blue markers).

At each grid point, the SSSC and the corresponding modeling error are estimated based on the formulae presented above. As an example, Figure 12 shows the reduced travel-time curves versus distance for the IASPEI91 model (thick black curve) and for the subregions surrounding station

BRVK, as described in Section 2. The regional travel-time curves are used in the calculation of the Pn SSSC for BRVK. Also shown in Figure 12 are the reduced travel times to BRVK for underground nuclear and chemical explosions (UNE's and UCE's, respectively) at the Semipalatinsk test site (STS), peaceful nuclear explosions (PNE's) in the Former Soviet Union, and UNE's at the Lop Nor test site in China.

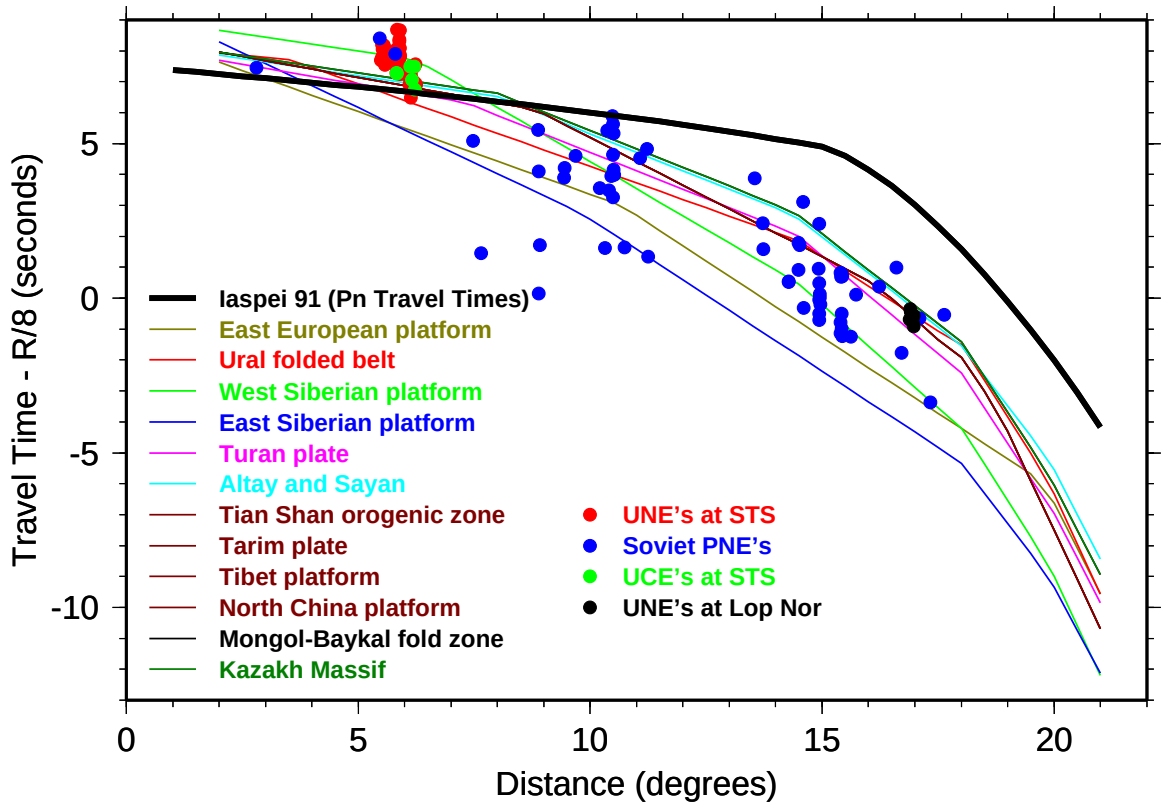

Figure 12. Reduced travel-time curves of Pn versus distance for IASPEI91 and for the subregions surrounding station BRVK. Also shown are the reduced travel times to BRVK for underground nuclear and chemical explosions (UNE's and UCE's, respectively) at the Semipalatinsk test site (STS), peaceful nuclear explosions (PNE's) in the Former Soviet Union, and underground nuclear explosions at the Lop Nor test site in China.

Using this regionalized travel-time curves, the resulting Pn SSSC grid for BRVK that is computed by Bondár's method is shown in Figure 13. The associated modeling-error grid is shown in Figure 14. These figures also show the Pn travel-time residuals, after applying the SSSCs, for the same set of explosions in Figure 12. These residuals are quantified below, after describing the kriging algorithm. It can be seen from Figure 13 that the Pn SSSC for BRVK consists mostly of

negative travel-time corrections, by as much as 7 to 8 seconds in some areas. The estimated modeling errors, depicted in Figure 14, are typically about one to two seconds. No corrections or modeling errors are obtained for distances beyond 20 degrees from the station.

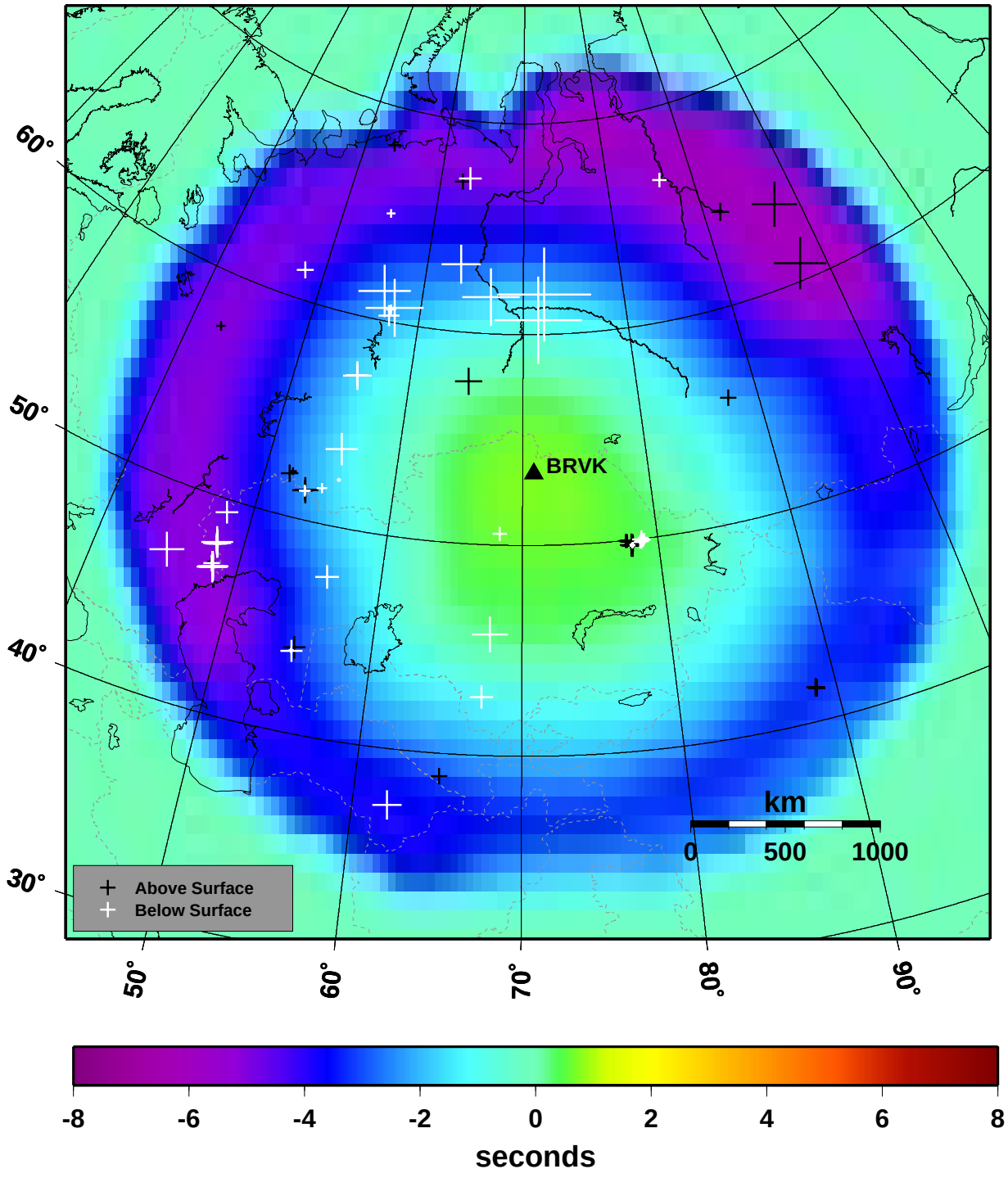

Figure 13. Model-based Pn SSSC for station BRVK. The markers (plus signs) indicate the locations of the calibration events. Black and white markers represent positive and negative residuals, respectively, with marker size proportional to the travel-time residual relative to the predicted travel times by Bondár's method.

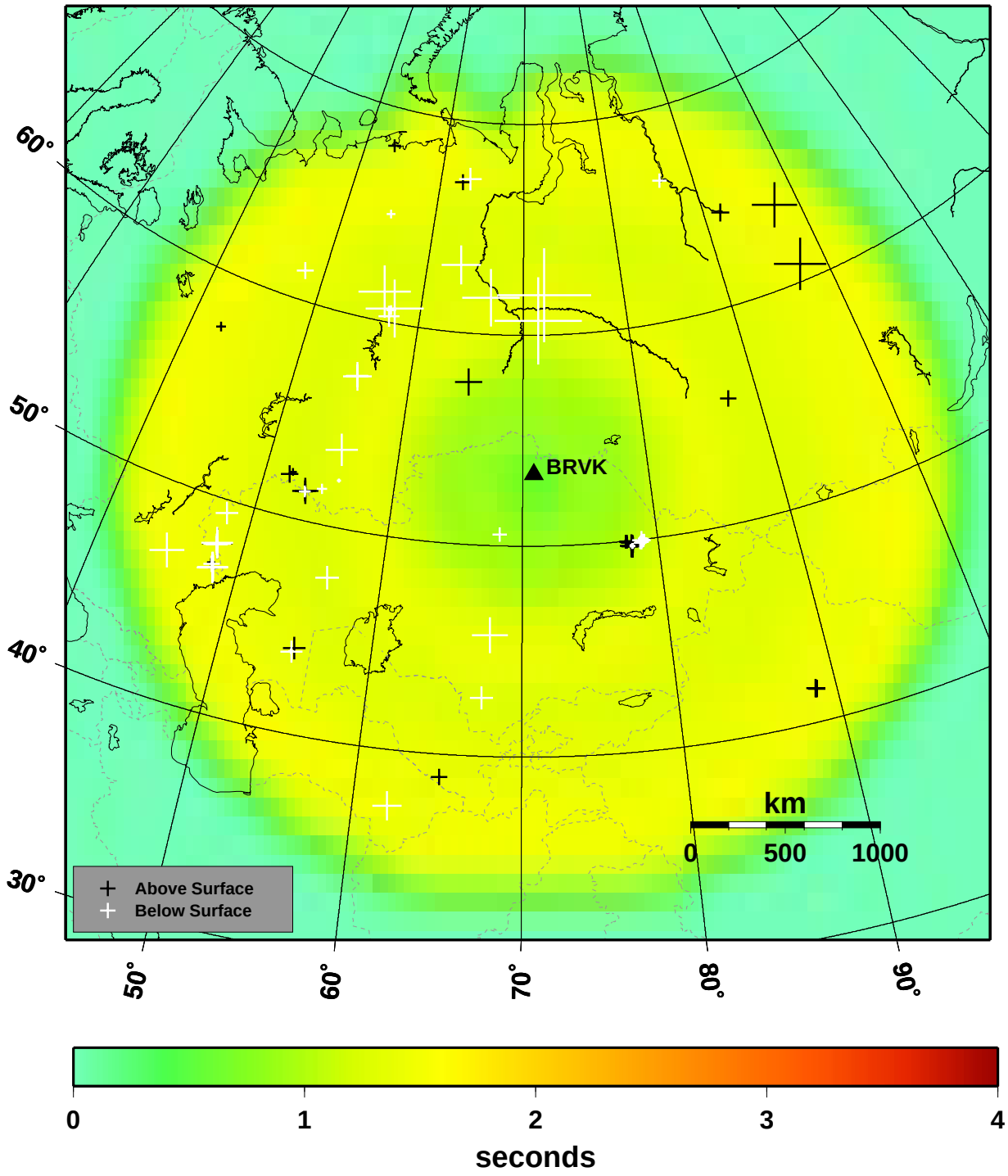

Figure 14. Modeling errors associated with the SSSC computed using Bondár's method for station BRVK. Markers are defined as in Figure 13.

4.2. Kriging

Kriging is a method of optimal spatial prediction, which generally refers to making inferences at a new location, given previously measured data at *N* separate locations, in a way that minimizes the uncertainty of that prediction under given statistical assumptions. It is a minimum variance, linear estimation technique that models nonuniformly distributed data as a continuous surface with uncertainty estimates that depend on second-order (covariance) properties (Rogers et al., 1999). It assumes that the spatial data result from a random process, meaning that samples are considered as outcomes of a random variable that is a function of spatial coordinates. Given reference data, kriging provides optimal prediction at a new location expressed as a weighted linear combination of data, with greater weight conferred to data that are spatially closer to the prediction location. The predictions at a set of spatial points may be used as a prediction (or correction) surface.

Given *N* data values, $x(\mathbf{s}_1), \ldots, x(\mathbf{s}_N)$, at locations $\mathbf{s}_1, \ldots, \mathbf{s}_N$, (in our case $x(\mathbf{s}_i)$ is the measured travel-time residual at position $\mathbf{s}_i$), the kriging optimal predictor for the mean at a location $\mathbf{s}_0$ is given by the weighted linear combination of data:

$$\hat{\mu}(\mathbf{s}_0) = \sum_{i=1}^{N} w_i x(\mathbf{s}_i).$$

The set of all predictions, $\hat{\mu}(\mathbf{s}_0)$, over all $\mathbf{s}_0$, provides a prediction, or correction, surface. A corresponding uncertainty surface, $\sigma^2(\mathbf{s}_0)$, also results from the calculation.

The weights w_i and the kriged variance, $\sigma^2(\mathbf{s}_0)$, depend on the correlations, ρ_{ij}, between the means of data located at $\mathbf{s}_i$ and $\mathbf{s}_j$, the calibration variance, σ_c^2, and residual variance, σ_r^2:

$$w_i = F(\sigma_c^2, \sigma_r^2, \rho_{ij}); \; \sigma^2(s_0) = G(\sigma_c^2, \sigma_r^2, \rho_{ij}).$$

The correlations, ρ_{ij}, between the means located at $\mathbf{s}_i$ and $\mathbf{s}_j$, are assumed to depend only on the distance $\Delta(\mathbf{s}_i,\mathbf{s}_j)$ between $\mathbf{s}_i$ and $\mathbf{s}_j$, and are taken to be given by the exponential function

$$\rho_{ij} = \exp(-\Delta(\mathbf{s}_i, \mathbf{s}_j) / \alpha),$$

where α is the correlation length.

Required input parameters for the kriging algorithm are σ_c^2, σ_r^2, and α. In practice these parameters are estimated from data using the variogram, which is defined by

$$2\gamma(h) = \mathrm{var}(x_i - x_j),$$

and is assumed to depend only on the distance h separating the locations of x_i and x_j. If we model data x_i at location $\mathbf{s}_i$ as

$$x_i = x(\mathbf{s}_i) = \mu_i + e_i,$$

where μ_i is the mean of the data at $\mathbf{s}_i$ with covariance $\rho_{ij}\sigma_c^2$ and e_i has mean zero and variance σ_r^2 and is uncorrelated with μ_i, it can be shown that the semivariogram, $\gamma(h)$, is given by

$$\gamma(h) = \sigma_r^2 + \sigma_c^2[1 - \exp(-h/\alpha)],\ h > 0.$$

The parameters, σ_c^2, σ_r^2, and α, can be estimated by computing the covariance of all data pairs with separations approximately equal to h, for various values of h. The resulting set of values as a function of h can then be fit with the semivariogram equation to estimate σ_c^2, σ_r^2, and α.

In our application of kriging, the spatial reference data are travel-time residuals for GT events at a given station, relative to the model-based SSSC value for that station and event location. The kriged correction surface, when added to the model-based SSSC, corresponds to an updated travel-time correction grid in the same form as the model-based SSSCs. The resulting kriged correction surface approaches the local mean of data with small uncertainty, equal to the residual variance, for well calibrated areas, and approaches the SSSC background model with large uncertainty, equal to the sum of the residual and calibration variances, for areas far from any calibration data.

An example of a kriged grid of Pn SSSCs for BRVK is shown in Figure 15. The superimposed plus signs indicate the Pn travel-time residuals of the calibration events relative to the predicted travel-times. Marker size is proportional to the size of the residuals, black for negative values and white for positive values. The corresponding modeling errors obtained by kriging are shown in Figure 16, which indicates that they are comparable to those in Figure 14, except near calibration data, where the estimated modeling errors are generally lower.

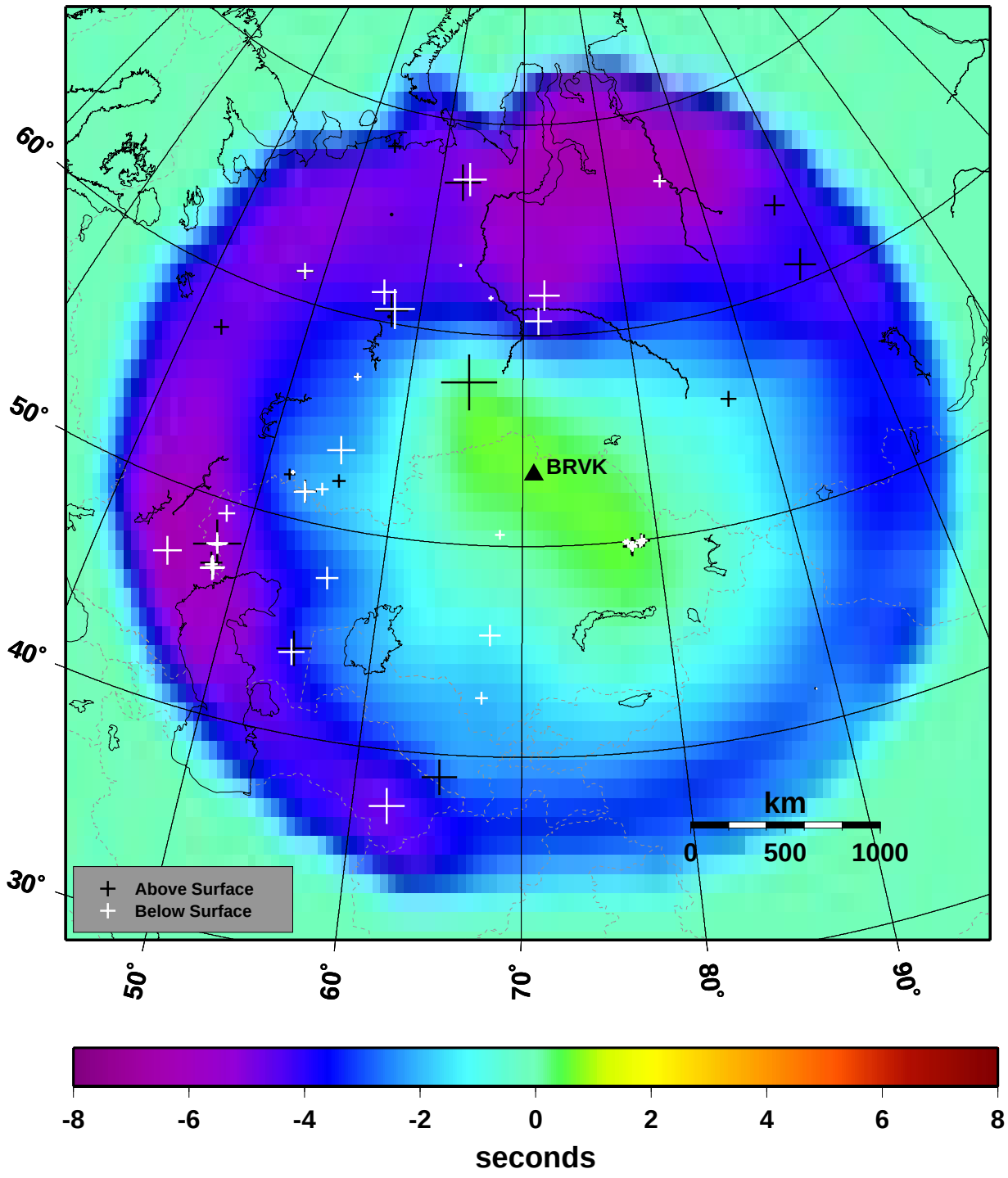

Figure 15. Model-based and kriged Pn SSSC for station BRVK. Markers are defined as in Figure 13.

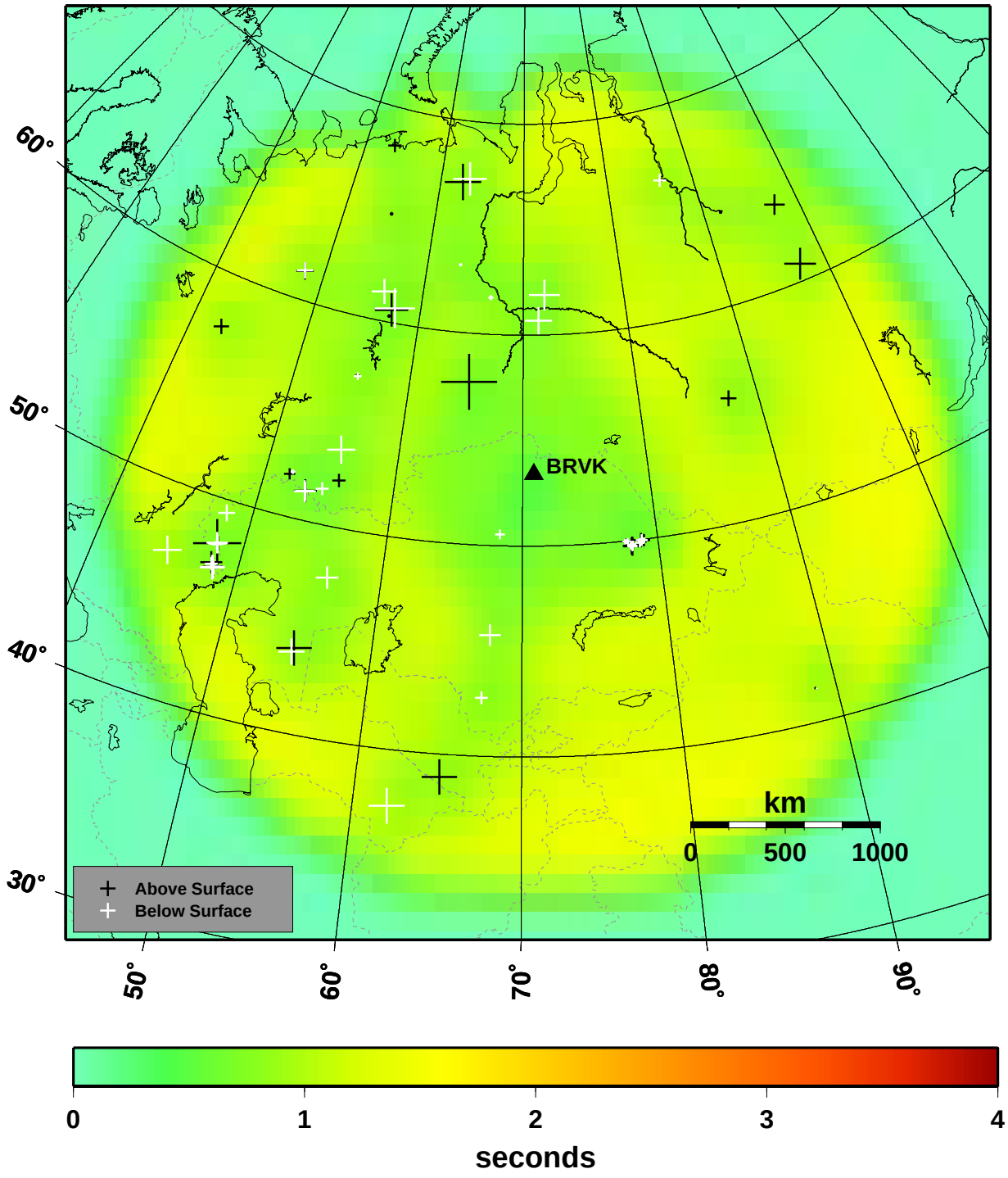

Figure 16. Grid of kriged modeling errors associated with the SSSC computed for station BRVK. Markers are defined as in Figure 13.

It is interesting to compare the travel-time residuals before and after applying either the model-based or kriged SSSCs. Figure 17 shows travel-time residuals versus epicentral distance for 145 Pn arrivals at station BRVK, corresponding to historical Soviet-era PNE's and UNE's at the former Soviet Semipalatinsk test site and the Chinese Lop Nor test site. The residuals are relative to IASPEI91 without corrections (red squares) and after applying the model-based SSSCs computed by Bondár's method (green circles). It is clear the model-based SSSCs generally reduce the travel-time residuals. Figure 18 shows a similar plot using the SSSCs computed by Bondár's method and kriging, which shows that application of kriging provides further reduction of the Pn travel-time residuals at BRVK.

These results are quantified in Table 5 in terms of the mean and standard deviation of the Pn travel-time residuals for the various sets of explosions and the overall results. In all cases, both the mean travel-time bias and the standard deviation of the travel-time residuals are progressively reduced by applying the model-based SSSCs and the model-based plus kriged SSSCs. Although these results for BRVK were shown because of the geographical distribution of GT events and the quantity and quality of the Pn phase picks, which we carefully reviewed by inspection of the waveforms, they are qualitatively representative of the reductions in mean travel-time bias and residual variance that we obtain at other stations in Asia.

Table 5. Comparison of Pn travel-time residuals for station BRVK.

Case	IASPEI91		Model-Based SSSCs		Model + Kriged SSSCs	
	$\mu_{\Delta T}$	$\sigma_{\Delta T}$	$\mu_{\Delta T}$	$\sigma_{\Delta T}$	$\mu_{\Delta T}$	$\sigma_{\Delta T}$
Semipalatinsk UNE's	0.51	0.45	0.11	0.44	-0.02	0.30
Soviet PNE's	-3.91	1.96	-0.51	1.35	-0.05	1.09
Lop Nor UNE's	-2.52	0.04	0.85	0.04	0.02	0.04
Overall	-1.56	2.56	-0.15	1.01	-0.02	0.76

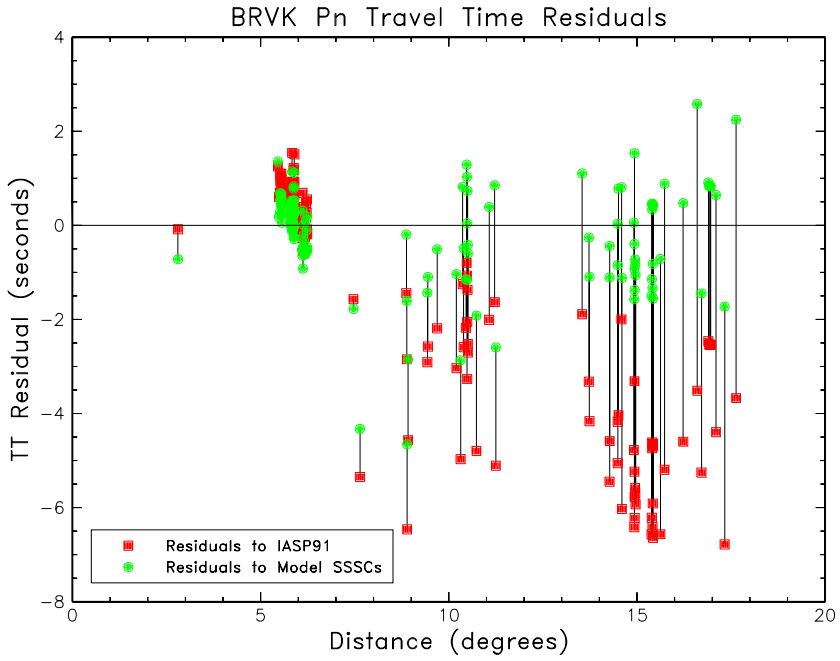

Figure 17. Pn travel-time residuals versus epicentral distance for station BRVK, before (red squares) and after (green circles) applying model-based Pn SSSCs computed by Bondár's method.

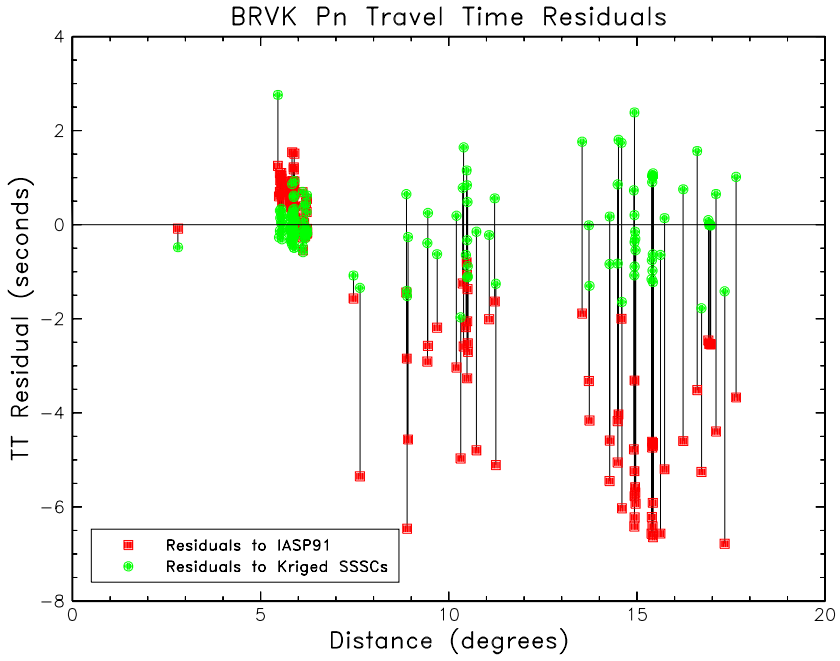

Figure 18. Pn travel-time residuals versus epicentral distance for station BRVK, before (red squares) and after (green circles) applying model-based plus kriged Pn SSSCs.

5. VALIDATION TESTING AND PERFORMANCE METRICS

5.1. Introduction

Validation testing of Pn SSSCs for Asia consists mainly of relocating events to demonstrate improvements in location performance relative to using IASPEI91 travel times. Using the CMR location software *EvLoc*, relocations are computed with and without the SSSCs to assess the impact of these corrections on location and error ellipse estimation. Improvements are quantified using standard evaluation metrics of mislocation errors, error ellipse area, 90% error ellipse coverage, and standard deviations of the phase arrival-time observations.

There are two main objectives of the validation tests: (1) model validation and (2) evaluation of the kriged SSSCs. The first is to validate the regionalized travel-time model and model-based SSSCs computed by Bondár's method. The model-based SSSCs rely solely on the regionalization (boundaries of subregions within which travel times show little evidence of lateral variability) and the 1-D travel time curves for each subregion. By relocating events with the model-based SSSCs, we attempt to show reductions in mislocations and error ellipse size, while maintaining adequate coverage of the error ellipses with the GT locations. The goal is to demonstrate that this model provides an effective representation of travel times in Central Asia. This is a critical step in the validation process because events may occur at locations far from calibration points used by the kriging algorithm, where the grids are asymptotically equivalent to the model-based SSSCs.

The second main objective is to assess the location performance using the kriged SSSCs. To do this, we relocate the events using the kriged SSSCs with a leave-one-out procedure (to avoid using the same events to both compute and test the grids) and quantify the results in terms of the same performance metrics used in the model validation. The results are compared to those in which the relocations were performed without SSSCs and with the SSSCs computed by Bondár's method.

To perform these tests we use the data sets described in Section 3, including 156 GT explosions in Kitov's data set and 18 additional GT explosions in Kazakhstan, China, India, and Pakistan. Although most of the stations associated with Kitov's data set are not in the IMS, they are especially useful for validating our regionalized model over a very broad and diverse range of geological conditions. To assess the impact of the SSSCs for the IMS stations under study (Table 1), we conducted a second test using the 18 GT explosions.

5.2. Model Validation

For model validation we use 156 events recorded at 93 stations (Kitov's data set). The test consists of relocating these events using Pn arrivals (2626 picks). All the relocations are performed with depth fixed at the surface. Figure 19 shows the distributions of events and seismographic stations used in this analysis. The relocation procedure is first applied using the IASPEI91 travel-time tables, without any SSSCs. This is followed by relocating the same events using the SSSCs. Both sets of relocation results are saved in a database at the CMR. Executing *EvLoc* with and without SSSCs resulted in 156 events with location estimates that converged.

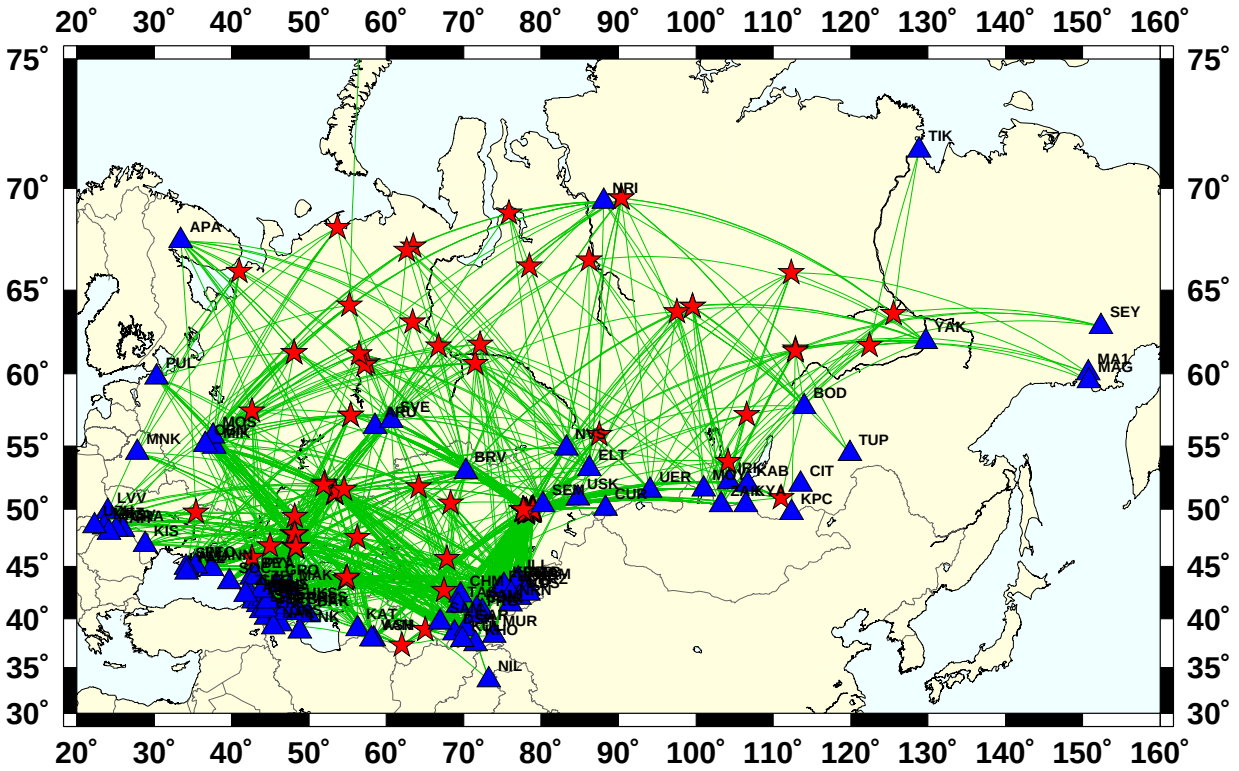

Figure 19. Map of events (red stars) and recording seismic stations (green triangles) of Kitov's data set used for model validation. Also shown are great circle paths between events and stations.

Relocation performance is quantified using evaluation metrics that conform with the guidelines from the 1999 Location Workshop (CTBT/WGB/TL-2/18) held in Oslo, Norway, which include the following:

- the median mislocation of GT events should be significantly reduced;
- mislocation should be reduced by 20% or more for the majority of events;
- median confidence ellipses should be reduced in area, and the coverage should be the same or better;

- confidence ellipses should be reduced by 20% or more for the majority of events;
- variance of travel-time residuals should be similar or smaller.

5.2.1. Mislocation

Mislocation is expressed as the difference in distance between the GT location and the location obtained by *EvLoc*. Of the 156 events, the locations using SSSCs improved for 99 events (63%) and deteriorated for 57 events (37%). The median mislocation was reduced from 12.2 km to 9.5 km. For 82 events (53%) the solutions improved by more than 20%, while for 37 events (24%) the deterioration is more than 20%. Figure 20 shows the mislocation results. The green symbols represent the events for which the relocation with SSSCs is closer to the GT location than without SSSCs. The red symbols show the events for which the mislocation without SSSCs is smaller than with SSSCs.

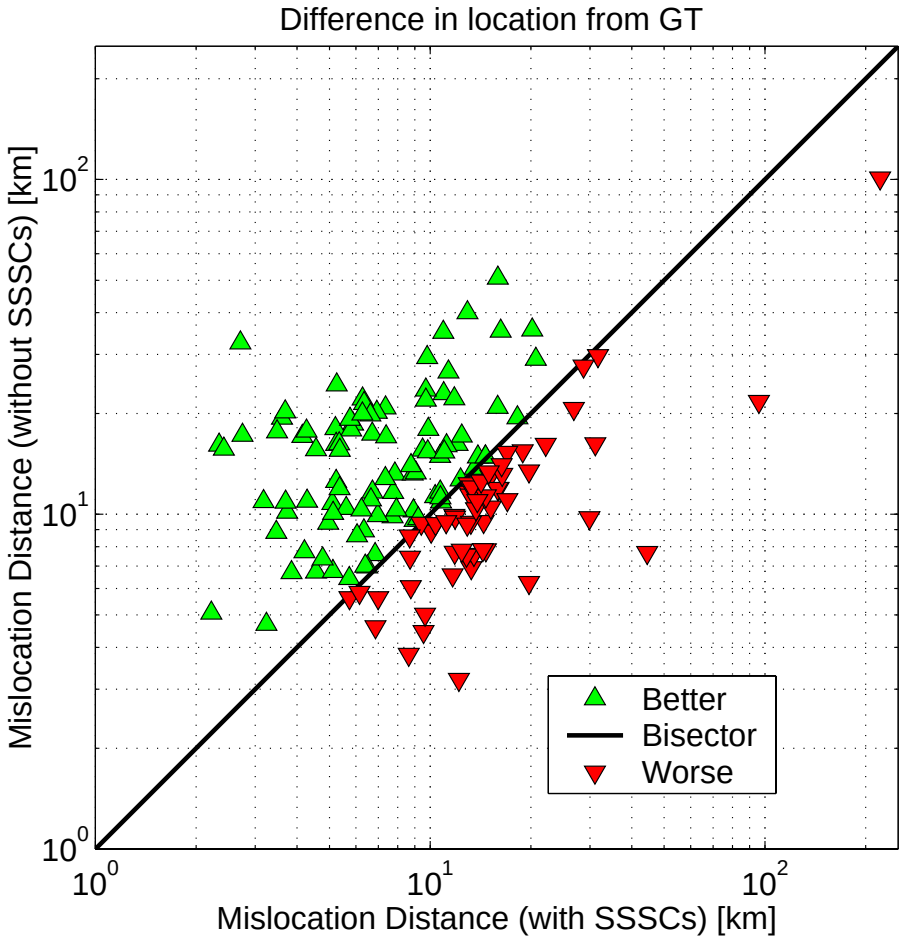

Figure 20. Mislocation distances with and without using model-based SSSCs with respect to corresponding GT locations. The green symbols show the events for which the mislocation error is smaller using SSSCs than

without. Red symbols show the events for which the mislocation errors are smaller without using SSSCs. The bisecting line corresponds to equivalent mislocation errors for the two solutions (with and without SSSCs).

Figure 21 shows the differences of mislocations, without and with the model-based SSSCs, versus number of defining phases [*ndef*] (upper plot) and azimuthal gap (lower plot). Green (red) markers indicate solutions with smaller (larger) mislocations when SSSCs are used. Large mislocation errors when using the SSSCs generally occur when *ndef* is less than 6 and the gap is greater than 200 degrees. In such cases the locations are poorly constrained with or without use of SSSCs.

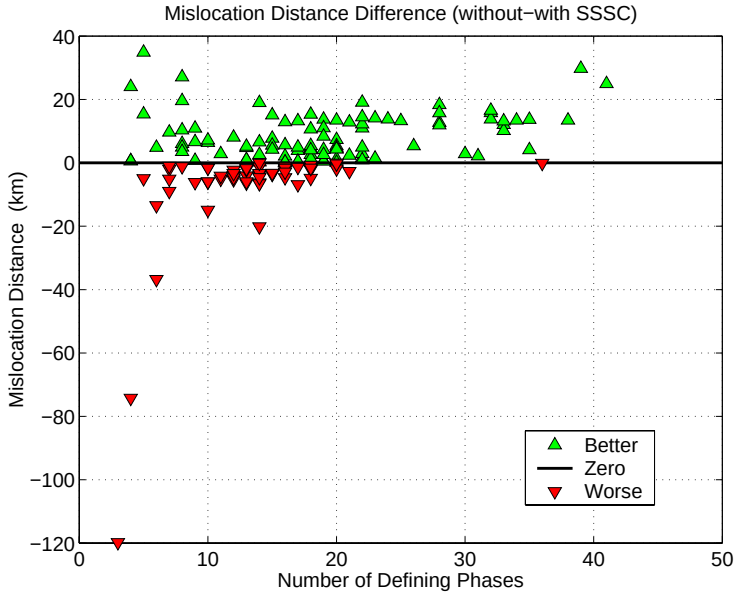

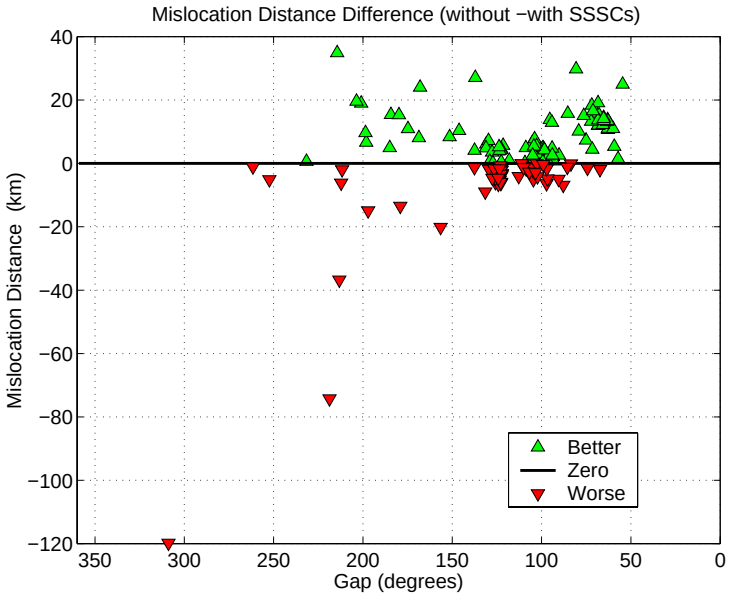

Figure 21. Differences of mislocation distances, without and with model-based SSSCs, versus the number of defining phases (upper plot) and azimuthal gap (lower plot). Green markers indicate solutions with smaller mislocation distances when SSSCs are used, while red markers indicate solutions with larger mislocation distances when SSSCs are used.

5.2.2. Error Ellipse Area and Coverage

The error ellipses have systematic reduction in area by using the SSSCs than not. The difference in the error ellipse calculations for the two cases is due to a difference in the modeling errors. Since the modeling error for the SSSCs is always less than for IASPEI91 (see Figure 11), we expect the error ellipses for the SSSC case to always be smaller than for the IASPEI91 case. In fact, all 156 solutions (100%) are improved by more than 20% (Figure 22). The decrease in the median error ellipse area is 1,146 km^2 (from 1,596 km^2 to 450 km^2).

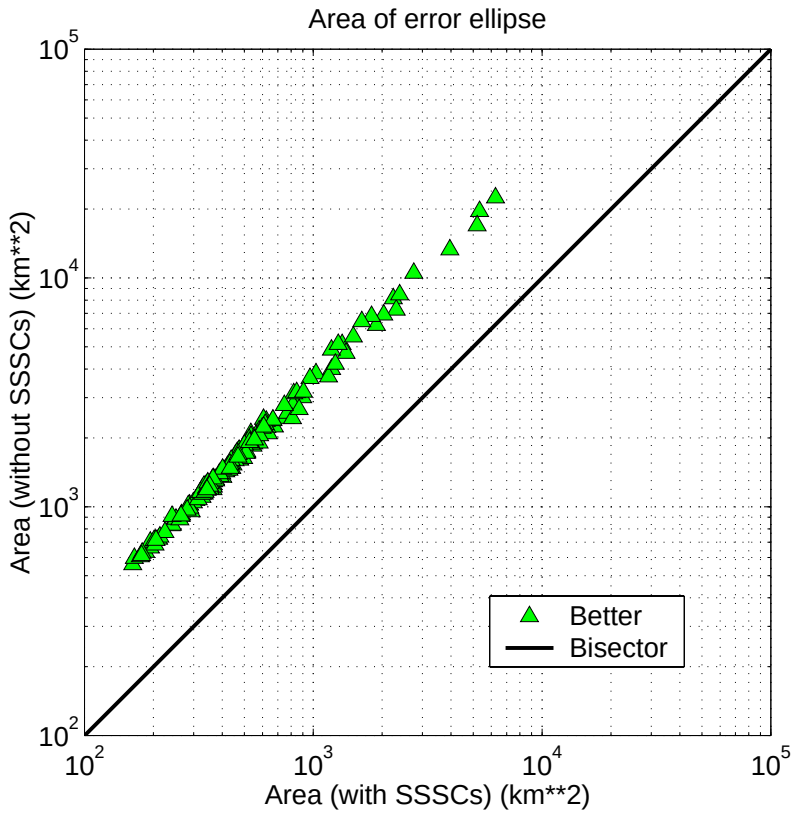

Figure 22. Scatter plot of error ellipse areas computed with (x-axis) and without (y-axis) using model-based SSSCs. Green symbols represent error ellipse areas that are smaller when using the SSSCs than without.

Error ellipse coverage is defined as the percentage of GT event locations that fall within the corresponding 90%-confidence error ellipse. For relocation solutions without using SSSCs, 151 events (97%) have 90%-confidence ellipses contain the GT locations. Using SSSCs, 146 events (94%) have 90%-confidence ellipses that contain the GT locations. Although the coverage is slightly lower when using the SSSCs, in both cases they are above the target of 90%, while the median area of the error ellipses is reduced substantially for all the events relocated with SSSCs.

5.2.3. Standard Error of Observations

The standard error of observations, a measure of the fit that depends on the root-mean-squared (rms) travel-time residuals, shows improvement for 110 solutions (71%) and deterioration for 46 solutions (29%). Sixty solutions (39%) are improved by more than 20% and 20 solutions (13%) deteriorated by more than 20%.

5.2.4. Discussion

The relocation results using the model-based SSSCs show the following:

- 63% of the events are located closer to the GT location than without using SSSCs;
- error ellipse area is smaller by 20% or more for 100% of the events;
- the coverage of the error ellipses is better than 90%.

Given the large number of source regions, stations, and ray paths that sample very diverse and extensive geological structures (represented by the 25 regions with corresponding travel times), we expect that SSSCs computed by Bondár's method for other stations in the same general area of Asia will, on average, perform as well as for the stations used to compile these evaluation metrics.

5.3. Evaluation of Kriged SSSCs

We now evaluate location performance using the kriged SSSCs. At locations near calibration data, the kriged corrections converge to the mean of the nearby data values and the uncertainty converges to the residual (i.e., local) variance. For grid points far from calibration data, the correction surface asymptotically approaches the model-based SSSC, with larger uncertainty that is the sum of the calibration and residual variances. Thus, the kriged SSSCs should perform at least as well as the model-based SSSCs, and much better for locations close to calibration points.

In this analysis, we use a "leave-one out" procedure in which the event to be relocated is excluded from the kriging calculation of the SSSCs. We then relocate each of the 156 events with kriged SSSCs that are re-computed for each event so that we do not use the same data to both compute and test the SSSCs. The new SSSCs and the relocation processing are executed by a script, *run_lv1out.csh,* that includes the following steps:

- start a loop based on origin IDs of the events in the file *ORID.lst*
- for each *orid* do a loop over stations in the file *STA.lst*
- if there are picks at the station for the given *orid,* omit the picks from the data file and apply kriging to the SSSCs computed with Bondár's method for that station
- repeat for all the stations that have arrivals for the given *orid*
- at the end of the loop over stations, reformat the SSSCs into PIDC format and install the SSSCs in the appropriate directory
- execute the script *run_evloc_wk* for the selected *orid*, relocating the event with the updated SSSCs (parameter *sssc_level*=1 in the *EvLoc* par file)

- repeat for all the events in *ORID.lst*

The location solutions are stored in the database and are used to compute the same location performance metrics, as above. The metrics are compared to those obtained using the model-based SSSCs and without any SSSCs (i.e., using IASPEI91). The following subsections describe the metrics for mislocation, error ellipse area, coverage, and standard errors of observations.

As an example, Figure 23 shows relocation results without SSSCs, with model-based SSSCs, and with kriged SSSCs for a PNE, Meridian-2, that was detonated on 19 September 1973 in the Former Soviet Union. Only regional Pn phases were used in the location analysis. The kriged SSSCs reduce the mislocation error from 20.2 km to 6.1 km and reduce the error ellipse area from 879 km^2 to 221 km^2. For this event, the relocation results do not differ significantly when using the model-based or kriged SSSCs. Also, the error ellipses are smaller when using either version of the SSSCs, and contain the GT location, unlike the error ellipse based on IASPEI91 without SSSCs.

5.3.1. Mislocation

Of the 156 GT events, 145 solutions (93%) have smaller mislocation errors using kriged SSSCs than those obtained using just the IASPEI91 travel-time tables. Of these, 139 events (89%) have mislocation errors that are reduced by more than 20%. Only 11 solutions (7%) deteriorated, but not dramatically. The median mislocation is reduced from 12.2 km to 2.7 km when kriged SSSCs are used. Figure 24 shows a scatter plot of the mislocation distances, relative to the GT locations, obtained with (x-axis) and without (y-axis) using the SSSCs. As in Figure 20, the green symbols represent events for which location estimates using the kriged SSSCs are closer to the GT locations, while the red symbols show solutions that are better without using SSSCs.

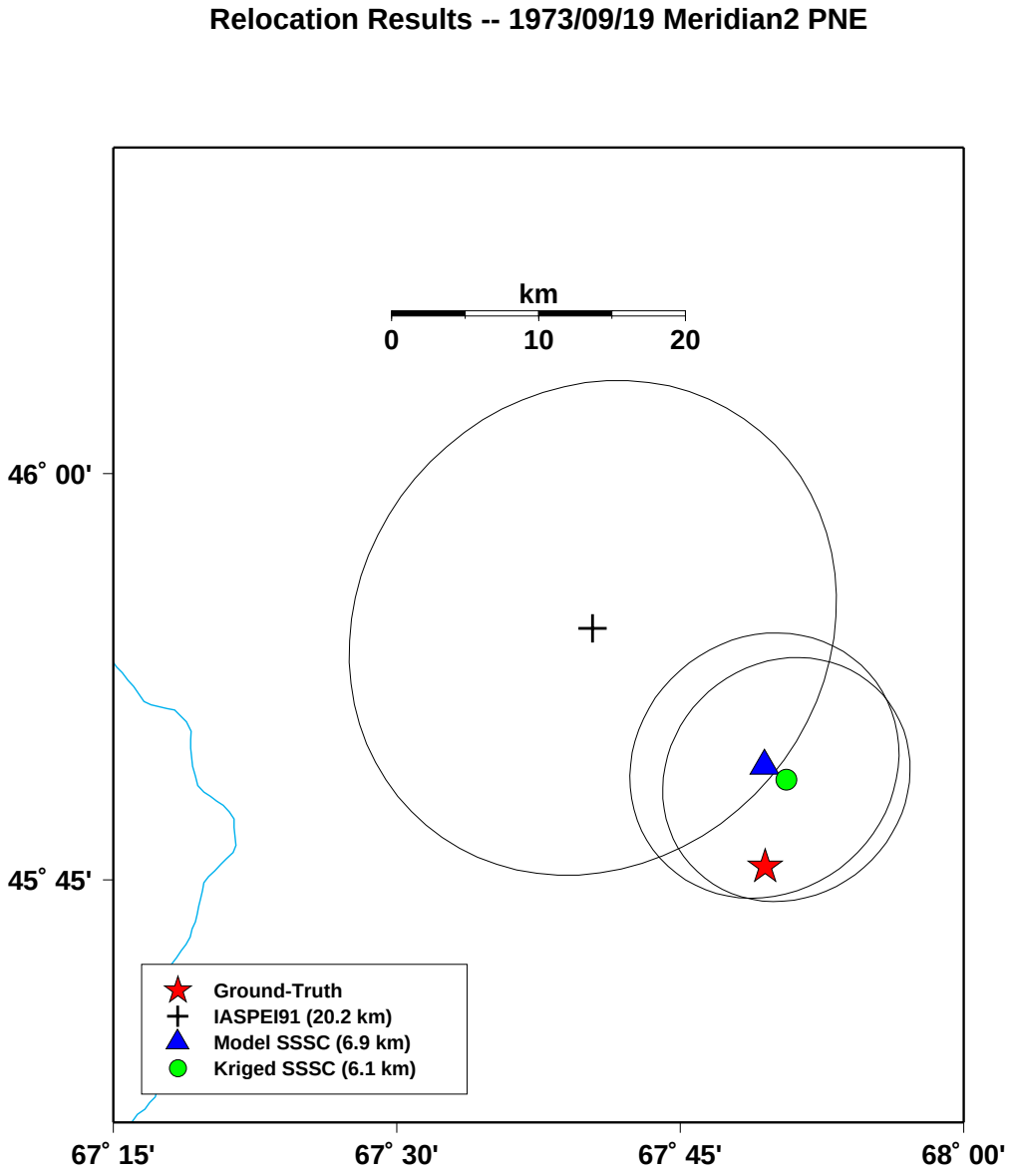

Figure 23. Relocation results, with and without using SSSCs, for a PNE (Meridian-2) in the Former Soviet Union on 19 September 1973. Mislocation errors relative to the ground-truth location are 20.2 km without using SSSCs, 6.9 km using model-based SSSCs, and 6.1 km using kriged SSSCs. The error ellipse areas are 879 km^2 without using SSSCs, 261 km^2 using model-based SSSCs, and 221 km^2 using kriged SSSCs.

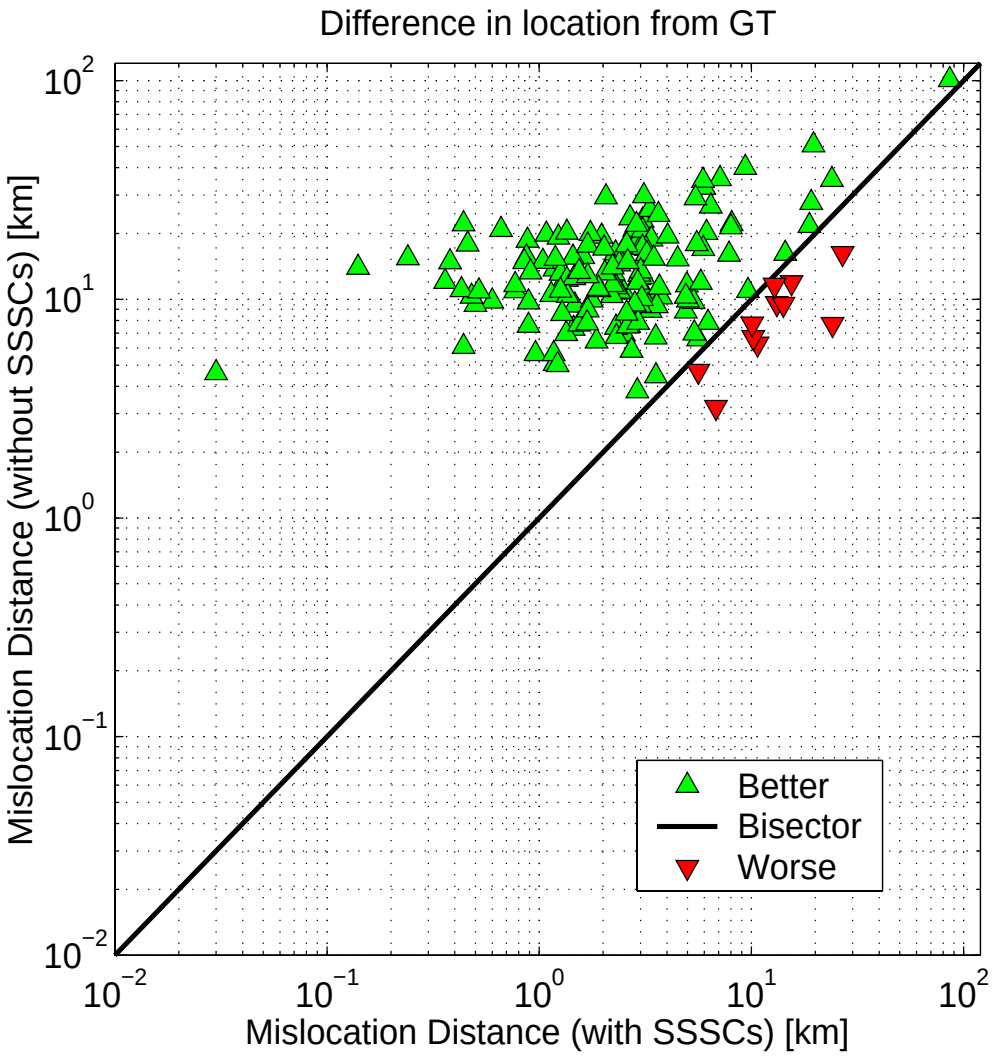

Figure 24. Mislocation distances with and without using kriged SSSCs with respect to corresponding GT locations. Markers and the line are defined as in Figure 20.

Figure 25 shows the differences of mislocation distances, without and with using kriged SSSCs, versus the number of defining phases [*ndef*] (upper plot) and azimuthal gap (lower plot). Green markers indicate solutions with smaller mislocation distances when SSSCs are used, while red markers indicate solutions with larger mislocation distances when SSSCs are used. These plots indicate that larger mislocation errors generally occur when *ndef* is less than 6 and the azimuthal gap is greater than 200 degrees.

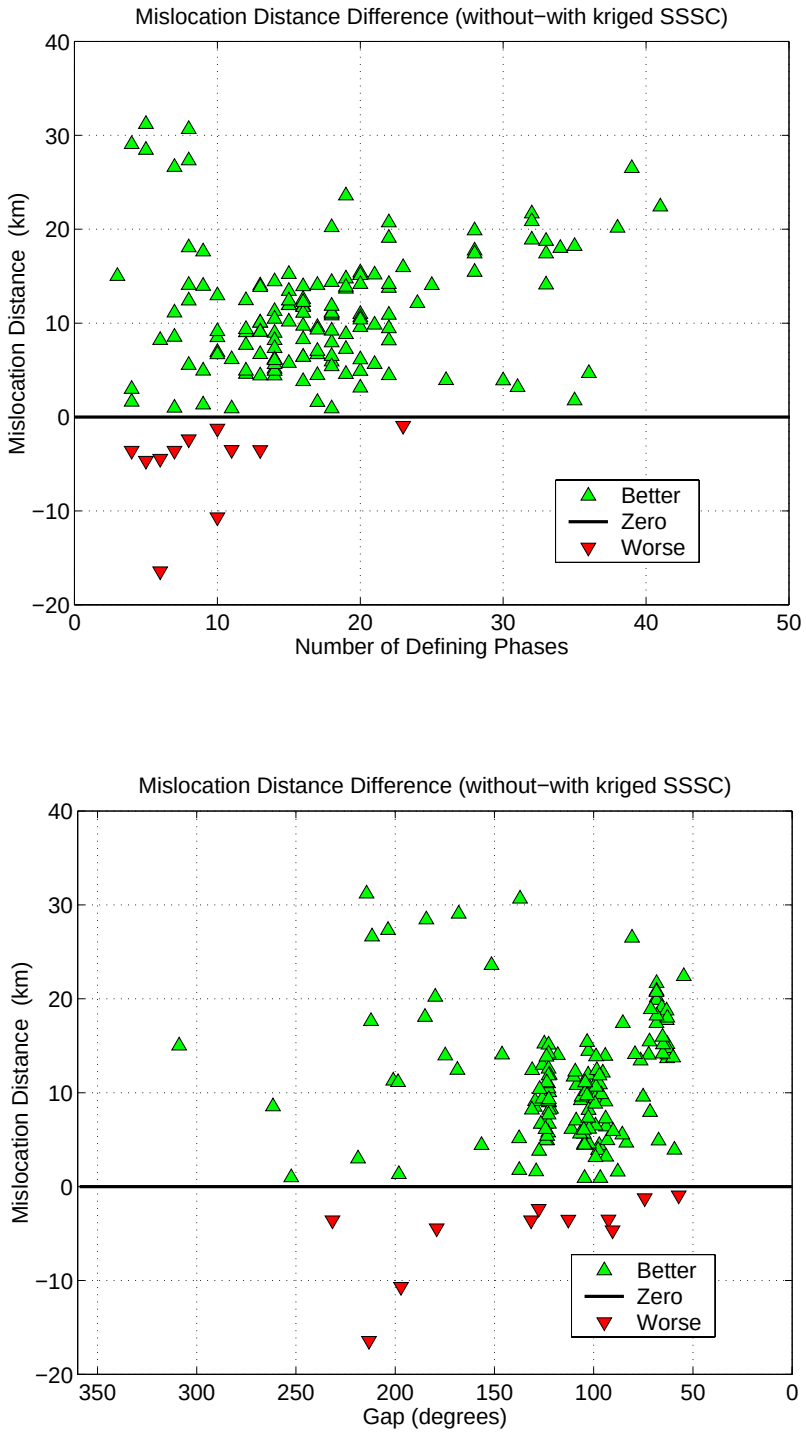

Figure 25. Differences of mislocation distances, without and with kriged SSSCs, versus the number of defining phases (upper plot) and azimuthal gap (lower plot). Markers are defined as in Figure 21.

We now provide a comparison of the three sets of solutions. Figure 26 shows the mislocation vectors for three cases: (1) without using SSSCs (red), (2) using model-based SSSCs (blue), and (3) using model+kriged SSSCs (green). The black vector in the upper right-hand corner of the map is scaled to 20 km. It can be seen that the green vectors are typically the smallest. Note that there are two events for which the mislocation vectors are significantly larger than for the remainder of the events. One of these events has only 3 defining phases and an azimuthal gap of about 310 degrees. The other event has 4 defining phases and an azimuthal gap of about 220 degrees

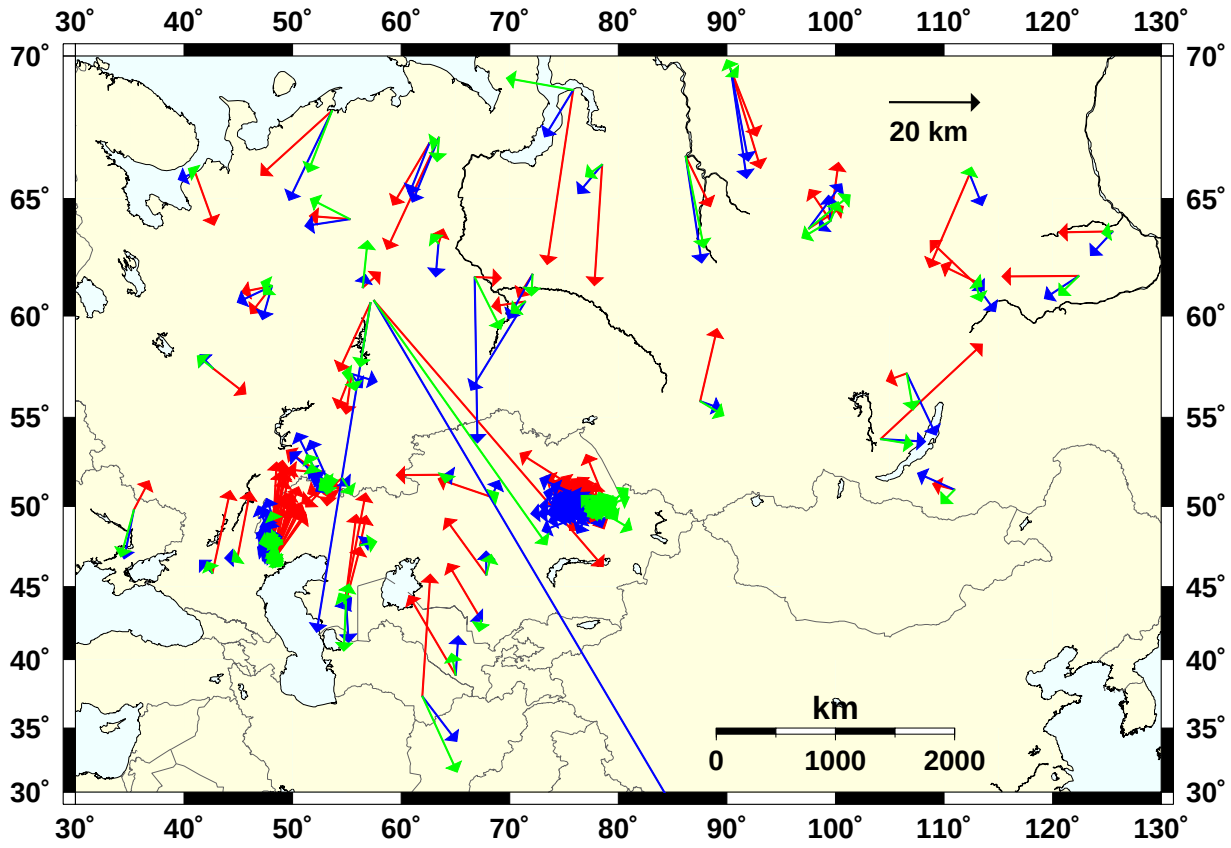

Figure 26. Mislocation vectors relative to the GT locations for 156 explosions (1) without using SSSCs (red vectors), (2) using model-based SSSCs (blue vectors), and (3) using model+kriged SSSCs (green vectors). The black vector in the upper right-hand corner of the map is scaled to 20 km.

5.3.2. Error Ellipse Area and Coverage

Using kriged SSSCs, error ellipse area is reduced for 153 of 156 solutions (98%), 152 of which (97%) are improved by more than 20%. Only 3 solutions (2%) do not have smaller error ellipses. The median ellipse area is reduced from 1,596 km^2 to 196 km^2. The results are shown in Figure 27. Error ellipse coverage, computed as the percentage of GT event locations contained within the 90%-confidence error ellipses, is 100% (all 156 GT events) when using the kriged SSSCs, as compared to 97% (151 GT events) without using SSSCs (i.e., using IASPEI91 only).

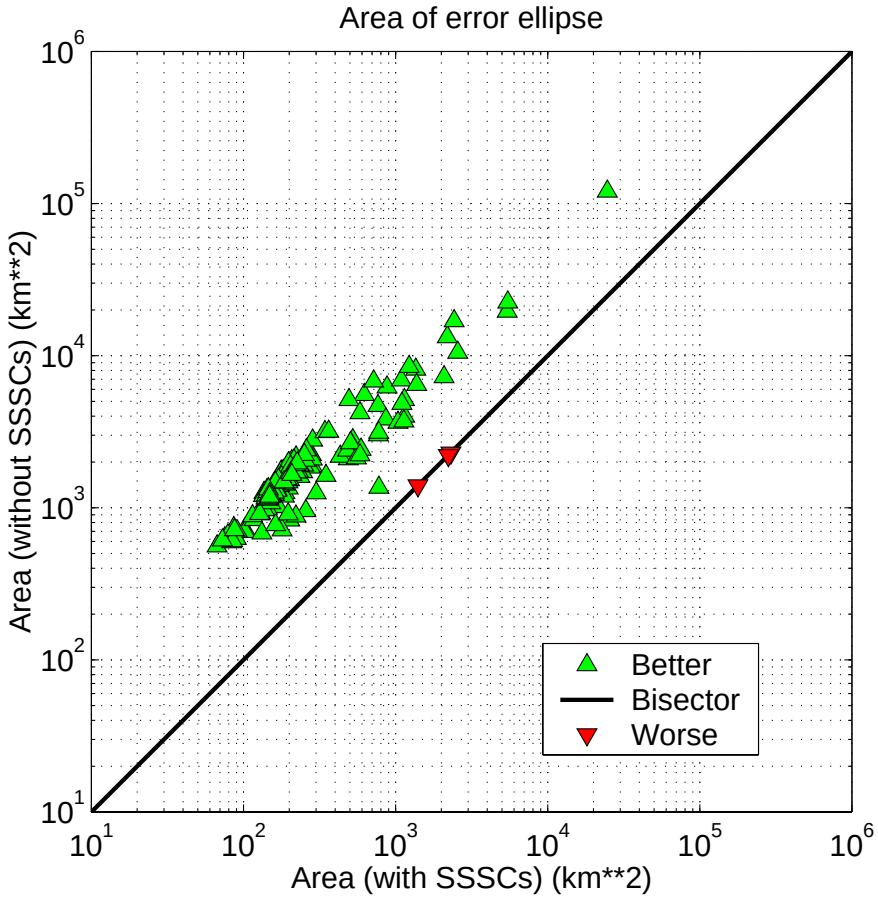

Figure 27. Scatter plot of error ellipse areas computed with (x-axis) and without (y-axis) using kriged SSSCs. Markers are defined as in Figure 22.

5.3.3. Standard Error of Observations

The results presented in Figure 28 show that 92% of the solutions have smaller standard errors of the travel-time observations (87% improved by more than 20%) and 8% deteriorated.

5.3.4. Discussion

The relocation results using kriged SSSCs show significant improvements for all location performance metrics. Specifically,

- 93% of the events are located closer to the GT location with median mislocation errors reduced from 12.2 km to 2.7 km;
- error ellipse area is reduced by 20% or more for 97% of the events;
- median error ellipse area is reduced from 1,596 km^2 to 196 km^2, while achieving 100% coverage of the error ellipses with the GT event locations.

These results are very encouraging and show that our regionalized travel-time model of Asia, and the combined computational methods of Bondár (1999) and kriging, yield useful Pn SSSCs and modeling errors for stations in Asia. It is important to note that location performance of events in areas far from existing calibration data should be, on average, comparable to the results obtained using the model-based SSSCs (i.e., without kriging).

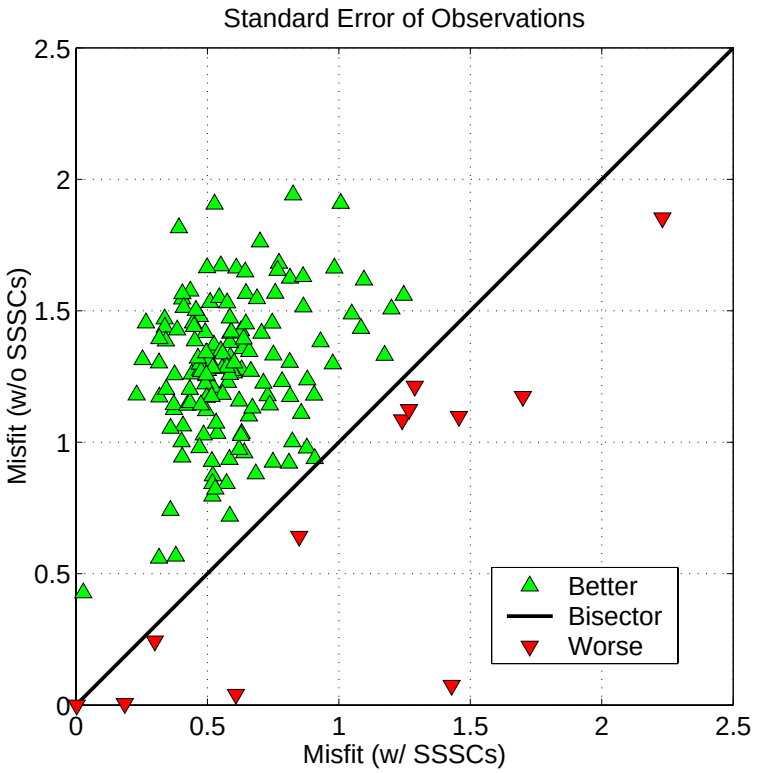

Figure 28. Scatter plot of the standard error of observations with (x-axis) and without (y-axis) using kriged SSSCs. The green symbols represent solutions with smaller standard errors using SSSCs, while the red symbols show the solutions with smaller standard errors without using SSSCs.

5.4. Validation of Pn SSSCs for IMS Stations in Central Asia

In Sections 5.2 and 5.3 we tested our regionalized travel-time model of Asia and showed that the methods of Bondár and kriging produce useful SSSCs. However, of the 30 IMS stations that we are trying to calibrate, Kitov's data set includes phase readings from only BRVK, NIL, MAG, NRI (NRIS), SEY, TIK (TIXI) and YAK. To validate the SSSCs for other IMS stations in Central Asia (AAK, AKTO, KURK, MAKZ and ZAL), we use 18 GT nuclear or chemical explosions (9 UNE's at the Lop Nor test site in China, 7 UCE's in Kazakhstan, 1 UNE in India, 1 UNE in Pakistan) with regional Pn arrivals. Locations of the IMS stations and the 18 GT events are shown in Figure 29. Pn arrivals at stations TLY (Talaya, Russia) and ULN (Ulan Bator, Mongolia) were also used. Plots of the Pn SSSCs and model errors are shown in the Appendix for these nine stations.

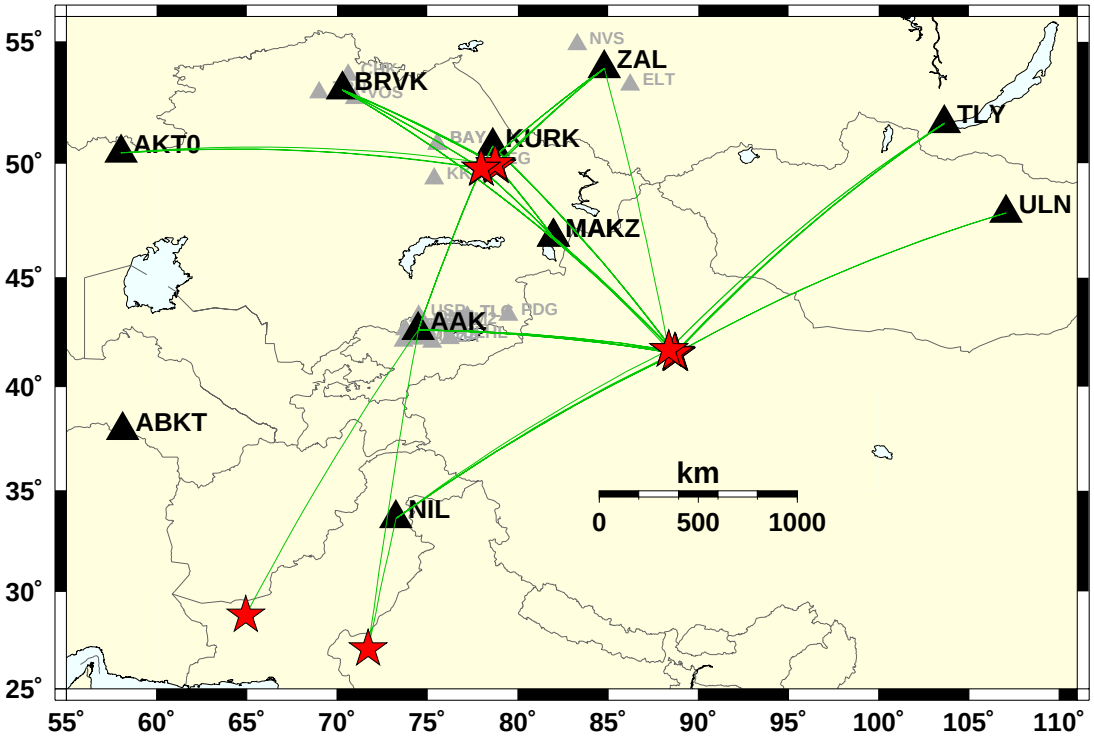

Figure 29. Map of additional events (stars) and IMS seismic stations (triangles) used for validation tests.

Relocation tests were performed for cases without SSSCs, with model-based SSSCs, and with model+kriged SSSCs. The 7 UCE's in Kazakhstan were relocated using Pn arrivals only because most of these events were too small to have useful teleseismic phases; the 9 Lop Nor UNE's were located using only Pn arrivals, and using P and Pn; the UNE's in India and Pakistan were located

using P and Pn arrivals because only a couple of regional stations recorded these events. Figure 30 illustrates the relocation results for a Lop Nor explosion on 15 May 1995. Results are shown for cases using (1) only regional Pn arrivals and (2) using Pn and P arrivals. For both of the respective cases, the mislocations and error ellipses are smaller using SSSCs. Note that the mislocation is smallest for the case of using only Pn phases, corrected by the SSSCs. This is due to having very good calibration of the Pn travel times, while no corrections were used for teleseismic P phases.

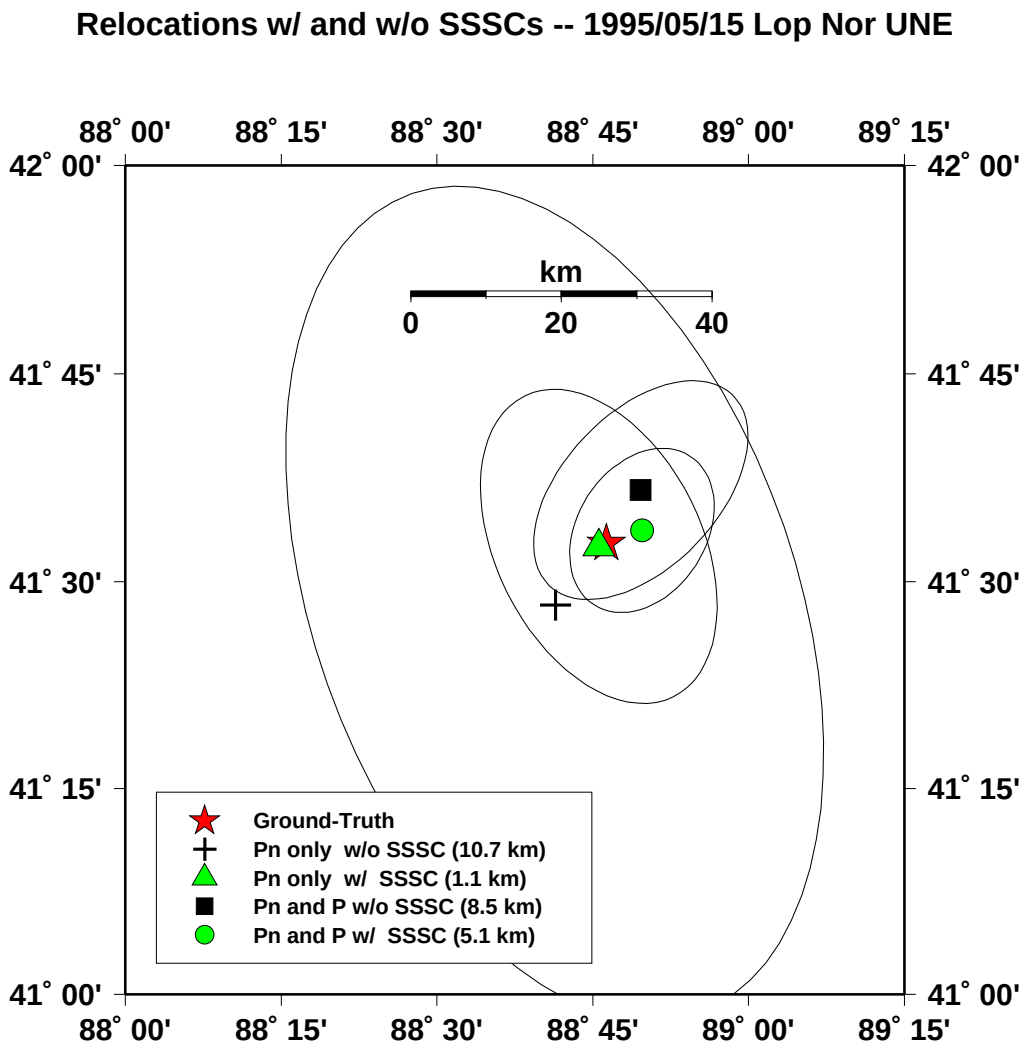

Figure 30. Comparison of relocation results, with and without using kriged SSSCs, for an underground nuclear explosion at the Lop Nor test site on 15 May 1995. Mislocation errors relative to the ground-truth location are provided in the legend for the various solutions.

5.4.1. Mislocation

The relocation results using the model-based SSSCs (but without kriging) show that 12 of 18 events (67%) have smaller mislocations than just using IASPEI91, while 6 solutions (33%) deteriorated. When kriging was applied (using the leave-one-out procedure, as above), 17 location estimates (94%) improved and only 1 (6%) deteriorated. The median mislocation is 7.2 km without using SSSCs, 4.6 km using model-based SSSCs, and 3.5 km using model+kriged SSSCs. Figure 31 shows the results for the case using model-based SSSCs. Figure 32 shows the results for the case using model+kriged SSSCs.

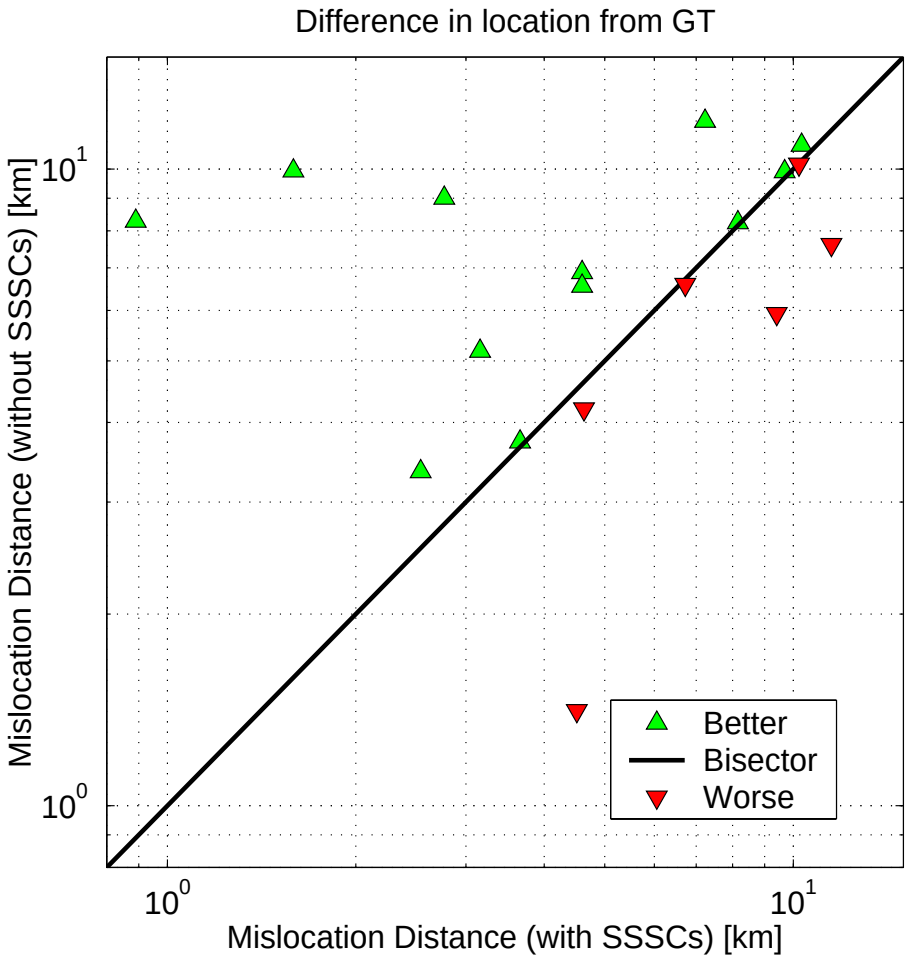

Figure 31. Comparison of mislocations, relative to GT locations, with and without using model-based SSSCs.

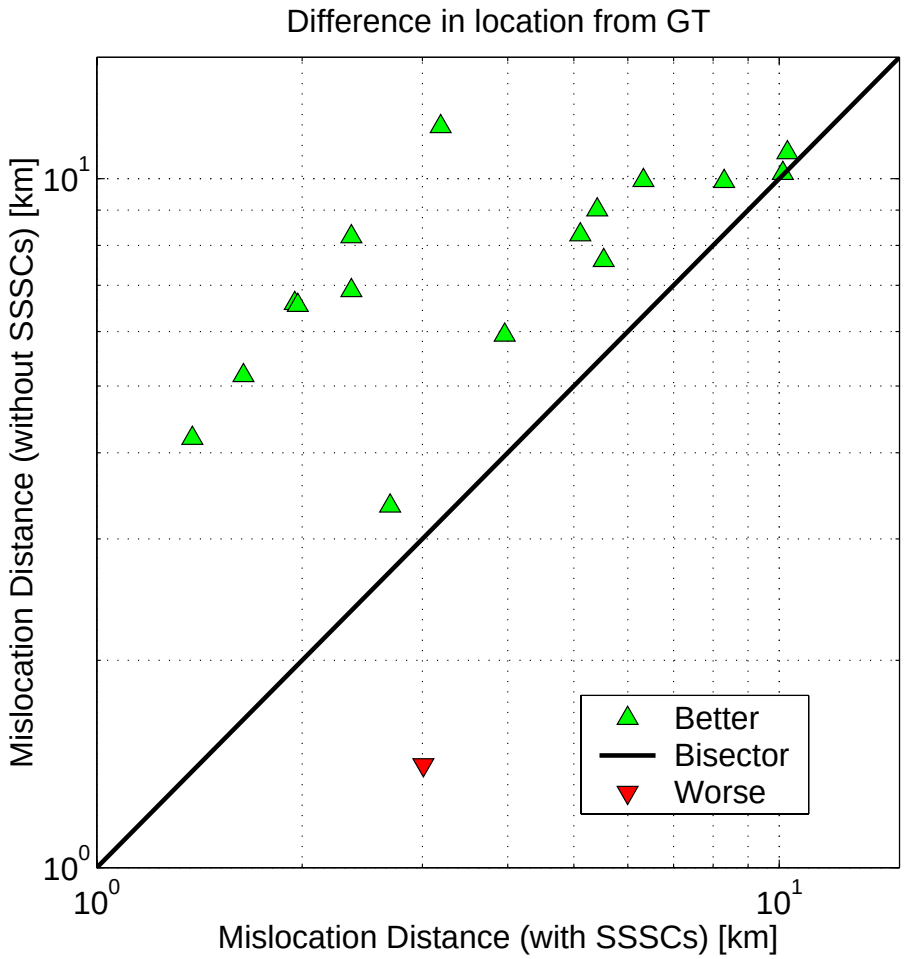

Figure 32. Comparison of mislocations, relative to GT locations, with and without using kriged SSSCs.

5.4.2. Error Ellipse Area and Coverage

In both cases (using model-based or kriged SSSCs) 100% of the events have smaller error ellipses. The median area decreases from 1412 to 669 km^2 without kriging and from 1412 to 551 km^2 when kriging was used. The error ellipse coverage is 100% for all cases, i.e., using IASPEI91 without SSSCs, using model-based SSSCs, and using model+kriged SSSCs.

5.4.3. Discussion

While the number of events used for this test is small, the results are consistent with the previous validation test results using Kitov's data set. Namely, mislocations and areas of error ellipses are reduced by using the model-based SSSCs, without compromising coverage, and location performance is further improved by refining the SSSCs by kriging the travel-time residuals.

6. CONCLUSIONS AND RECOMMENDATIONS

The goal of the tests presented in this report was to validate our regionalized travel-time model of Asia and evaluate the effectiveness of the regional Pn SSSCs developed by the Group 1 consortium. As the regionalization is an important part of our current SSSC computation, a significant portion of the report was also devoted to specifying the boundaries of the subregions and reviewing a wide variety of data and literature to obtain the best available estimates of the travel times, as a function of distance, within each subregion.

The SSSCs were computed for each station using the approach of Bondár (1999) and refined by spatially correcting the travel-time residuals at each grid point using kriging. The kriging approach assures that the correction converges to the mean of nearby calibration data for areas with ground truth, and the uncertainty converges to the residual variance of the local data. Far from empirical calibration data, the correction surface reverts to the background model-based SSSC, with larger uncertainty that is the sum of the residual and calibration variances.

To quantify improvements in location performance due to our Pn SSSCs, we performed two series of tests on two distinct data sets. The main objective of the first test was validate the regionalized travel-time model and demonstrate that the resulting SSSCs improve location performance. To directly test the validity of the model, we first performed relocation tests that did not use kriging to refine the model-based SSSCs. To evaluate the additional benefit of kriging, we performed a second set of relocation tests using kriged model-based SSSCs. Although kriging significantly enhances the calibration of the SSSCs, as shown, a direct test of the model is important to demonstrate that even in areas and at stations without empirical calibration data, the model-based SSSCs provide useful improvements in location performance.

Using a data set of phase arrival times assembled by Kitov and his colleagues at the IDG in Moscow, and published information regarding GT locations and origin times of the corresponding events, we relocated 156 events recorded by various combinations of 93 regional stations, with and without using SSSCs. The results show reductions in mislocations for 63% of events when the model-based SSSCs were used, and 93% when using model-based SSSCs refined by kriging. The median mislocation improved from 12.2 km to 9.5 km and 2.7 km, respectively. The median area of the error ellipses was reduced from 1,596 km^2 to 450 km^2 and 196 km^2, respectively. Error

ellipse coverage, as a percentage of GT event locations within the corresponding error ellipses, is 97% without using SSSCs, 94% using model-based SSSCs, and 100% using kriged SSSCs. These results were obtained for source locations, stations, and paths that sample very extensive and diverse geological provinces throughout Central and Northern Asia (Figure 10). Thus, we believe the results indicate the general validity of the model and the resulting SSSCs for this region.

To directly evaluate the Pn SSSCs for IMS stations in Central Asia, we then performed relocation tests using 18 GT explosions in western China, eastern Kazakhstan, India, and Pakistan. Although this data set is small, comparable reductions in mislocations and error ellipse areas were obtained for these tests, as for the tests against Kitov's data set.

In all cases, the results demonstrate that the regionalization and travel-times curves, developed by the Group 1 consortium, along with the computational methods of Bondár (1999) and kriging, have produced Pn SSSCs and modeling errors that improve the performance of location and uncertainty estimates in Asia.

We have delivered these SSSCs (model-based with kriging) and GT data sets to the CMR, along with an Integration Test Plan. We expect that these SSSCs will perform, on average, as well as indicated by the validation test results for the model-based SSSCs, and substantially better for regions surrounding the Lop Nor, Semipalatinsk, Indian and Pakistani nuclear test sites, where calibration data have been utilized. We are coordinating with CMR staff to conduct an integration test of these SSSCs on the CMR Testbed system, to verify that no unexpected problems occur in an operational setting. We then plan to present a proposal to the Configuration Control Board (CCB) to install the SSSCs in the operational system at the CMR.

Future efforts will focus on improving and extending the model, computational methods, and resulting SSSCs. Specifically, we plan to (1) update these SSSCs as better models and GT data are obtained; (2) generate SSSCs for secondary regional phases (Pg, Sn, Lg) at IMS stations; and (3) generate SSSCs at additional IMS stations in Eastern Asia.

7. REFERENCES

Anikanova, G. Thickness of the crust in the Western Khubsugul region. Russian Geology and Geophysics, 36, N12, pp.128-130, 1995.

Antonenko, A.N. The Deep Structure of the Kazakhstan Earth Crust (from seismic data). Nauka Publ. House, Alma-Ata, 242 p. 1984 (in Russian).

Atabaev, Kh.A., E.M. Butovskaya. Regional travel-time tables for some regions of Central Asia. Institute of Geophysics and Geology, Uzbek National Academy of Science, Tashkent, report. 36 pp., 1986 (in Russian).

Barker, B., M. Clark, P. Davis, M. Fisk, M. Hedlin, H. Israellson, V. Khalturin, W.-Y. Kim, K. McLaughlin, C. Meade, J. Murphy, R. North, J. Orcutt, C. Powell, P. Richards, R. Stead, J. Stevens, F. Vernon, and T. Wallace, Monitoring nuclear tests, Science, 281, 1967-1968, 1999.

Barkhin, G.S., L.N. Nikitina, V.Z. Ryaboy. Study of the structure of the upper mantle based on DSS profile observations. VINITI, 65 p., 1987.

Båth, M. Earthquakes in Sweden, 1951-1976. Travel times of regional phases in Scandinavia region for H = 0 km and H = 12 km. Uppsala, 1977.

Beloussov, V.V. et al. (editors). Deep structure of the USSR territory. Moscow, Nauka, 1991.

Beloussov, V.V., N.I. Pavlenkova and G.N. Kvyatkovskaya (editors), Structure of the Crust and Upper Mantle of the USSR, International Geology Review, V.34, N4, pp.213-445, 1992.

Bocharov, V.S., S.A. Selentov and V.N. Michailov, Characteristics of 92 Underground Nuclear Explosions at the Semipalatinsk Test Site, Atomaya Energia, Vol.87, Issue 3, 1989 (in Russian).

Bondár, I. Combining 1-D models for regional calibration, in Proceedings of a Workshop on IMS Location Calibration, Oslo, January 1999.

Bondár, I., X. Yang, K. McLaughlin, R. North, V. Ryaboy, and W. Nagy. Source Specific Station Corrections for Regional Phases at IMS Stations in North America and Fennoscandinavia, EOS Trans., AGU, 79 (45), Fall Meet. Suppl., F839, 1998.

Bondár, I., V. Ryaboy. Regional travel-time tables for the Baltic Shield region. Technical report CMR-97/24, 34 pp., 1997.

Bottone S., M.D. Fisk, and G.D. McCartor. Regional seismic event characterization a using Bayesian formulation of simple kriging, in press, Bull. Seism. Soc. Am., 2001.

Bune, V.I., E.M. Butovskaya,. Travel-time curves and Earth's structure studied by records of large explosions. Proceedings of Geophysical Institute, N32, pp.142-153, 1955 (in Russian).

Chan, W.W., C.Y. Wang, and W.D. Mooney. 3-D Crustal structure in southwestern China. 23rd Seismic Research Review, Wyoming, v.1, pp.12-20. 2001.

Egorkin, A.V., et al. Structure and properties of the Upper Mantle on the USSR territory. Moscow, Nauka Publ.House, 1980.

Egorkin, A.A., et al. Results of lithospheric studies from long-range profiles in Siberia. Tectonophysics, v. 140, pp.29-47, 1987.

Fedorov, S.A. (editor). Gazli earthquakes. Geological and geophysical nature of the source zones. Moscow, Nauka Publ.House, 200 pp., 1984.

Fisk, M.D. Accurate locations of nuclear explosions at the Lop Nor test site using cross-correlated seismograms and Ikonos satellite imagery, submitted to Bull. Seism. Soc. Am., 2001.

Golenetskiy, S.I. Travel time tables of seismic waves from Baykal region earthquakes. In the book: Seismicity and Deep Structure of Baykal Area. Novosibirsk, Nauka Publ. House, pp.30-38, 1978.

Golenetskiy, S.I., F.B. Novomeyskaya, and G.I. Perevalova. Travel times of seismic waves and Earth's crust thickness in the North-East part of Baykal zone. Geology and Geophysics, Novosibirsk, N2, pp.40-57, 1974.

Gorbunova, I.V,. Average travel time of P wave first arrivals for Central Asia and South Kazakhstan regions. Annual book: Earthquakes in the USSR in 1988. Moscow, Nauka Publ. House, pp. 59-63. 1990 (in Russian).

Hamburger, M.W., and S. Ghose. Velocity structure beneath the Northern Tien Shan, J. Geophys. Res., v103, 2725-2748, 1998.

Hearn, T.M., J. Ni. Tomography and location problems in China using regional travel-time data, 22-nd Seismic Research Symposium, New Orleans, v.2, pp.155-160, 2000.

IDC Documentation IDC7.1.5 - Event Location Software, 2001.

Karus, E.V. (editor). Investigation of the Earth's crust and upper mantle in the seismic active zone of the USSR. Moscow, Nauka Publ.House, 1984 (in Russian).

Kennett, B.L.N. (editor). IASPEI 1991 Seismological Tables, Research School of Earth Sciences, Australian National University, Canberra, Australia, 1991.

Khalturin, V.I. Regional version of Nersesov-Rautian (1964) travel-time table (unpublished report), 1974.

Khalturin, V.I., et al. Propagation of Lg waves and lateral variations in crustal structure. J. Geophys. Res., v82, n2, pp.307-316. 1977.

Khalturin, V.I, A.A. Lukk, A.I. Ruzaykin. Regional phase velocities and fine structure of its travel time curves from CSE stations observations of seismic events in North-West China at the distances 800-2400 km.(Part of unpublished CSE report to Soviet Military, Dec. 1978.).

Khalturin, V.I., T.G. Rautian, P.G. Richards. A study of small earthquakes and small explosions during 1961-1989 at the Semipalatinsk Test Site. Technical report to DOE/LLNL, 64p., 1994.

Khalturin, V.I., T.G. Rautian, P.G. Richards. A study of small magnitude seismic events during 1961-1989 on and near the Semipalatinsk Test Site, Kazakhstan, Pure and Applied Geophysics, v. 158, pp.143-172, 2001.

Khamrabaev, I.Kh. (editor). Earth's crust and upper mantle of Central Asia. Nauka Publ.House, Moscow, 210 pp., 1977.

Kirichenko, V.V., Y.A. Kraev. Development of regional travel-time tables for different geotectonic provinces of Northern Eurasia. Proceedings of 22nd Annual DoD/DOE Seismic Symposium, New Orleans, pp.305-315, 2000.

Kirichenko, V. V., and Y. A. Kraev. Results of 1-D location calibration studies related to the territory of Northern Eurasia, *Proceedings of the 23rd Seismic Research Review*, 2001

Kosminskaya, I.P. et al. (editors). Seismic models of the lithosphere of the main Geostructures in USSR territory. Moscow, Nauka Publ. House, 191 pp, 1980 (in Russian).

Krasnopevtseva, G.V. Deep structure of the Caucasus seismoactive region. Nauka, Publ.House, Moscow, 109 pp., 1984.

Krilov, S.V. et al. Seismic cross-section of the lithosphere at the Baykal Rift Zone. Geology and Geophysics, Novosibirsk, N3, 1975.

Lomakin, V.S, V.V. Kolmogorova, G.I. Parygin. Travel time table of seismic waves in Ural region. In the book: Seismic waves from mining explosions and study of the Earth's crust in the Ural. Ural Scientific Center of Acad.Sci. USSR, Sverdlovsk, pp.14-20, 1978.

Lukk, A.A., I.L. Nersesov. Deep Pamir-Hindu Kush earthquakes. Earthquakes in the USSR in 1966, Nauka Publ.House, 1967 (in Russian).

Mooney, W., et al., 2001. A review of new seismic constraints of crust and mantle from China and India. Proceedings of the 23rd Seismic Research Review. Wyoming, pp.90-99, 2001.

Molnar, P., and P. Tapponier. Cenozoic tectonics of Asia: effects of tectonic collision, Science, v 189, 419-426, 1975.

Molnar, P., and P. Tapponier. Active faulting and Cenozoic tectonics of the Tien Shan, Mongolian and Baykal regions, J. Geophys. Res., v84, 3425-3459, 1979.

Nersesov, I.L. Structure of the Earth's Crust. In the book: Methods of the Detailed Study of the Seismicity, Chapter 3. Moscow. Publ. House of Academy of Science, Moscow, pp. 30-46. 1960 (in Russian).

Nersesov, I.L. (editor). Deep Structure of the low seismicity regions of the USSR. Moscow, Nauka Publ.House, 223 pp., 1987 (in Russian).

Nersesov, I.L., T.G. Rautian. Kinematics and dynamics of seismic waves at epicentral distances less than 3,500 km. Proceedings of the Institute of the Physics of the Earth, N32, pp.63-84, 1964 (in Russian).

Pavlenkova, N.I. Crust and upper mantle structure in Northern Eurasia from seismic data. Advances in Geophysics, v. 37, Academic Press, 1996.

Roecker, S.W., et al. Three-dimensional velocity structure of the Western and Central Tien Shan, J. Geophys. Res., v99, 15779-15795, 1993.

Ryaboy, V.Z. Lower lithosphere and asthenosphere of the Central and Eastern regions of Northern Eurasia based on seismic data. Physics of the Solid Earth (English edition), Soviet Academy of Sciences, v.21, N2, pp.100-110, 1985.

Ryaboy, V.Z. Upper mantle structure studies by explosion seismology in the USSR. Delphic Associates, 154 pp., 1989.

Ryaboy, V.Z. The Earth's crust and upper mantle structure and lateral inhomogeneities beneath Northern Eurasia. Nuclear monitoring research at the Center for Seismic Studies. Sci. Report N1, 64 pp., 1991.

Sabitova, T.M. Seismic wave velocities in Northern Kyrgizia and their use for epicenter location. Seismicity of Tien-Shan, ILM Publ.House, Frunze, pp.27-49, 1989.

Schultz, C.A., S.C. Myers, J. Hipp, and C.J. Yooung. Nonstationary Bayesian Kriging: A predictive technique to generate spatial corrections for seismic detection, location and identification, Bull. Seism. Soc. Am., **88**, 1275-1288, 1998.

Seismic Models of the Lithosphere of the main Geostructures in territory of the USSR, Moscow, Nauka Publ. House, 311p, 1980 (in Russian).

Seleznev, V.S., V.M. Solovyev, I.V. Zhemchugova. Deep structure of Altay-Sayans region from the seismological systems of observations. Seismology in Siberia. Novosibirsk, Nauka Publ.House, pp.222-228, 2000 (in Russian).

Shatsilov, V.I. Methods of Evaluating Seismic Hazard, Nauka Publ. House, Alma-Ata, pp. 65-78, 1989.

Shatsilov, V.I., et al. Velocity Models of the Earth's Crust in Kazakhstan, Evrasia Publ. House, Almaty, 105 p 1993 (in Russian).

Starovoit, O.E., et al. in Proceedings of a Workshop on IMS Location Calibration, Oslo, 2000.

Sulatnov, D.D., J.R. Murphy, and Kh.D. Rubinstein. A Seismic Source Summary for Soviet Peaceful Nuclear Explosions, Bull. Seism. Soc. Am., 89, vol.3, pp. 640-647, 1999.

Travel time table of regional phases for several Chinese regions. Chinese Seismological Bureau. Beijing, 178 pages, 1989 (in Chinese).

Tsibulchik, G.M. Travel time data of the regional phases and the Earth's crustal structure in the Altay-Sayans region. In the book: Regional Geophysical Studies in Siberia. Novosibirsk, Nauka Publ. House, pp.159-169, 1967 (in Russian).

Ulomov, V.I., A.B. Aronov. Travel-time table of main P and S phases for seismic waves observed in Uzbekistan at epicentral distances up to 1000 km, Technical report, 1977.

Volvovsky, B. Probabilistic Geophysical Models of the Earth's Crust of the main structure of Central Asia. Moscow, Nauka Publ. House, 1991 (in Russian).

Working Group B, Recommendations for seismic event location calibration development, CTBT/WGB/TL-2/18, 1999.

Yang, X., I. Bondár, K. McLaughlin, and R. North. Source Specific Station Corrections for Regional Phases at Fennoscandinavian Stations, Pure Appl. Geophys. 158, pp. 35-57, 2001.

Yang, X., I. Bondár, K. McLaughlin, R. North, and W. Nagy. Path-Dependent Phase Travel-Time Corrections for the International Monitoring System in North America, Bull. Seism. Soc. Am., 91,6, pp. 1831-1850, 2001.

Yang, X. and C. Romney. PIDC Ground Truth (GT) Datatbase, CMR Technical Report, CMR-99/15, May 1999.

Yakovleva, I.B. Travel times for West Uzbekistan. In the book: Seismology and Seismogeology of Uzbekistan. FAN Publ. House, Tashkent, pp.52-60, 1971.

Zhao, L.S., J. Xie. Lateral variations in compressional velocities beneath the Tibetan Plateau from Pn travel time tomography, Geophys. J. In., v115, pp. 1970-1984, 1993.

Zunnunov, F.K. Lithosphere of Central Asia from seismic data. Tashkent, FAN Publishing House, 208 pp., 1985 (in Russian).

Appendix: Pn SSSCs and Modeling Errors

The following figures depict the Pn SSSCs and the corresponding modeling errors, computed with Bondár's method and refined by applying a kriging algorithm, for the 7 IMS stations (or sites of future IMS stations) listed in Table 1 (AAK, AKTO, BRVK, KURK, MAZK, NIL, ZAL). Also shown are the grids for stations MAG (Magadan, Russia), NRI (Norilsk, Russia), SEY (Seymchan, Russia), TIK (Tiksi, Russia), TLY (Talaya, Russia), ULN (Ulan Bator, Mongolia) and YAK (Yakutsk, Russia).

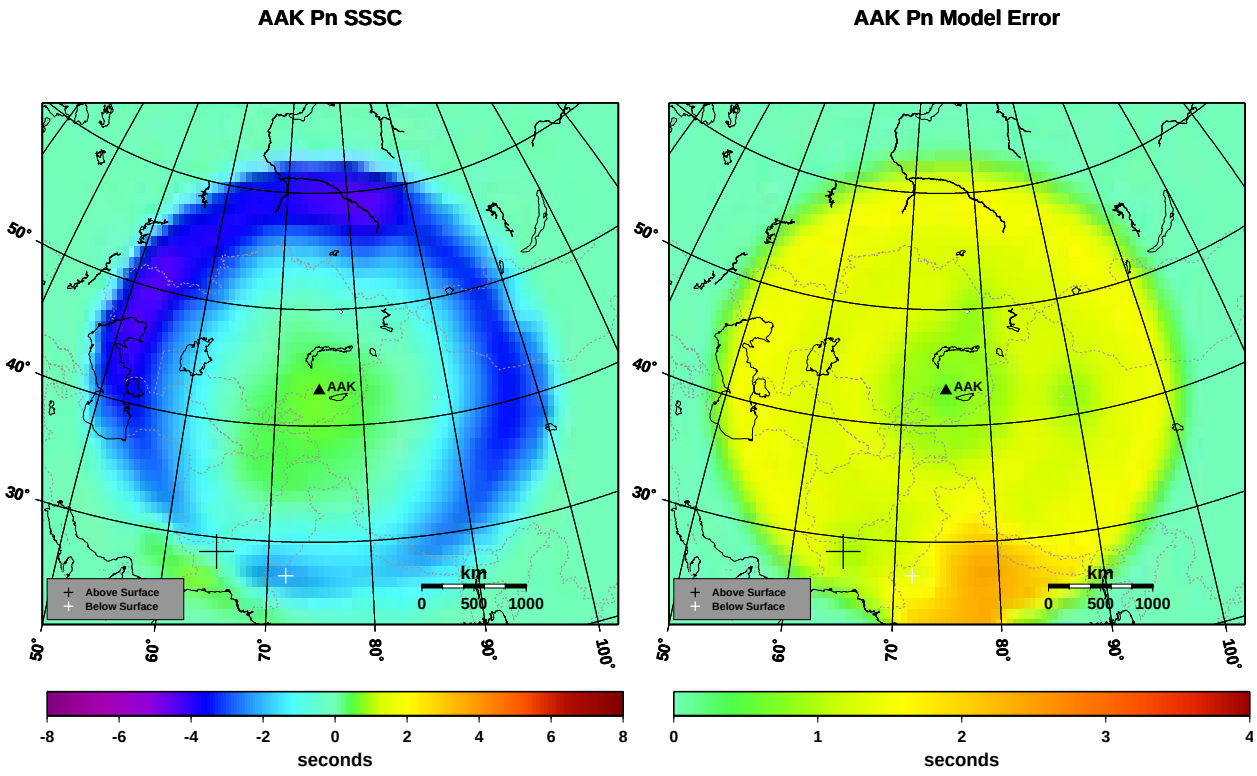

AKT0 Pn SSSC

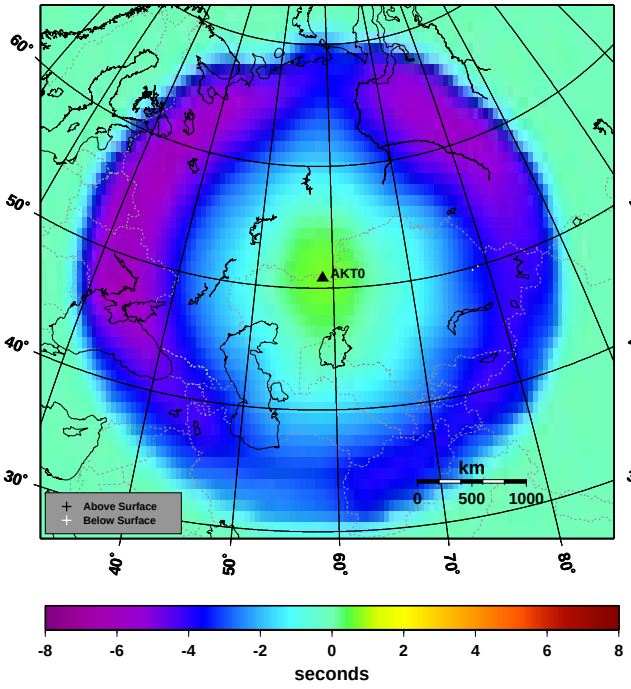

AKT0 Pn Model Error

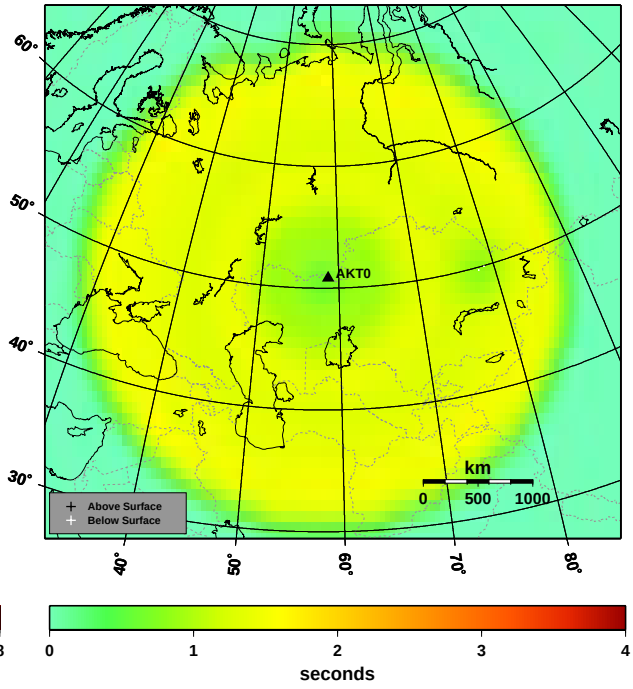

BRVK Pn SSSC

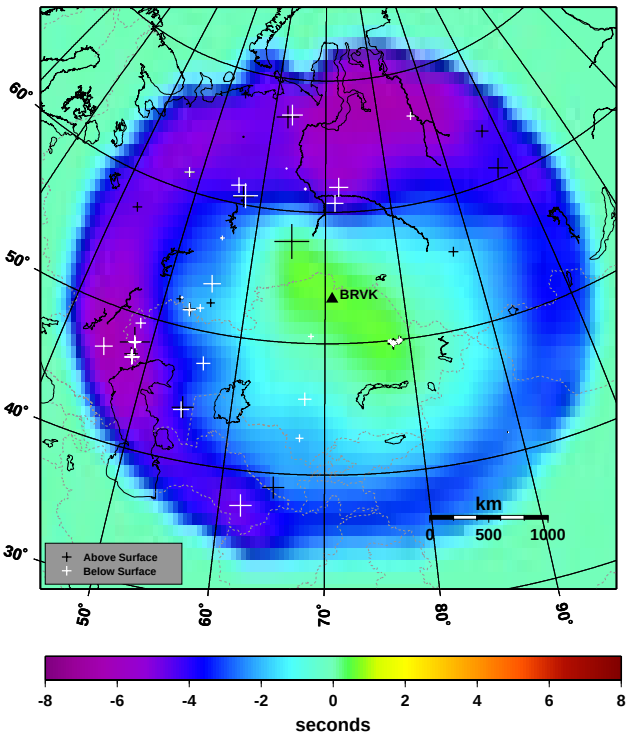

BRVK Pn Model Error

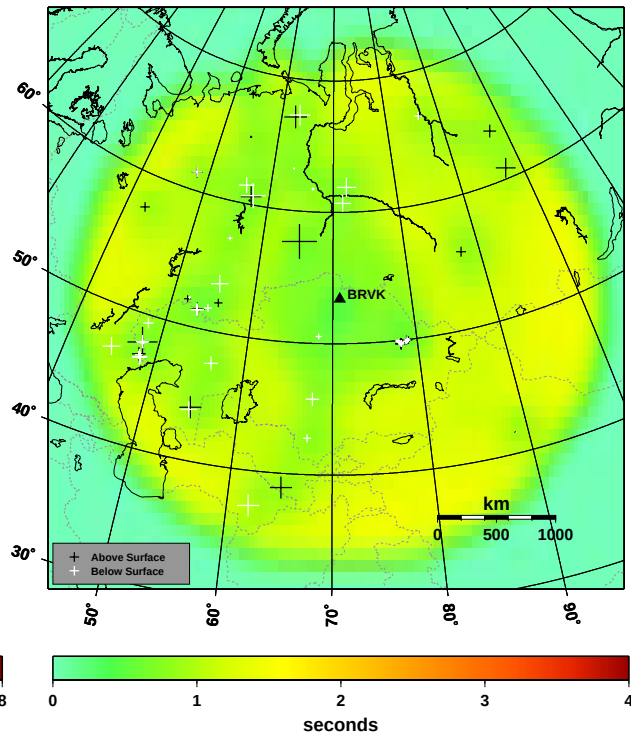

KURK Pn SSSC

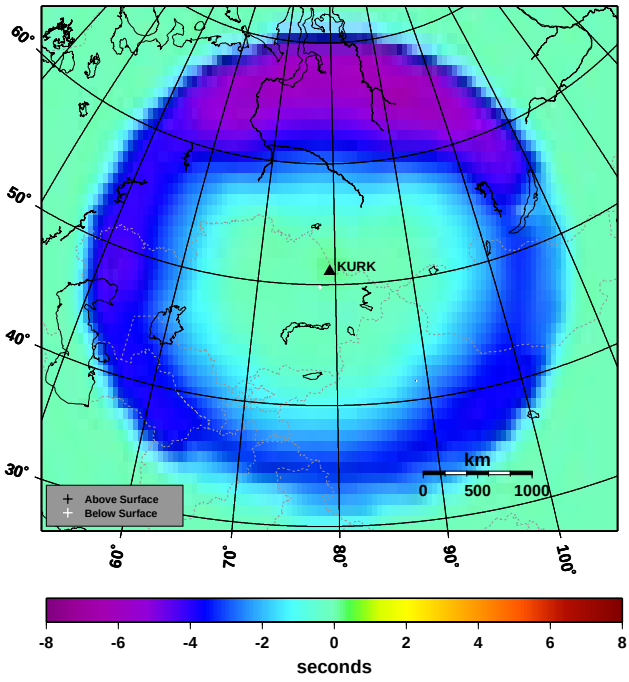

KURK Pn Model Error

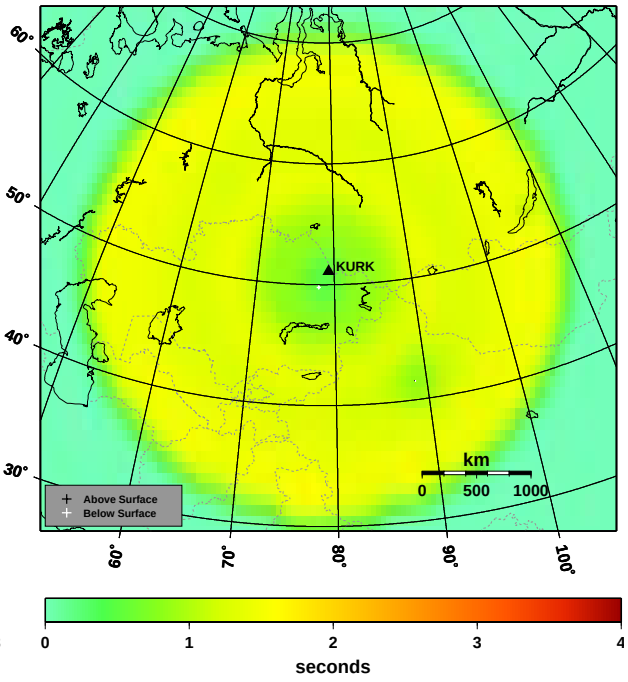

MAG Pn SSSC

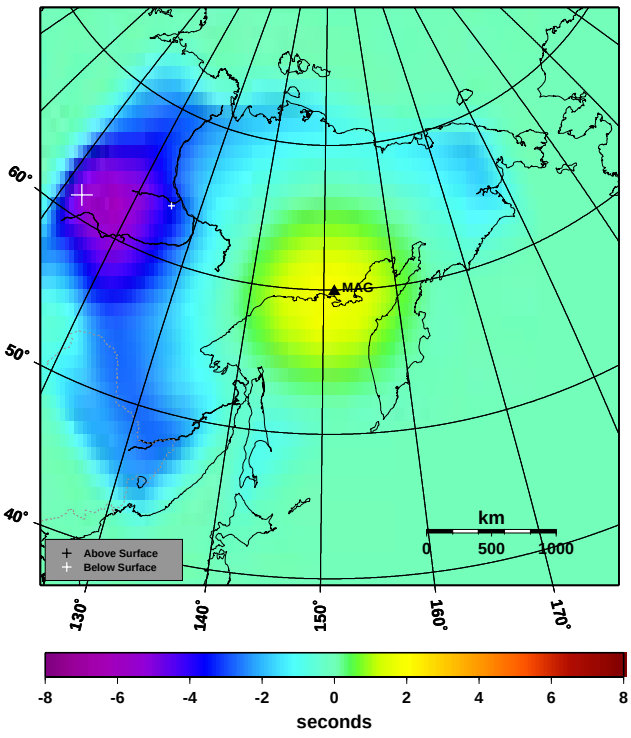

MAG Pn Model Error

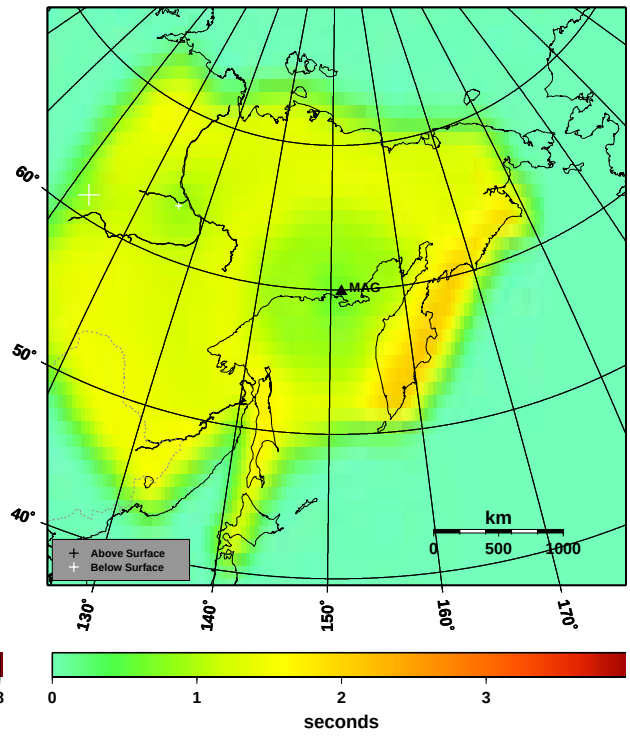

MAKZ Pn SSSC

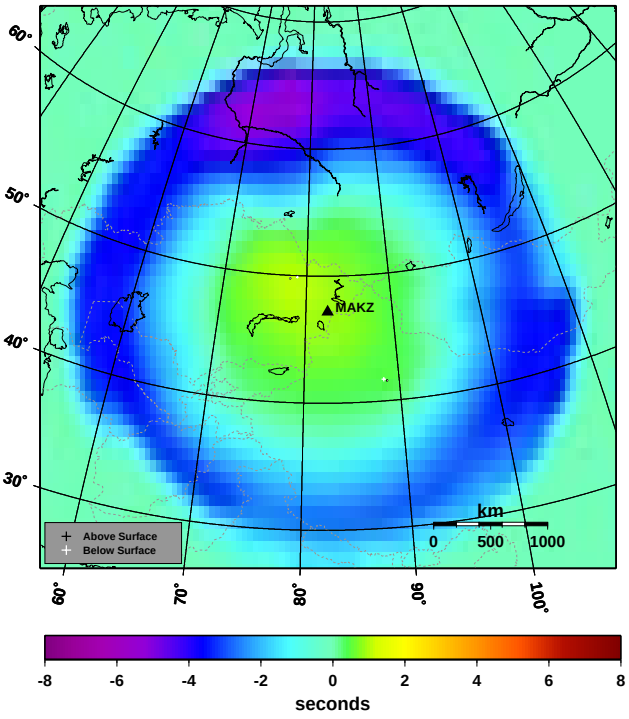

MAKZ Pn Model Error

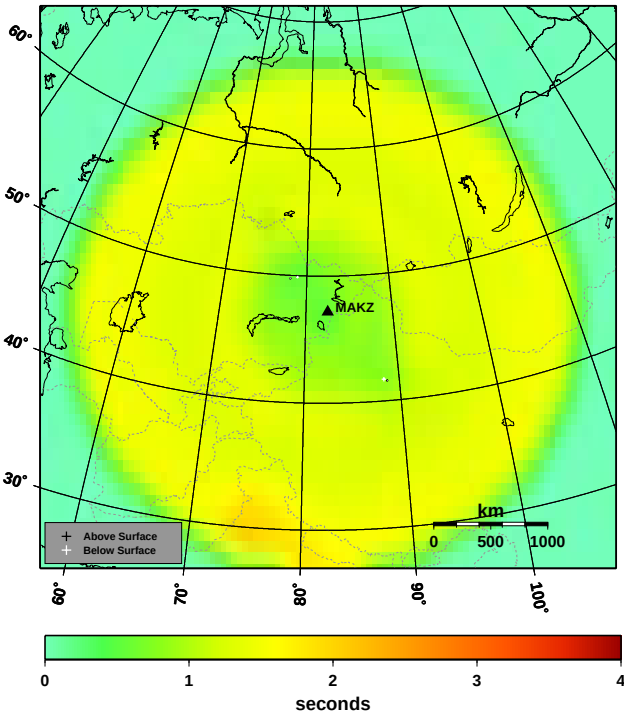

NIL Pn SSSC

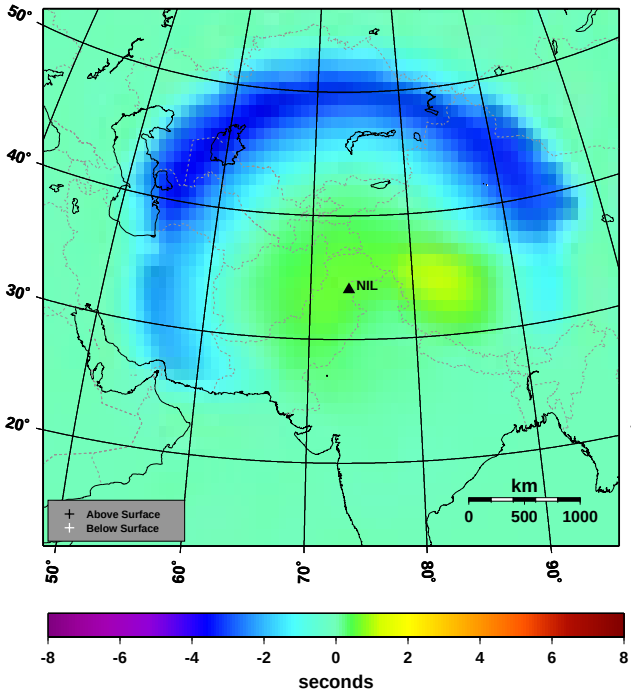

NIL Pn Model Error

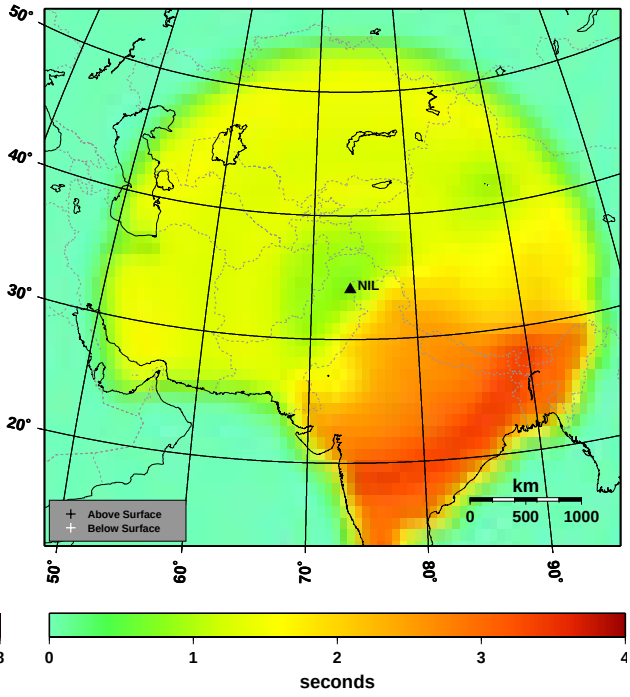

NRI Pn SSSC

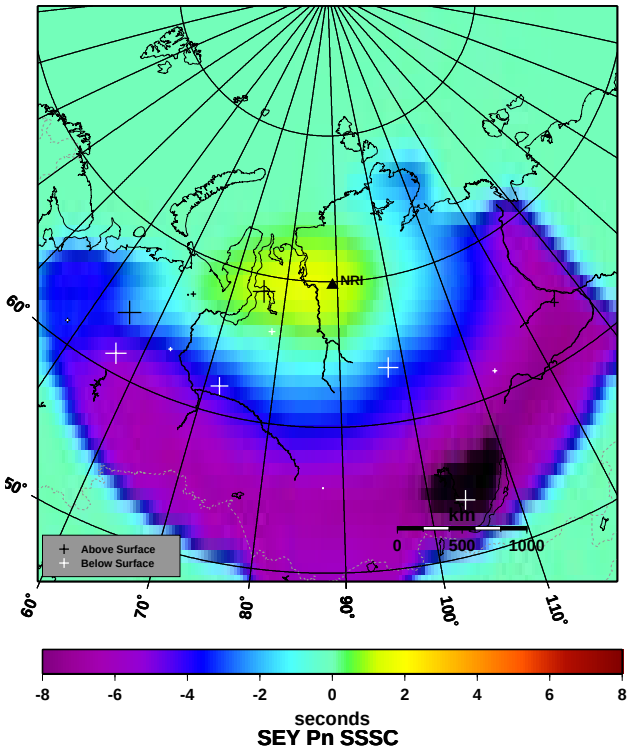

NRI Pn Model Error

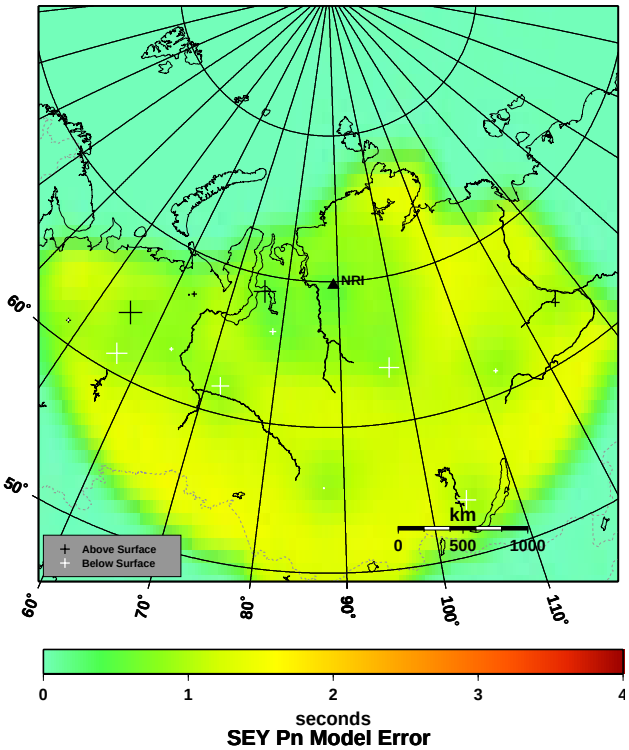

SEY Pn SSSC

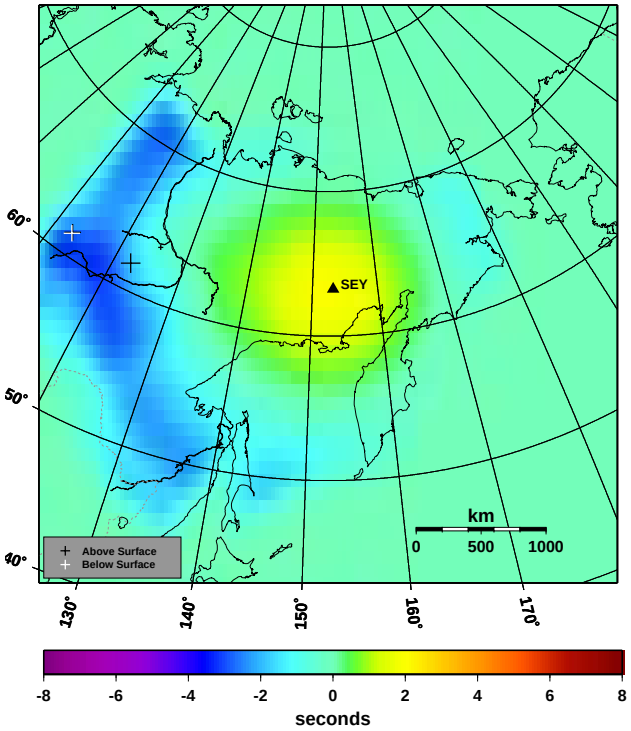

SEY Pn Model Error

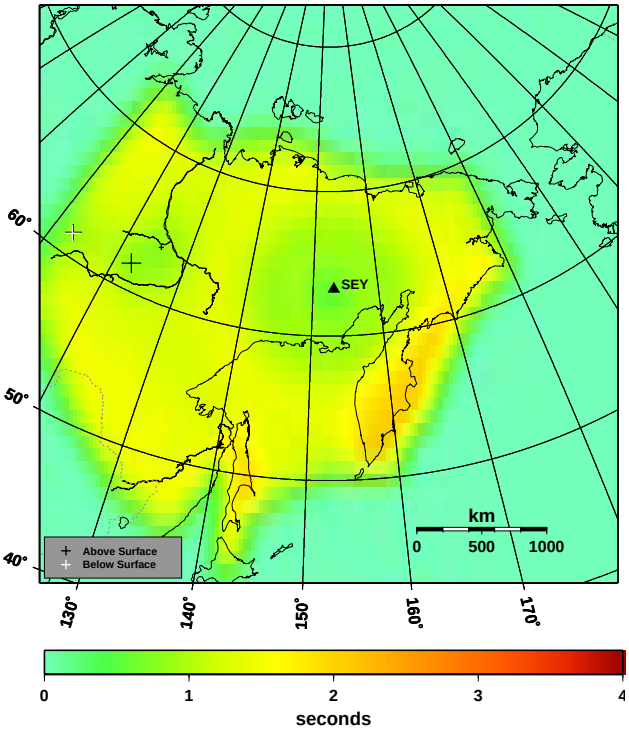

TIK Pn SSSC

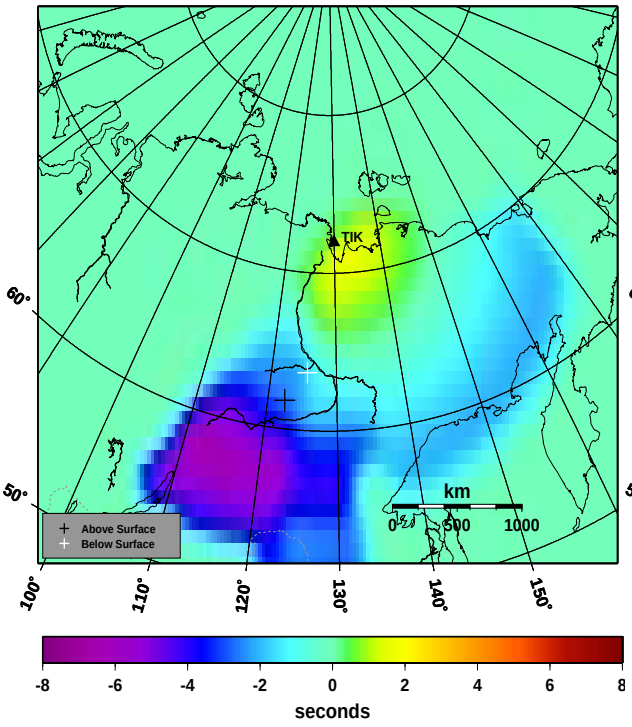

TIK Pn Model Error

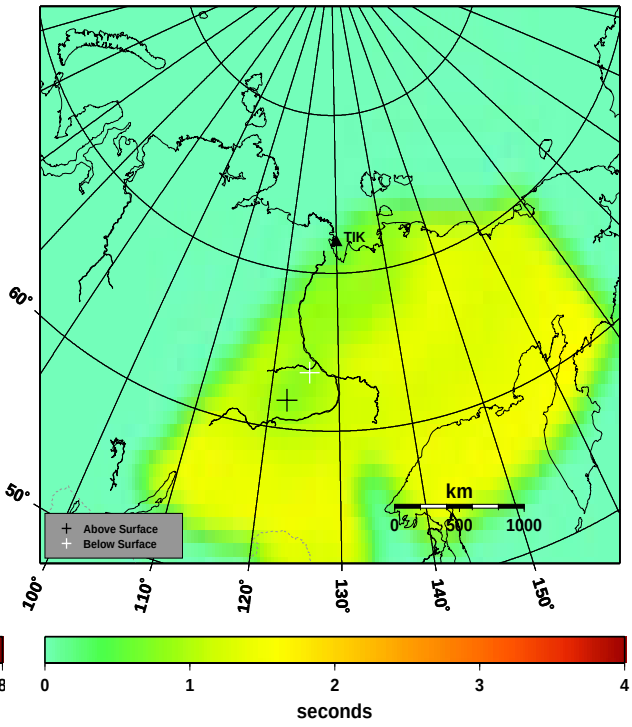

TLY Pn SSSC

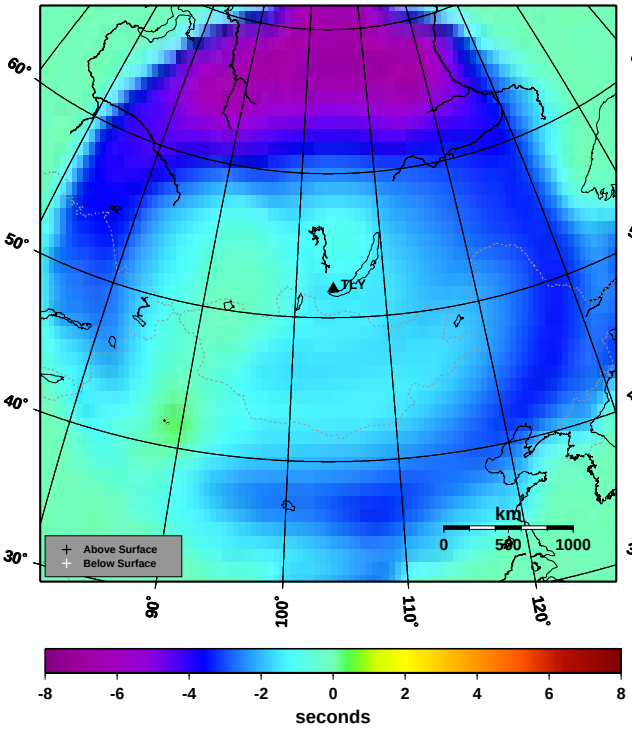

TLY Pn Model Error

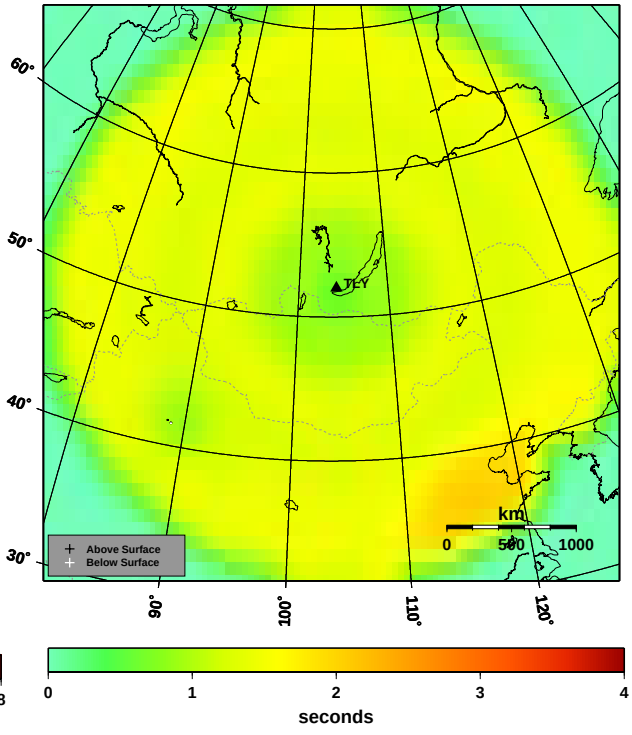

ULN Pn SSSC

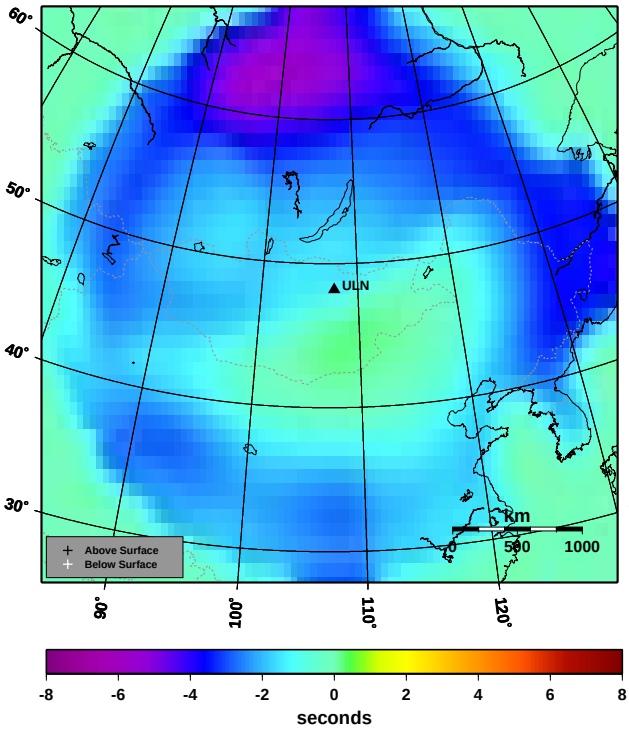

ULN Pn Model Error

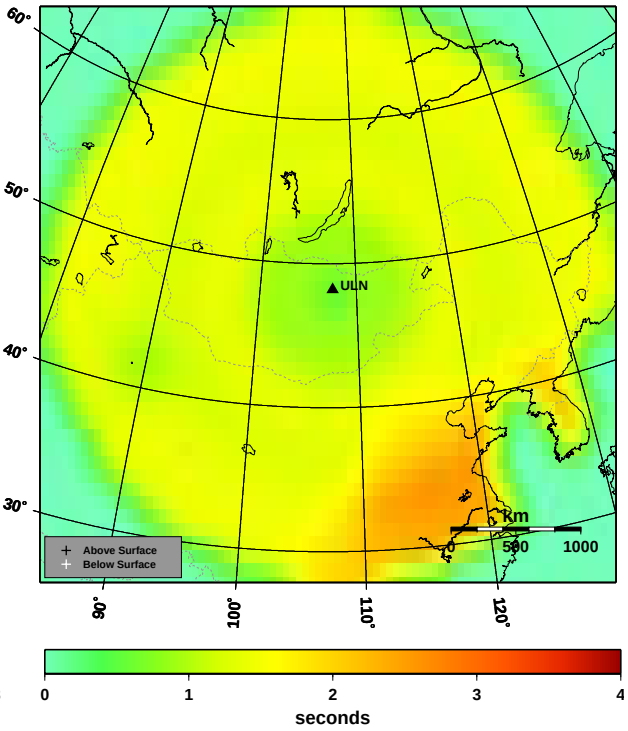

YAK Pn SSSC

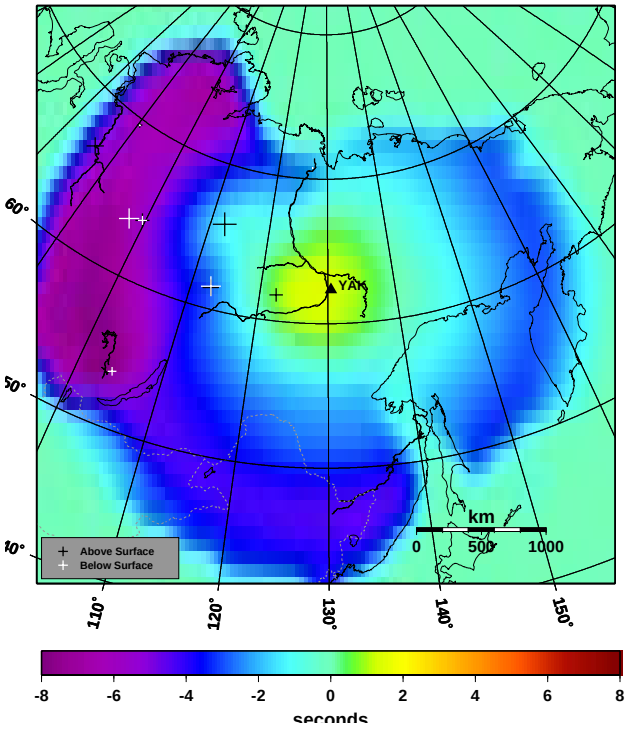

YAK Pn Model Error

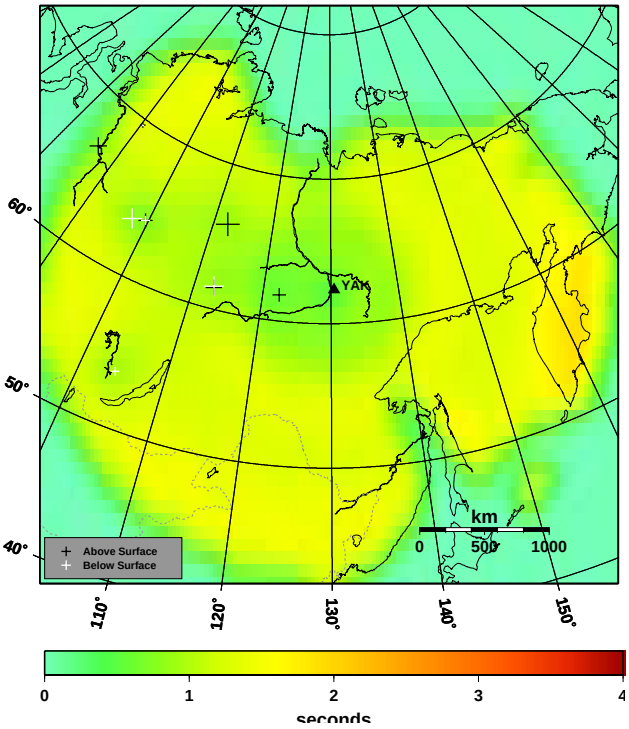

ZAL Pn SSSC

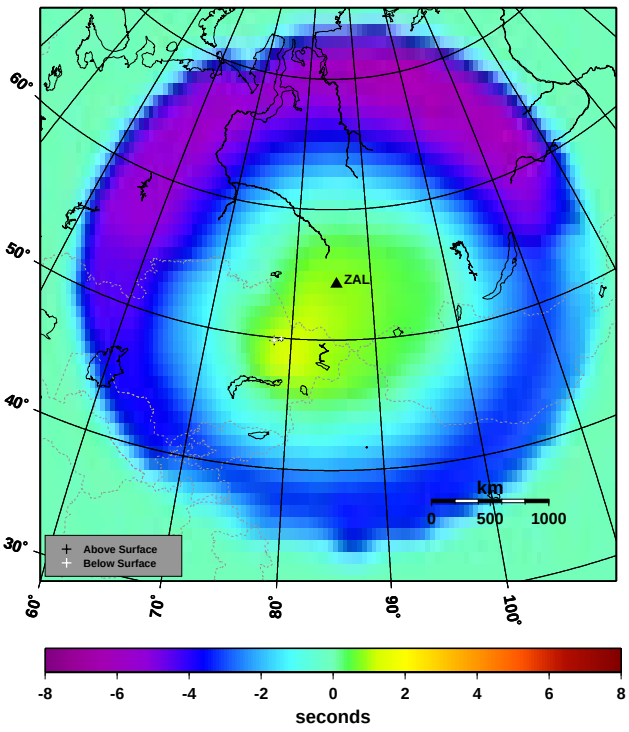

ZAL Pn Model Error